



THE HONG KONG
POLYTECHNIC UNIVERSITY

香港理工大學

Pao Yue-kong Library

包玉剛圖書館

Copyright Undertaking

This thesis is protected by copyright, with all rights reserved.

By reading and using the thesis, the reader understands and agrees to the following terms:

1. The reader will abide by the rules and legal ordinances governing copyright regarding the use of the thesis.
2. The reader will use the thesis for the purpose of research or private study only and not for distribution or further reproduction or any other purpose.
3. The reader agrees to indemnify and hold the University harmless from and against any loss, damage, cost, liability or expenses arising from copyright infringement or unauthorized usage.

IMPORTANT

If you have reasons to believe that any materials in this thesis are deemed not suitable to be distributed in this form, or a copyright owner having difficulty with the material being included in our database, please contact lbsys@polyu.edu.hk providing details. The Library will look into your claim and consider taking remedial action upon receipt of the written requests.

**OMICS-BASED CHARACTERIZATION OF
ANAEROBIC METABOLISM IN
METHANOGENIC SYSTEM AND CHAIN
ELONGATION PROCESS**

YANG PEIXIAN

PhD

The Hong Kong Polytechnic University

2019

The Hong Kong Polytechnic University
Department of Civil and Environmental Engineering

**OMICS-BASED CHARACTERIZATION OF
ANAEROBIC METABOLISM IN METHANOGENIC
SYSTEM AND
CHAIN ELONGATION PROCESS**

YANG PEIXIAN

A thesis submitted in partial fulfillment of the requirements for the Degree
of Doctor of Philosophy

August 2018

CERTIFICATE OF ORIGINALITY

I hereby declare that this thesis is my own work and that, to the best of my knowledge and belief, it reproduces no material previously published or written, nor material that has been accepted for the award of any other degree or diploma, except where due acknowledgement has been made in the text.

_____ (Signed)

YANG PEIXIAN (Name of student)

ABSTRACT

The thesis is to explore possible improvement of anaerobic fermentation system and to reveal the underlying mechanism. Specifically, the microbial communities and interspecies interactions of two methanogenic systems were investigated. One is a novel staged anaerobic fluidized bed ceramic membrane bioreactor (SAF-CMBR) with granular activated carbon (GAC) as fluidized biofilm carriers for low-strength synthetic wastewater (250 mg COD/L Na-propionate and acetate) treatment, another is a SAF-CMBR with GAC and polyethylene terephthalate (PET) beads as fluidized biofilm carriers, respectively. Microbial communities of the two systems were examined for a comparative study between GAC and PET beads as carriers. By using GAC as carrier, anaerobic treatment was achieved mainly by microorganism grown on the GAC particles in which propionate-degrading syntrophs (*Syntrophobacter* and *Smithella*), acetoclastic methanogens *Methanothrix* and exoelectrogenic *Geobacter* dominated. Whereas PET beads are less selective environment for microorganisms associated with methane production. Notably, methanogenesis would be promoted by the syntrophic cooperation between methanogens with *Geobacter* via direct interspecies electron transfer (DIET) for increased methane production. The conductive GAC could facilitate DIET and resulted in relatively high efficiency and methane yield, but not the non-conductive PET.

Metagenomic and metatranscriptomic analyses were performed to

further decipher the microbial interactions on the granular activated carbon (GAC) fluidizing media. Metabolic pathway reconstructions and metatranscriptomics mapping revealed that the syntrophic propionate oxidizing bacteria (SPOB) degraded propionate into acetate, which was further converted into methane and CO₂ by *M. concilii* via the acetoclastic methanogenesis pathway. Concurrently, *G. lovleyi* oxidized acetate into CO₂ and released electrons into the extracellular environment. By accepting these electrons through direct interspecies electron transfer (DIET), *M. concilii* was capable to perform CO₂ reduction for further methane formation. Most notably, our study has, for the first time, showed that an alternative RuBisCO-mediated CO₂ reduction (the reductive hexulose-phosphate (RHP) pathway) is transcriptionally-active in *M. concilii*. The RHP pathway enables *M. concilii* to gain dominance and energy. Moreover, the RHP pathway could constitute a third methanogenesis route in *M. concilii* via a methyl-H₄MPT intermediate. Further analysis verified that the acetoclastic methanogenesis, coupling of acetoclastic methanogenesis and CO₂ reduction pathways for methane formation are thermodynamically favorable even under very low substrate condition. Such tight interactions involving both mediated and direct interspecies electron transfer (MIET and DIET) promoted the overall efficiency of bioenergy processes.

Another anaerobic mix-culture bioprocess, carboxylate chain elongation process in which acetate is converted into valuable biochemicals,

caproate, with ethanol as an electron donor, was studied. The feasibility of upgrading lignocellulosic ethanol (LE) to produce value-added chemical, caproate, via the chain elongation process was examined. Also, the effects of yeast extract and cellulose containing in the LE were evaluated separately. Fermentation performance showed that using LE as feedstock greatly shortened the lag phase of caproate production (4 days), and the similar enhancement effects were observed in the experimental group with extra supplement of yeast extract (6 days), and cellulose (9 days) compared with the control group (17 days) without extra supplement. Depletion of ethanol limited further elongation into caproate, resulting in comparable caproate yields and carbon conversion ratios. Microbial community and microbial kinetics analysis revealed that yeast extract could be metabolized by protein-utilizing bacteria into short chain carboxylates (SCCs), which facilitated biological chain elongation. Meanwhile, yeast extract boosted microbial growth by serving as nitrogen and other nutrient sources. Furthermore, cellulose was utilized and further converted into SCCs, or even caproate, by cellulolytic bacteria. Together, caproate production was enhanced with high microbial activities and intermediates formation using LE.

Yeast extract was commonly added as a supplement in the CE process. In this study, the effects of casamino acids, the main composition in the yeast extract, and the conductive GAC particles on medium chain carboxylates (MCCs) production via CE process were evaluated, respectively. The results showed that the addition of casamino acids

greatly shortened the lag phase for caproate production. While the addition of GAC extended the lag phase for the butyrate production (the first step of chain elongation), presumably because microorganisms needed longer time to adapt and enrich on GAC particles than these without such interference. But once the community was well-enriched, the microorganisms cooperated and functioned efficiently and resulted in shorter lag phase of caproate production compared to the Control. Further microbial analysis indicated that the reactors Control and AA showed high similarity of community structure over time. Whereas the communities of the reactor GAC showed great variations, suggesting that the addition of GAC induced adaptation and reformation of microbial consortia. While after 51 days of fermentation, the communities of three reactors converged and became similar after cultivation and enrichment.

A sample was taken from the reactor AA (with casamino acids supplement) on Day 14 (significant caproate production) for further interspecies metabolic interactions exploration via metagenomics and transcriptomics analysis. The high-quality genome bins that phylogenetically identified to be closely related to the genomes of *Clostridium kluyveri*, *Proteiniphilum acetatigenes* and *Clostridium aminophilum* were recovered, which together represented the majority of the microbial community in the reactor AA. The complete ethanol-acetate fermentation pathway for caproate production via the reversed β -oxidation pathway was fully recovered in the genome bin closely

related to *C. kluyveri*. Also, metatranscriptomics analysis confirmed that the genes involved in this pathway were actively-transcribed and contributed to the caproate production in the CE process. Moreover, in the genome bin of *Proteiniphilum acetatigenes* and *Clostridium aminophilum*, the pathways of amino acids, such as serine and glycine to produce butyrate were reversed and found to be transcriptionally-active. It indicated that amino acids could not only support microbial growth, but also be directly involved in the CE metabolism and attributed to increased efficiency of the process.

PUBLICATIONS ARISING FROM THE THESIS

Journal Papers:

1. **Yang, P.**, Tan, G.-Y., Aslam, M., Kim, J. & Lee P.-H. (2019). Metatranscriptomic evidence for classical and RuBisCO-mediated CO₂ reduction to methane facilitated by direct interspecies electron transfer in a SAF-CMBR system. *Scientific Reports*, 9:4116.
2. **Yang, P.**, Leng, L., Tan, G.-Y., Dong, C., Leu, S.-Y., Chen, W.-H. & Lee P.-H. (2018). Upgrading Lignocellulosic Ethanol for Caproate Production via Chain Elongation Fermentation. *International Biodeterioration & Biodegradation*, 135, 103-109.
3. Leng, L [†], **Yang, P** [†], Singh, S., Zhuang, H., Xu L., Chen W.-H., Dolfing, J., Li, D., Zhang, Y., Zeng, H., Chu W., & Lee P.-H. (2017). A review on the bioenergetics of anaerobic microbial metabolism close to the thermodynamic limits and its implications for digestion applications. *Bioresource Technology*, 247, 1095-1106 (co-first author).
4. **Yang, P.**, Lee P.-H. (2019). Metagenomic insight into the microbial networks and metabolic mechanism in chain elongation for caproate production enhanced by casamino acids. (under submission).
5. Leng, L., **Yang, P.**, Mao, Y., Wu, Z., Zhang, T., & Lee P.-H. (2017). Thermodynamic and physiological study of caproate and 1,3-propanediol co-production through glycerol fermentation and fatty acids chain elongation. *Water Research*, 114, 200-209.
6. Aslam, M., **Yang, P.**, Lee P.-H., KIM, J. (2018). Novel staged anaerobic fluidized bed ceramic membrane bioreactor: Energy

reduction, fouling control and microbial characterization. *Journal of Membrane Science*, 553, 200-208.

7. Leng, L., Nobu, M. K., Narihiro, T., **Yang, P.**, Amy Tan, G.-Y., & Lee, P.-H. (2019). Shaping microbial consortia in coupling glycerol fermentation and carboxylate chain elongation for Co-production of 1,3-propanediol and caproate: Pathways and mechanisms. *Water Research*, 148, 281-291.
8. Leng, L., Wang, Y., **Yang, P.**, Narihiro, T., Nobu, M. K., Narihiro, Amy Tan, G.-Y., Lee, P.-H. (2019). Unraveling a microbial synergy to boost caproate production via carboxylates chain elongation with ethanol. *HKIE Transactions* (THIE-2018-0041.R2) (accepted).
9. Aslam, M., **Yang, P.**, Lee P.-H., Kim, J. (2018). The effects of different biofilm carriers on organic removal, microbial distribution and biofilm development in staged anaerobic fluidized bed ceramic membrane bioreactor treating low-strength wastewater treatment (In preparation).

Conference Presentation:

1. **Yang, P.**, (presenter), Lee P.-H., Microbial Communities & Kinetics Associated with Caproate Production in the Chain Elongation Systems, The 5th GIGCAS-HKPOLYU-SYSU Joint Workshop on Environmental Science and Engineering, Zhuhai, Jun 2017.
2. G.-Y.A. Tan, **Yang, P.**, C. Shin, A. Muhammad, J. Kim, J. Bae, P.-H. Lee (2018). The Selective Enrichment of Syntrophs, Methanogens and Exoelectrogens on Granular Activated Carbon in Stage Anaerobic Fluidized Bed Membrane Bioreactors (SAF-MBRs). *10th Asian*

Symposium on Microbial Ecology (ASME 2018), 11-13 Jul, Okinawa,
Japan.

ACKNOWLEDGEMENTS

Foremost, I would like to express my sincere gratitude to my supervisor, Dr. Po-Heng Lee, for his consistent guidance, support and encourage during my Ph.D. study and research. His critical instruction and suggestion inspired me a lot during my Ph.D. study. His invaluable guidance and encourage motivated me to overcome the obstacles I encountered in the research. His character and morals are the most valuable things I have learned and appreciated. Also, I would like to express my thanks to the technicians in the Water and Wastewater Laboratory, especially Mr. Lam Wai-Shung for his technical supports and patient assistance during the past four years.

My sincere thanks also goes to my optimistic and passionate colleagues, Mr. Leng Ling, Dr. Giin-Yu Amy Tan, Mr. Zhuang Huichuan, Ms. Xu Linji, Mr. Zheng zhen, Mr. Ji Xiaoming, Dr. Wu Zhuoying, Dr. Huang Xiaowu, Mr. Dong Chengyu and Dr. Wang Ying. I sincerely thank them for their advices, help, and encouragement throughout this difficult but precious time.

Moreover, I genuinely appreciate the Research Grants Council (RGC) of the Hong Kong Special Administrative Region, China for financial support of my higher degree under the Hong Kong Ph.D. Fellowship Scheme (PF13-12713).

Last but foremost, I would like to express my sincere gratitude to my beloved parents who support and trust me all the time. They are always my strongest backing, bringing me happiness and spiritual strength to my life.

TABLE OF CONTENTS

ABSTRACT	I
PUBLICATIONS ARISING FROM THE THESIS	VI
ACKNOWLEDGEMENTS	IX
TABLE OF CONTENTS	XI
LIST OF FIGURES	XV
LIST OF TABLES	XX
LIST OF ABBREVIATIONS	XXII
1. Chapter 1. Introduction	1
1.1 Background	1
1.2 Objectives	3
1.3 Thesis Organization	4
2. Chapter 2. Literature review	7
2.1 Conversion of wastes to energy and bioproducts	7
2.1.1 Environmental issues, energy crisis, sustainable approaches. 7	
2.1.2 Sustainable bioenergy processes	8
2.2 Methanogenic anaerobic digestion system	10
2.2.1 Anaerobic syntrophy	11
2.2.2 Interspecies electron transfer/flow in anaerobic digestion ...	27
2.2.3 The RHP pathway	32
2.3 Carboxylates chain elongation for caproate production	33
2.3.1 Applications and manufacture of caproate	33
2.3.2 Ethanol-acetate fermentation for caproate production	35
2.3.3 Caproate formation microbiomes and biological pathways .	39
2.3.4 Challenges and opportunities	45

3. Chapter 3. Materials and Methodology	46
3.1 Inoculum and medium for CE fermentation.....	46
3.2 CE fermentation experiment in batch	48
3.3 CE fermentation in semi-continuous reactor	49
3.4 Analytical procedures.....	50
3.5 DNA extraction and high-throughput sequencing.....	52
3.5.1 SAF-CMBR systems	52
3.5.2 CE batch fermentation	54
3.5.3 CE fermentation reactors	54
3.6 Genomic analysis.....	55
3.6.1 16S rDNA gene-based analysis	56
3.6.2 Metagenomic analysis	57
3.6.3 Metatranscriptomic analysis.....	60
3.7 Microbial kinetics calculation.....	61
3.8 Thermodynamics calculation of biochemical reactions	68
3.8.1 MATLAB programs for thermodynamics calculation	70
4. Chapter 4 Microbial communities of two methanogenic SAF-CMBR system using conductive GAC and non-conductive PET beads as biofilm carriers.....	73
4.1 Overview	73
4.2 Results and discussion	77
4.2.1 Microbial community of the SAF-CMBR with GAC as carrier	77
4.2.2 Microbial community of the SAF-CMBR with different biofilm carriers: PET beads and GAC	81

4.3 Chapter summary	86
5. Chapter 5 Metatranscriptomic evidence for classical and RuBisCO-mediated CO₂ reduction to methane facilitated by direct interspecies electron transfer in a methanogenic system	87
5.1 Overview	87
5.2 Results and discussion	90
5.2.1 Overview of the metagenome bin and metatranscriptomes .	90
5.2.2 Propionate oxidation and acetoclastic methanogenesis.....	99
5.2.3 Acetate oxidation and DIET-dependent CO ₂ reduction	101
5.2.4 CO ₂ reduction via the RHP pathway	104
5.2.5 Thermodynamics estimation of the CO ₂ reduction pathways	106
5.3 Chapter summary	112
6. Chapter 6 Upgrading lignocellulosic ethanol for caproate production via chain elongation fermentation	114
6.1 Overview	114
6.2 Results and discussion	116
6.2.1 Caproate yield and lag phase	116
6.2.2 Bacterial community characterization.....	120
6.2.3 Microbial kinetics characterization	129
6.3 Chapter summary	133
7. Chapter 7 Metagenomic insight into the microbial networks and metabolic mechanism in chain elongation for caproate production enhanced by casamino acids	134
7.1 Overview	134

7.2 Results and discussion	137
7.2.1 Shortening the lag phase of caproate production	137
7.2.2 Microbial community and community composition convergence in chain elongation	140
7.2.3 Reconstruction of highly active pathways in the reactor AA 147	
7.3 Chapter summary	151
8. Chapter 8 Conclusions and Recommendations	153
8.1 Conclusions	153
8.2 Recommendations for Future Work	157
Appendix I Coding DNA sequences (CDS) predicted to be involved in the metabolism of main pathways.	158
Appendix II Genes expression of the of main pathways (propionate degradation, methane generation) in <i>S. fumaroxidans</i> , <i>M. concilii</i> and <i>G.</i> <i>lovleyi</i>	179
Appendix III Coding DNA sequences (CDS) predicted to be involved in the metabolism of main pathways associated with caproate production..	190
Appendix IV Genes expression of the of main pathways associated with caproate production.	199
References	204

LIST OF FIGURES

Figure 2-1. Intricate food web of methanogenic anaerobic digestion. Several trophic groups of microorganisms work together to convert complex organic material into methane and carbon dioxide (Adopted from (Angenent et al., 2004)).....	12
Figure 2-2. Proposed methylmalonyl-CoA pathway.....	16
Figure 2-3. Proposed pathway for propionate conversion by <i>Smithella propionica</i> (adopted from (Frank AM de Bok, Alfons JM Stams, Cor Dijkema, & David R Boone, 2001)).....	17
Figure 2-4. The window of opportunity for propionate degradation in methanogenic bioreactors at 25 °C.....	23
Figure 2-5. The proposed pathways for acetoclastic methanogenesis in <i>Methanosarcina mazei</i> (adopted from (K. S. Smith & Ingram-Smith, 2007)).	25
Figure 2-6. DIET-based metabolism in digester samples and defined co-cultures of <i>Geobacter metallireducens</i> and <i>Methanothrix harundinacea</i> as revealed by metatranscriptomics (adopted from (A. E. Rotaru et al., 2014)).	31
Figure 2-7. Proposed RHP pathway and related metabolic processes in archaea (adopted from (Kono et al., 2017)).	33
Figure 2-8. Examples of commercial applications of caproate.	35
Figure 2-9. Chain elongation of acetate with ethanol as electron donor in <i>Clostridium kluyveri</i> (adopted from (Seedorf, Fricke, Veith, Bruggemann, Liesegang, Strittmatter, et al., 2008)).	41

Figure 3-1. Source of the inoculum sludge used in our study (Drainage Services Department, Hong Kong).....	46
Figure 3-2. Schematic diagram of the semi-continuous fermentation system.....	50
Figure 3-3. The HPLC system (SHIMADZU) used for quantification of the target compounds and GC system (Agilent) used for quantification of the target gases.	52
Figure 3-4. Illustration of samples collection.....	54
Figure 3-5. Flowchart of 16S rRNA gene-based amplicon sequencing for microbial analysis.....	57
Figure 3-6. Flowchart of (a) metagenomics analysis pipeline and (b) software used in the analysis.	59
Figure 3-7. Illustration of metagenomics analysis pipeline via hybrid <i>de novo</i> assembly.	60
Figure 4-1. Schematic diagram of the staged anaerobic fluidized bed ceramic membrane bioreactor (SAF-CMBR) system (adopted from (Aslam et al., 2018)).....	75
Figure 4-2. Schematic diagram of the staged anaerobic fluidized bed ceramic membrane bioreactor (SAF-CMBR) system with different biofilm carriers (GAC and PET beads) (adopted from an unpublished work (Aslam et al., 2018)).....	76
Figure 4-3. Beta diversity analysis (a) Dendrograms describing the similarity of the microbial communities of the samples to each other; (b) Braycurtis heat map at distance 0.03.....	78

Figure 4-4. Taxonomic classification of the communities displaying both bacteria and archaea developed on fluidized GAC and bulk suspension (collected on day 162); (a) at phylum level; (b) at genus level.	80
Figure 4-5. Beta diversity analysis (a) Dendrograms describing the similarity of the microbial communities of the samples to each other; (b) Thetayc heat map at distance 0.16.....	84
Figure 4-6. Taxonomic classification of the microbial communities displaying both bacteria and archaea developed on the biomass carriers and bulk (collected on day 135): (a) at phylum level; (b) at genus level. Phylum or genus occurred at abundance more than 1 % in at least one sample was annotated whereas the rest were grouped as “others”.	85
Figure 5-1. Metabolic interactions between <i>Methanotherix concilii</i> and <i>Geobacter lovleyi</i> in the SAF-CMBR system.	90
Figure 5-3. Phylogenetic tree of genome bins closely related to (a). <i>Syntrophobacter fumaroxidans</i> , (b). <i>Geobacter lovleyi</i> and (c). <i>Methanotherix concilii</i> using PhyloPhlAn.	94
Figure 5-2. CheckM plot for the quality assessment of the genomes bins for further annotation and analysis.	95
Figure 5-4. Annotated pathways of acetate oxidation, acetocalstic methanogenesis, classical CO ₂ reduction and CO ₂ reduction via RHP for methane production.	103
Figure 5-5. Transformed Gibbs free energy values ($\Delta G'_{298K}$) in KJ/mol at pH of 7 and pressure of 1 atm as a function of acetate concentration and partial pressure ratio of CH ₄ /CO ₂ for (a) Eq. 1: acetoclastic methanogenesis (b) Eq. 4 (complete acetate reduction via classical CO ₂ reduction) and Eq. 5	

(complete acetate reduction via RHP pathway). The red curve represents Eq. 4, and the red orange one represents Eq. 5. 111

Figure 6-1. Illustration of the batch experiment and improvement of fermentation performance. 116

Figure 6-2. Profile of concentrations of substrates and products during the fermentation cycle in group (a) EtOH; (b) CL; (c) LE; (d) YE..... 117

Figure 6-3. Beta-diversity analysis among groups with (a) UNIFRAC tree; (b) braycurtis heatmap..... 123

Figure 6-4. Taxonomic classification of bacterial communities of the four groups at (a) phylum and (b) genus levels. Relative abundance is defined as the number of reads affiliated with any given taxon divided by the total number of reads per sample. Phylogenetic groups with a relative abundance lower than 1% were classified as “others”. 126

Figure 6-5. Canonical Correspondence Analysis (CCA) of microbial community patterns. The experimental variables (EVs), lignocellulosic ethanol, yeast extract and cellulose, are represented as arrows, whose direction explains most of the bacterial patterns and length indicates the magnitude of contribution of that EV in explaining variation in bacterial profiles. Dots represent the four experimental groups. 129

Figure 7-1. Experimental groups to enhance caproate production via chain elongation process, and the essential substrates flow in the experiment with extra supplement of casanimonic acids. 136

Figure 7-2. The concentration of substrates and products in the three CE reactors: (a) Control; (b) AA and (c) GAC. 139

Figure 7-3. The concentration of electrons based on e- equivalent in the formed products across the whole fermentation.....	140
Figure 7-4. Beta-diversity analysis among groups with UNIFRAC dendrogram tree;.....	143
Figure 7-5. Principal coordinate analysis (PCoA) of community similarity comparing the 19 samples. Principal coordinate 1 (axis 1) vs. Principal coordinate 2 (axis 2) are represented. axes 1 and 2: 63.94 %. Each dot was named after the form of “sampling day_the reactor”.	144
Figure 7-6. Taxonomic classification of the bacterial communities of the raw sludge and the three reactors (Control, GAC and AA) on different days (a) at phylum level; (b) at genus level. Phylum or genus occurred at abundance more than 1 % in at least one sample was annotated whereas rests were grouped as “others”.	147
Figure 7-7. Annotated metabolic pathways of ethanol-acetate fermentation for butyrate and caproate production (in blue) and degradation of glycine and serine for butyrate production (in yellow) in the reactor AA on Day 14.	151

LIST OF TABLES

Table 2-1. Summary of the bioprocessing strategies for energy and value-added chemicals from waste(waters).....	9
Table 2-2. The window of opportunity corresponding to estimated range of H ₂ concentration comparing the Smithella pathway and the methylmalonyl CoA (MMC) pathway coupled to hydrogenotrophic methanogenesis.....	20
Table 2-3. Reactions involved in propionate oxidation and responsible microbes along with standard Gibbs free energy.	21
Table 2-4. Comparison of syntrophic propionate degradation using smithilla pathway and methylmalonyl CoA pathway.	22
Table 2-5. Reactions involved in propionate conversion to methane and responsible microbes along with standard Gibbs free energy.	26
Table 2-6. Physical Properties and price comparison of different bio-products.	34
Table 2-7. Metabolic stoichiometry in butyrate and caproate formation by <i>Clostridium kluyveri</i> (adopted from (Ding et al. 2010)).	42
Table 2-8. Possible reactions for butyrate and caproate formation (revised from (Ding, Tan, & Wang, 2010)).	44
Table 3-1. Composition of synthetic medium for fermentation.	47
Table 3-2. The step reactions involved in classical CO ₂ reduction, half reactions of electron carriers and their standard Gibbs free energy changes (ΔG^0) at 298 K, pH 7.0 and all compounds at 1 molar activity.	69
Table 5-1. Summary of the 4 metagenomes.	96
Table 5-2. High-quality recovered genome bins that are closely related to methanogens, syntrophs and <i>Geobacter</i>	97

Table 5-3. The step reactions involved in classical CO ₂ reduction, half reactions of electron carriers and their standard Gibbs free energy changes (ΔG^0).	108
Table 5-4. Reactions of methane production in the system and the corresponded standard Gibbs free energy.	109
Table 6-1. Summary of concentrations of products, carbon conversion percentages and lag phase of caproate production in the four experimental groups.	119
Table 6-2. The reads and coverage obtained for bacteria communities. .	121
Table 6-3. Alpha-diversity indices of the four microbial communities at 3% cutoff.....	122
Table 6-4. Values of half-maximum rate concentration K and growth rate μ in the initial stage of fermentation ($t < 10$ days).	132
Table 7-1. The coverage and alpha-diversity indices of the 19 microbial communities at 3% cutoff.....	141
Table 7-2. High-quality genome bins recovered from sample in reactor AA on Day 14.	148

LIST OF ABBREVIATIONS

MIET	mediated interspecies electron transfer
DIET	Direct interspecies electron transfer
GAC	Granular activated carbon
AFBR	Anaerobic fluidized bed bioreactor
AFCMBR	Anaerobic aerobic fluidized bed ceramic membrane bioreactor
SAF-CMBR	Staged anaerobic fluidized bed ceramic membrane bioreactor
RHP	Reductive hexulose-phosphate
RuBisCO	Ribulose-1,5-bisphosphate carboxylase/oxygenase
TCA	Tricarboxylic acid
SPOB	Syntrophic propionate oxidizing bacteria
MMC	Methylmalonyl-CoA
SCC	Short chain carboxylate
SCFA	Short chain fatty acid
MCC	Medium chain carboxylate
SSF	Simultaneous saccharification and fermentation
LE	Lignocellulosic ethanol
CE	Chain elongation
MS	Municipal wastes
MSW	Municipal solid waste
T	Temperature
I	Ionic strength
AD	Anaerobic digestion

SWH	Shek Wu Hui
BESA	2-Bromoethanosulfonic acid
PBS	Phosphate Buffer Saline
SLP	Substrate-level phosphorylation
ETP	Electron transport phosphorylation
HRT	Hydraulic retention time
HPLC	High-performance liquid chromatography
RID	Refractive index detector
GC	Gas chromatography
TCD	Thermal conductivity detector
PE	Paired-end
SE	Single-end
RPKM	Reads Per Kilobase Million
bp	Base pairs
OTU	Operational taxonomic unit
CE	Chain elongation
PCoA	Principal coordinate analysis
SRB	Sulfate-reducing bacteria
G+C	Content Guanine-cytosine content
CDS	Coding DNA sequences
CCA	Canonical correspondence analysis
EV	Environmental variables
NCBI	National Center for Biotechnology Information
BLAST	Basic Local Alignment Search Tool

1. Chapter 1 Introduction

1.1 Background

Methanogenesis is a key process in anaerobic digestion, responsible for the generation of renewable energy, presenting an attractive technology for municipal and industrial wastes treatment. The well-formed and stable microbial syntrophic interactions are essential for achieving methanogenesis. Recent innovative bioprocess designs, such as anaerobic fluidized-bed membrane bioreactor (AFMBR), improves the bioenergy processes and enhances energy efficiency. Specifically, the supplementation of fluidizing medium granular activated carbon (GAC) particles, as an electrically-conductive biocarrier, promoted the enrichment of syntrophs, exoelectrogen *Geobacter* and methanogen *Methanotrix*, establishing both syntrophic and electric syntrophic methanogenesis. Crucially, direct interspecies electron transfer (DIET) is suspected to stimulate metabolism. From methanogen's perspective, inorganic carbon fixation using extracellular electrons would supply additional carbon to other important anabolic and energy-producing pathways. The recently-discovered reductive hexulose-phosphate (RHP) pathway, analogous to the Calvin-Benson cycle in plant photosynthesis, was speculated to the most ancient and widely distributed CO₂ fixation pathway in archaea. By assimilating CO₂ into cells and methane, the slow-growing *Methanotrix* may easily establish its dominance in the microbial community therefore contributed to the overall energy recovery. This manuscript studies the tight microbial interactions, particularly involving DIET, to elucidate microbial

behavior and provide strategies for the further improvement of bioenergy processes.

An alternative anaerobic bioprocess for wastes treatment and products recovery is chain elongation, in which short chain carboxylates (SCCs) are elongated to medium chain carboxylates (MCFAs), e.g. caproate, with alcohols as electron donors (Matthew T. Agler, Spirito, Usack, Werner, & Angenent, 2012; T. I. Grootsholten, K. J. Steinbusch, H. V. Hamelers, & C. J. Buisman, 2013; Grootsholten, Steinbusch, Hamelers, & Buisman, 2012; Steinbusch, Hamelers, Plugge, & Buisman, 2011). The properties of low solubility and high energy density make MCCs superior bio-products to SCCs (Steinbusch et al., 2011). There has been several studies accomplishing caproate production from miscellaneous low-grade organic wastes in both lab- (Matthew T. Agler et al., 2012; Ge, Usack, Spirito, & Angenent, 2015; T. I. M. Grootsholten, K. J. J. Steinbusch, H. V. M. Hamelers, & C. J. N. Buisman, 2013a; Grootsholten, Strik, Steinbusch, Buisman, & Hamelers, 2014) and pilot-scale (Angenent et al., 2016) systems at high rates and specificities. Approaches like a new reactor system, upflow anaerobic filter, and reducing the hydraulic retention time were successfully applied to improve the productivity of MCCs (T. I. Grootsholten et al., 2013; T. I. M. Grootsholten, K. J. J. Steinbusch, H. V. M. Hamelers, & C. J. N. Buisman, 2013b), suggesting the great application potential of chain elongation bioprocess. However, there is a limited understanding of the microbial interactions, metabolic potential of mixed populations. Other than the well-known and predominated chain elongating

bacteria, *Clostridium kluyveri*, the roles and metabolism of other dominated bacterial groups are also crucial to operate an efficient and stable CE process. Therefore, the potential approaches for enhancement of fermentation performance and their underlying mechanism in CE process still requires for further exploration. A deeper mechanistic understanding of the CE process with complex reactor microbiomes would benefit for shaping stable and functional community structures, therefore provides clues for the design and operation of an efficient and predictable engineered system.

1.2 Objectives

The broad aim of this study is to better understand the interspecies interactions and metabolic pathways involving interspecies electron transfer (IET) in methanogenic systems. In addition, the study was motivated to evaluate the upgrading of diluted wastes into value-added chemical, caproate, and to reveal the microbial networks and interactions facilitating the chain elongation process. The specific objectives of this study are shown as follows:

- (1) To examine the effects of electronic conductive and non-conductive fluidizing medium on the microbial community structures and dominance of microbial groups in methanogenic staged anaerobic fluidized bed ceramic membrane bioreactor (SAF-CMBR) systems.

- (2) To investigate the microbial interactions and the main metabolic pathways facilitated by direct interspecies electron transfer (DIET) for promoting the overall efficiency of a SAF-CMBR system.
- (3) To evaluate the feasibility of upgrading lignocellulosic ethanol (LE) for caproate production via chain elongation in a mix-culture fermentation, and to assess the effects of yeast extract and cellulose containing in LE on the chain elongation process.
- (4) To assess the physiological performance of ethanol-acetate fermentation for caproate production with extra addition of casamino acids and GAC, respectively. in a semi-continuous fermentation.
- (5) To inspect the microbial community associated with chain elongation and its response to the addition of casamino acids and GAC, and to reconstruct the main metabolically active pathways associated with caproate production.

1.3 Thesis Organization

This thesis is composed of eight chapters. The present chapter includes the background information, motivation, objectives and the structure of this thesis.

Chapter Two provides a comprehensive literature review of related study. Particularly, interspecies interactions in methanogenic system, including syntrophic relationship, MIET and DIET are introduced in detail. In addition, carboxylates chain elongation (CE) for caproate production via the ethanol-acetate fermentation are summarized and discussed in depth.

In Chapter Three, the specific descriptions of the experimental materials, experimental design and methodologies are provided.

Chapter Four reports a comparative study of the microbial communities in two methanogenic system using different biomass carriers. Specifically, one of them is SAF-CMBR system using the conductive GAC as the carriers, and the other is a SAF-CMBR but using GAC and PET, separately, as carriers.

In Chapter Five, the interspecies interactions in the SAF-CMBR system are revealed by reconstruction of the main metabolic pathways and identification of their activities through the metagenomics and meta-transcriptomics sequencing and analysis. In particular, the active DIET-facilitated CO₂-utilization pathways in the acetoclastic methanogen, *Methanotherix*, are discussed.

Chapter Six discusses the physiological performance of upgrading of lignocellulosic ethanol (LE) for caproate production via chain elongation fermentation, and the effects of yeast extract and cellulose containing in the LE on the fermentation performance. The microbial communities associated with the CE processes are examined, and microbial kinetics of the caproate-producing microbial group is evaluated theoretically.

Chapter Seven evaluates the performance of ethanol-acetate fermentation for caproate production with extra addition of casamino acids and GAC, respectively, to facilitate the CE process in semi-continuous fermentation. The responses of microbial communities, and their changes over time are described. In addition, the microbial interactions and the main metabolically active pathways associated with caproate production are investigated.

In the last chapter, conclusions of the whole work present in this thesis are summarized. Moreover, the limitations of the present study and recommendations for the future work are also proposed.

2. Chapter 2 Literature review

2.1 Conversion of wastes to energy and bioproducts

2.1.1 Environmental issues, energy crisis, sustainable approaches

The rapid growth of global population and accelerated urbanization and industrialization cause the production of huge amount of municipal wastes (MS), bringing tremendous pressure on the existing wastes treatment facilities and systems (P. Chen et al., 2016). Other than expansion of treatment and disposal capacity, implementation of sustainable strategies and technologies are necessary to recover and reuse the great proportion of nonrecyclable matters contained in the MW. These organic waste materials can be converted into energy in the forms of heat, electricity, or fuels and chemicals through a variety of processes, such as gasification, pyrolysis, anaerobic digestion and other biological platforms (Angenent, Karim, Al-Dahhan, & Domiguez-Espinosa, 2004; P. Chen et al., 2016; Marshall, LaBelle, & May, 2013).

On the other hand, the tremendous pressure on global demand for chemicals and fuels will continue to grow, simultaneously with environmental pollution, costly requirement to treat wastes and climate change from its usage. There is a clear need for reduction of dependency on fossil fuels. To mitigate this issue, one of the current practices is producing sustainable bioenergy as an alternative. Conversion of wastes to valuable chemicals would achieve a dual benefit, turn the challenge into an opportunity (Marshall et al., 2013). Consequently, the pressure of building a sustainable society shifts the focus on wastes from disposal to resource

exploitation. Many bioprocesses can provide bioenergy or valuable biochemicals while simultaneously achieving the objective of pollution control, including methanogenic anaerobic digestion, biological hydrogen production, microbial fuel cells and fermentation for production of valuable products, such as the carboxylate platform, microbial electrosynthesis and bioplastic production (Angenent et al., 2004; Marshall et al., 2013).

2.1.2 Sustainable bioenergy processes

Bioprocessing has long been considered one of the best strategies for resource mining from waste(waters), because it is suitable to generate bioenergy or valuable chemicals, while simultaneously achieving the objective of waste treatment by microbiome. It consists of a mixed microbial community adapted to an environmental niche to synthesize valuable products from waste materials and is considered as attractive and environmental-friendly hosts (Marshall et al., 2013). Specifically, energy, such as methane (CH₄), hydrogen (H₂) and electricity, and value-added chemicals are two common targeting products obtained from bioprocessing. Comparatively, gases and electricity produced from these bioprocesses are easily separated as summarized in Table 2-1. These processes mostly utilize selection and adaptation of mixed microbial community according to their specific functions, thereby leading to efficient metabolic interactions among microbes to achieve energy and chemical formation (Angenent et al., 2004). Although pure-culture or co-culture has higher specificity of products in some cases, mix-culture fermentation is still an attractive approach due to its potential benefits. The non-sterilization of waste

streams before bioprocesses is well suited to waste streams of complex compositions and microbial environment. In addition, the properties of different waste streams will naturally select for the specific microbiome that consists of the most efficient and effective microbial catalysts. Importantly, the well-formed microbial community is robust and resilient to adverse disturbance, therefore it can be recovered rapidly when encounters abrupt environmental upset (Marshall et al., 2013). Although bioprocesses cannot fully satisfy the demand for energy needs, bioenergy still reduces the burden of infinite requirement for fuels to some extent and handles the issue of wastes treatment at the same time. The continuous development and exploration of bioprocesses will lead to more large-scale implementations of economically feasible platforms for conversion and recovery of valuable products.

Table 2-1. Summary of the bioprocessing strategies for energy and value-added chemicals from waste(waters).

Bioprocess strategy	Level of maturity	Separation of products	Culture	Value added
Anaerobic digestion	Mature, operational	Easy, gas	Mixed	Low
Hydrogen fermentation	Laboratory phase	Easy, gas	Mixed	Low to medium
Microbial fuel cell	Laboratory phase	Easy, electricity	Mixed	Low

Biochemical production	Scale-up phase	Hard, soluble	Pure, co or mixed	Medium to high
---------------------------	-------------------	------------------	----------------------	-------------------

* Revised from (Angenent et al., 2004).

2.2 Methanogenic anaerobic digestion system

Methanogenic anaerobic digestion (AD) is a representative example of conversion waste streams to an attractive fuel by degrading organic matters into methane in wastewater. AD is a mature and robust process and is widely applied worldwide even in full-scale installations. Its early applications for the treatment of organic waste can be traced back to decades ago, and the amount of digester has emerged notably in recent years attributed to its merits. The mix-culture AD process not only avoid sterilization, but also circumvents pre-treatments, such as pre-drying step, since it can treat waste streams or biomass with high water content (Appels et al., 2011). Additionally, low emission of hazardous pollutants from the process makes it environmentally friendly (Appels et al., 2011). Although methane is a relatively low-value product, AD still represent the most economically feasible bioprocess, because produced gases can be upgraded to natural gas purity or to catalytic conversion to syngas, which can be used to produce liquid fuel and high-value products through conventional chemical manufacturing processes (Latif, Zeidan, Nielsen, & Zengler, 2014). Nowadays, the challenges in energy and environment necessitate the constant upgrade of AD systems aiming to improve treatment efficiency and energy harvest. The efficient microbial cooperation is crucial for biomass growth and methane production, even under low-substrate

conditions in AD systems. A close insight into the microbial interactions and their metabolic behaviour is essential to unveil this complex system and upgrade this process to a new renaissance (Leng et al., 2018).

2.2.1 Anaerobic syntrophy

Anaerobic digestion mineralizes complex organic materials to methane via a series of correlated steps and interactions among metabolically distinct groups of microorganisms. As indicated in Fig. 2-1, polymeric substrates, such as proteins, lipids and polysaccharides, are first hydrolyzed to monomers, which are further oxidized to acetate and H₂ through the acetogenesis process. Acetate is oxidized to methane and carbon dioxide by acetoclastic methanogens. Meanwhile, the hydrogen-producing acetogenic bacteria are obligated to form a syntrophic association with hydrogenotrophic methanogens, who produce methane from H₂ (and CO₂) and maintain a low partial pressure of H₂ to ensure the acetogenesis step is thermodynamically favorable (referred as interspecies hydrogen transfer) (Angenent et al., 2004; Thauer, Jungermann, & Decker, 1977). Methane production is achieved by a cooperation that is not only a simple dependency on the food chain, but also has a thermodynamic rationale. The oxidation of short chain fatty acids (SCFAs) is thermodynamically unfavorable under standard conditions (298K, pH 7, and 1 atm) without inorganic electron acceptors, unless methanogens metabolize their products make the reactions spontaneous. Consequently, the products from SCFAs oxidation promoted methane production. The establishment of anaerobic syntrophy allows unfavorable reactions to proceed. Specifically,

interspecies electron transfer, the concentrations of electron carriers, metabolic synchronization of the syntrophic partners, or even close physical contact are essential for maintaining such syntrophic metabolism (Leng et al., 2018; McInerney, Sieber, & Gunsalus, 2009).

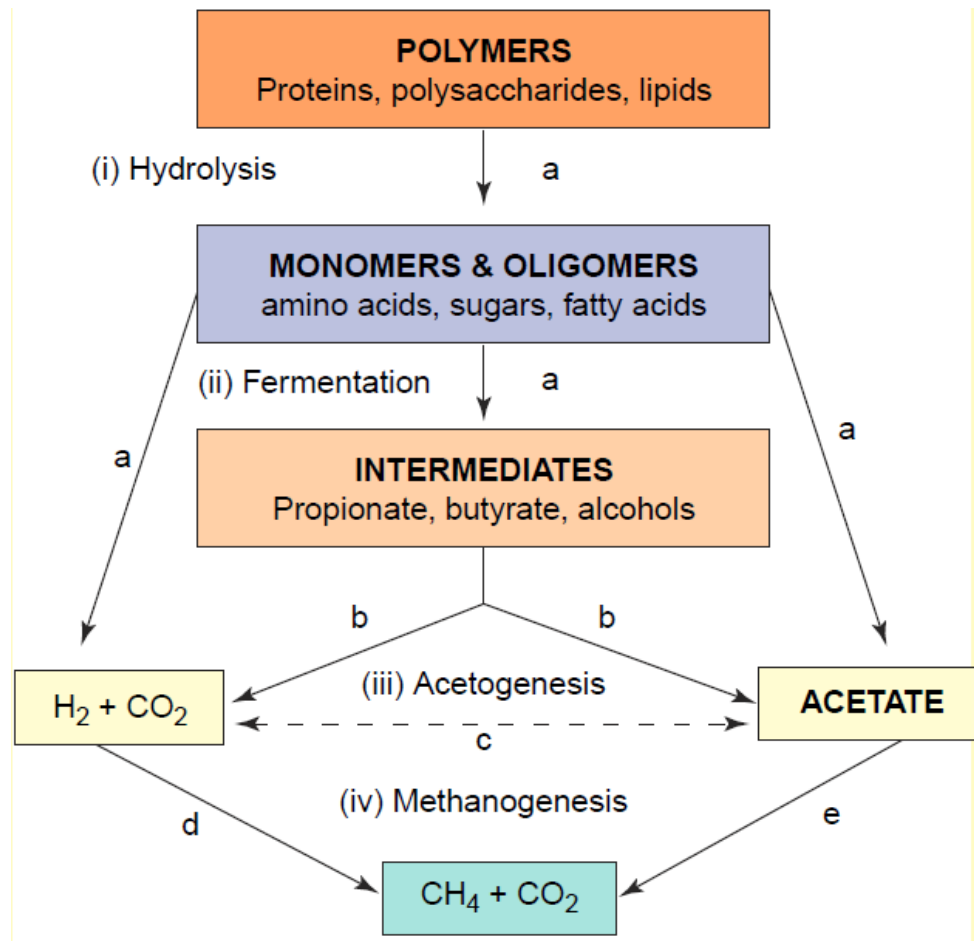


Figure 2-1. Intricate food web of methanogenic anaerobic digestion. Several trophic groups of microorganisms work together to convert complex organic material into methane and carbon dioxide (Adopted from (Angenent et al., 2004)).

AD for methane production is less exergonic than aerobic degradation or alternative forms of anaerobic respiration (Leng et al., 2018). For instance,

the energy generated from degradation of hexose to methane and carbon dioxide only account for 15% of that released from aerobic degradation (Schink, 1997). Owing to such limited energy production in AD, the microorganisms are obligated to form a tight and efficient cooperation. Particularly, anaerobic syntrophy is regarded as a thermodynamically interdependent partnership in which typically occurs between a compounds degrader, usually acetogens, with a second microorganism, usually a methanogen. Especially, within such obligately mutualistic metabolism, neither partner can operate without the other. The end products of compounds degradation, usually H_2 , formate, and acetate, are consumed by methanogens and maintained at very low concentrations (McInerney et al., 2009; Morris, Henneberger, Huber, & Moissl-Eichinger, 2013).

2.2.1.1 Propionate oxidation

The intermediates formed in the acidogenesis step, such as butyrate, propionate and ethanol, are further degraded by a group of syntrophic acetogens into acetate, formate, and H_2/CO_2 , which are directly uptaken by methanogens to produce methane. The degradation of propionate to acetate and H_2/CO_2 (and then to CH_4) accounts for approximately 6–35% of the total methanogenesis, and its accumulation causes acidification of anaerobic digestion systems and deterioration of digestion performance (D. P. Smith & Mccarty, 1989). Propionate degradation is generally regarded as a bottleneck in methanogenic bioreactors (Gallert & Winter, 2008), and various thermodynamics calculations have been performed to elucidate the thermodynamics of propionate degradation (P. L. McCarty & Bae, 2011; D.

P. Smith & Mccarty, 1989). Accordingly, the syntrophic propionate-oxidizing bacteria (SPOB) plays an essential role in the well-functioned AD systems. Generally, syntrophic acetogens include *Syntrophobacter*, *Pelotomaculum*, *Smithella*, *Syntrophus*, *Syntrophomonas*, and *Syntrophothermus* (Leng et al., 2018). The first three genera are usually associated with the oxidation of propionate, and the others are commonly involved in the degradation of butyrate and other fatty acids (Cai et al., 2016; Venkiteshwaran, Bocher, Maki, & Zitomer, 2015).

Normally, the acetogenesis step is hindered since the reaction is thermodynamically unfavorable under standard conditions. However, with the syntrophic partnership, methanogens consume the end products of acetogens, H₂, formate and acetate, maintaining their concentration/partial pressure at a low level to turn the reactions thermodynamically unfavorable to proceed (Stams & Plugge, 2009). For the propionate oxidizing bacteria, it is feasible to oxidize propionate facilitated by syntrophic association between the hydrogenotrophic methanogens (McInerney et al., 2009). The syntrophic propionate metabolism should have a free energy change of about -20 kJ mol^{-1} to allow the net synthesis of one third of an ATP molecule (Scholten & Conrad, 2000), while the measured values across propionate metabolism ranges from -30 kJ mol^{-1} to lower than -10 kJ mol^{-1} depending on the growth conditions (Scholten & Conrad, 2000).

Generally, there are two known pathways that are responsible for propionate metabolism. Most of the syntrophic propionate oxidation is

accomplished via the randomizing methylmalonyl-CoA (MMC) pathway, also referred to as the classical pathway (Kosaka et al., 2006a) as shown in Fig. 2-2. So far, at least ten species have been identified as SPOB, belonging to the genera *Syntrophobacter*, *Smithella*, *Pelotomaculum* and *Desulfotomaculum*. The MMC pathway is more common and can be found in many propionate oxidizers such as *Syntrophobacter* (S. Chen, Liu, & Dong, 2005), *Desulfotomaculum thermobenzoicum* subsp. *thermosyntrophicum* (Plugge, Balk, & Stams, 2002), *Pelotomaculum thermopropionicum* (Hiroyuki Imachi et al., 2002), and *Pelotomaculum schinkii* (F. A. de Bok et al., 2005).

As shown in Fig. 2-3, Liu et al. (1999) identified a propionate-degrading syntroph of the genus *Smithella*, which produces less methane and more acetate than the previously identified syntrophic propionate degraders such as *Syntrophobacter* (Y. Liu et al., 1999). It differed greatly in the substrate range and catabolic products, forming small amounts of butyrate during propionate degradation. *Smithella* spp. utilize propionate in a non-randomizing pathway in which propionate is dismutated to acetate and butyrate via a six-carbon intermediate before being degraded via β -oxidation (F. A. de Bok, A. J. Stams, C. Dijkema, & D. R. Boone, 2001). This novel dismutation pathway is also known as the *Smithella* pathway (F. A. de Bok et al., 2001).

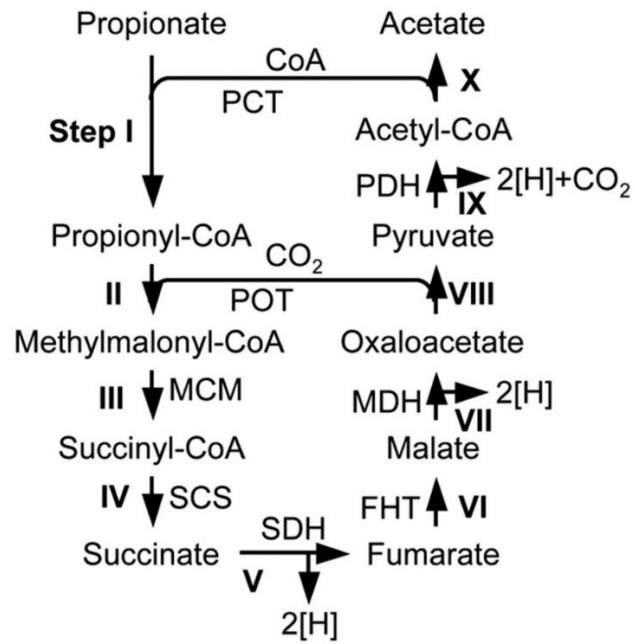


Figure 2-2. Proposed methylmalonyl-CoA pathway.

* PCT, propionate CoA transferase; POT, propionyl-CoA:oxaloacetate transcarboxylase; MCM, methylmalonyl-CoA mutase; SCS, succinyl-CoA synthetase; SDH, succinate dehydrogenase; FHT, fumarate hydratase (fumarase); MDH, malate dehydrogenase; PDH, pyruvate dehydrogenase (adopted from (Kosaka et al., 2006b)).

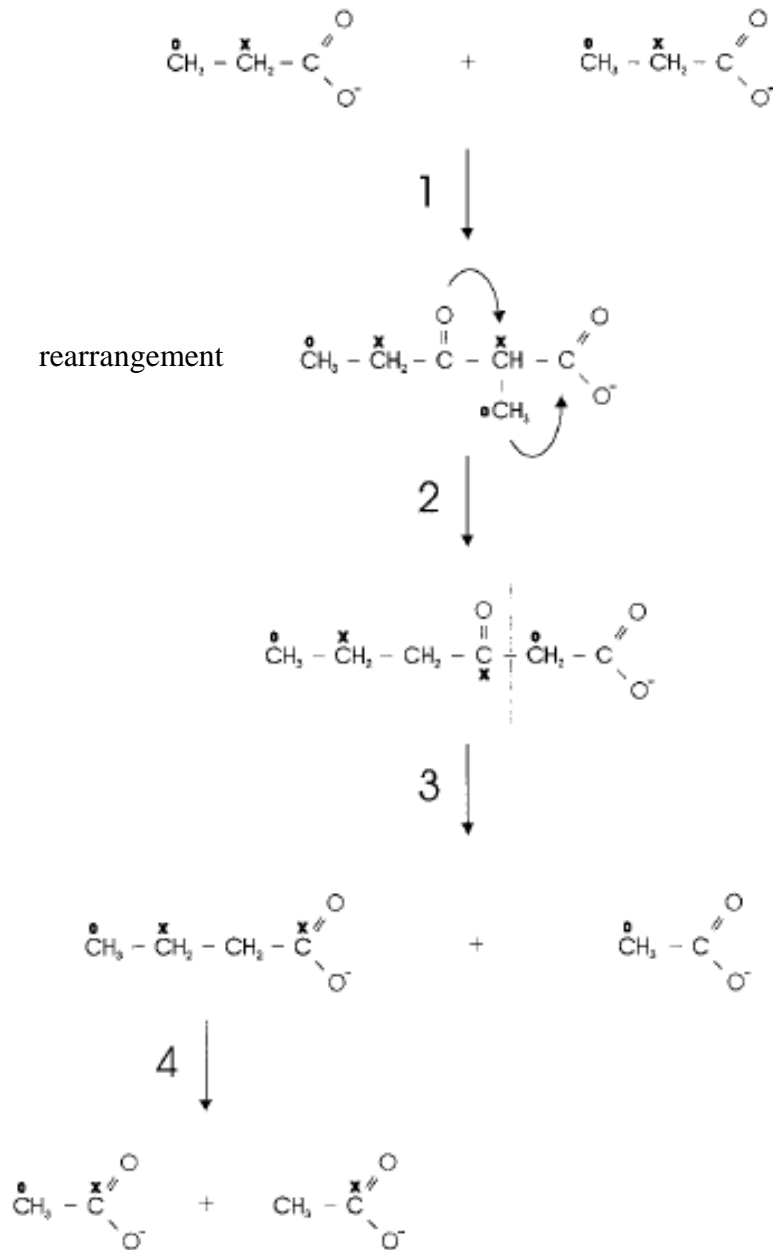


Figure 2-3. Proposed pathway for propionate conversion by *Smithella propionica* (adopted from (Frank AM de Bok, Alfons JM Stams, Cor Dijkema, & David R Boone, 2001)).

The partial pressure of H_2 (P_{H_2}) is crucial in the control of a syntrophic partnership between SPOB bacteria and hydrogenotrophic methanogens.

P_{H_2} measured at steady-state conditions were in the range of $1\text{--}20 \times 10^{-5}$ atm,

under which propionate consumption is thermodynamically favorable (Perry L McCarty & Smith, 1986). J. Doling (2013) calculated the Gibbs free energy for these two pathways and concluded that the *Smithella* pathway is less sensitive to H_2 and is more thermodynamically favorable in a certain range of H_2 than the MMC pathway. The *Smithella* bacteria in syntrophic partnership with hydrogenotrophic methanogens have a larger H_2 window than the classical SPOB due to a different propionate degradation pathway (J. Doling, 2013). Also, *Smithella* species are known to utilize the six-carbon pathway via butyrate and have been detected in various anoxic environments (Wenzong Liu et al., 2016), suggesting that this pathway is widespread. A significant range of conditions exist under which propionate oxidation via the *Smithella* pathway is exergonic whereas the MMC pathway is endergonic (J. Doling, 2013). Table 2-2 shows the windows of opportunity under specific conditions for the MMC and *Smithella* pathways with hydrogenotrophic methanogenesis at 25 °C and 55 °C, respectively, and Figure 2-4 shows the Gibbs free energy change over a wide range of P_{H_2} for both the processes under specific conditions. Accordingly, in both temperatures (i.e. 25 °C and 55°C), the *Smithella* pathway coupled to hydrogenotrophic methanogenesis has a wider range of P_{H_2} to occur spontaneously ($\Delta G < 0$) compared to MMC pathway coupled to hydrogenotrophic methanogenesis.

Reactions involved in syntrophic conversion of propionate to methane along with responsible microbes and standard Gibbs free energy values are provided in Table 2-3. Many factors, including operational conditions such

as pH, temperature, P_{H_2} , and the presence of volatile fatty acids (VFAs), organic compounds, and toxins, as well as the reactor configuration, affect the biodegradation of propionate and lead to different biokinetic characteristics.

Table 2-2. The window of opportunity corresponding to estimated range of H₂ concentration comparing the *Smithella* pathway and the methylmalonyl CoA (MMC) pathway coupled to hydrogenotrophic methanogenesis.

Pathway	Hydrogen concentration at 25 °C (Pa)	Hydrogen concentration at 55 °C (Pa)	Reference
<i>Smithella</i> pathway with hydrogenotrophic methanogenesis	0.002 - 500.34 ^a	1.8 - 580 ^b	^a (Leng et al., 2018) ^b Jan Dolfig (2017)
Methylmalonyl-CoA pathway with hydrogenotrophic methanogenesis	0.002 - 1.82 ^a	1.8 - 7.3 ^b	^a (Leng et al., 2018) ^b Jan Dolfig (2017)

Conditions: [acetate] = [propionate] = 1 mM; [bicarbonate] = 50 mM; P_{CH₄} = 1 atm; pH=7.

Table 2-3. Reactions involved in propionate oxidation and responsible microbes along with standard Gibbs free energy.

Reactions involved	ΔG° (kJ/reaction)	Functional microbes	Reference
$CH_3CH_2COO^- + 3H_2O \rightarrow CH_3COO^- + HCO_3^- + 3H_2 + H^+$	76.5 ^a	<i>Syntrophobacter fumaroxidans</i> ; <i>Desulfotomaculum thermobenzoicum subsp. thermosyntrophicum</i> ; <i>Pelotomaculum thermopropionicum</i> ; <i>Pelotomaculum schinkii</i>	(S. Y. Chen & Dong, 2005); (Plugge et al., 2012); (H. Imachi et al., 2002); (F. A. M. de Bok et al., 2005)
$2CH_3CH_2COO^- + 2H_2O \rightarrow 3CH_3COO^- + 2H_2 + H^+$	48.4	<i>Smithella propionica</i>	(Y. Liu et al., 1999)

^a Calculation based on G_f° values tabulated by Thauer et al. (1977).

Table 2-4. Comparison of syntrophic propionate degradation using smithilla pathway and methylmalonyl CoA pathway.

	<i>Smithella</i> pathway	ΔG^0 (kJ/reaction)	Methylmalonyl-CoA pathway	ΔG^0 (kJ/reaction)
Propionate oxidation	$\text{CH}_3\text{CH}_2\text{COO}^- + \text{H}_2\text{O} \rightarrow 3/2\text{CH}_3\text{COO}^- + 1/2\text{H}^+ + \text{H}_2$	24.18	$\text{CH}_3\text{CH}_2\text{COO}^- + 3\text{H}_2\text{O} \rightarrow \text{CH}_3\text{COO}^- + \text{HCO}_3^- + \text{H}^+ + 3\text{H}_2$	76.5
Hydrogenotrophic methanogenesis	$\text{H}_2 + 1/4\text{HCO}_3^- + 1/4\text{H}^+ \rightarrow 1/4\text{CH}_4 + 3/4\text{H}_2\text{O}$	-33.9	$3\text{H}_2 + 3/4\text{HCO}_3^- + 3/4\text{H}^+ \rightarrow 3/4\text{CH}_4 + 9/4\text{H}_2\text{O}$	-101.7
Acetoclastic methanogenesis	$3/2\text{CH}_3\text{COO}^- + 3/2\text{H}_2\text{O} \rightarrow 3/2\text{HCO}_3^- + 3/2\text{CH}_4$	-46.44	$\text{CH}_3\text{COO}^- + \text{H}_2\text{O} \rightarrow \text{HCO}_3^- + \text{CH}_4$	-30.96
Overall equation	$\text{CH}_3\text{CH}_2\text{COO}^- + 7/4\text{H}_2\text{O} \rightarrow 7/4\text{CH}_4 + 5/4\text{HCO}_3^- + 1/4\text{H}^+$	-56.16	$\text{CH}_3\text{CH}_2\text{COO}^- + 7/4\text{H}_2\text{O} \rightarrow 7/4\text{CH}_4 + 5/4\text{HCO}_3^- + 1/4\text{H}^+$	-56.16

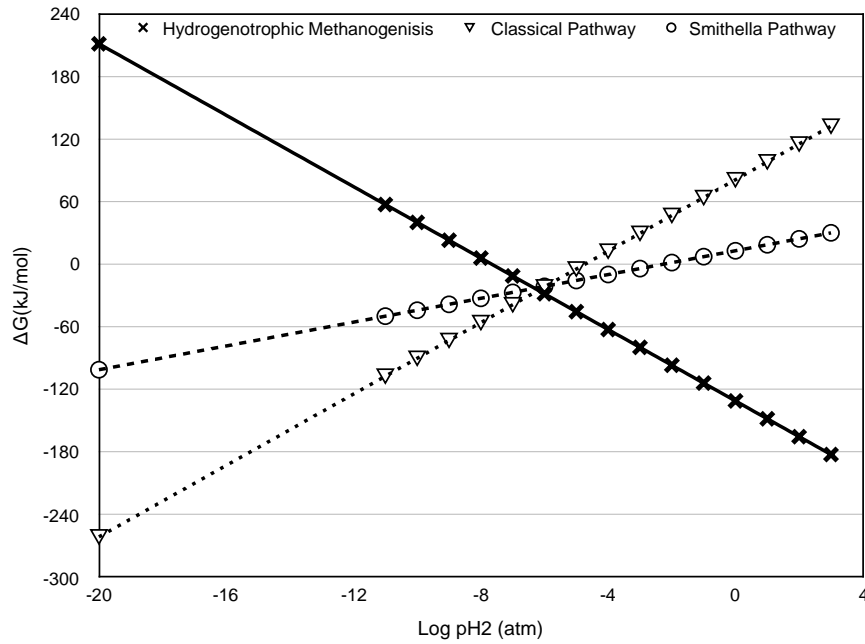


Figure 2-4. The window of opportunity for propionate degradation in methanogenic bioreactors at 25 °C.

* ΔG values of hydrogenotrophic methanogenesis (crosses) and propionate degradation (open triangle) via classical pathway. Window of opportunity: $2.2E-08$ atm to $1.8E-05$ atm. ΔG values for hydrogenotrophic methanogenesis (crosses) and propionate degradation (open circles) via smithella pathway. Window of opportunity: $2.2E-08$ atm to $5E-03$ atm. Conditions: [acetate] = [propionate] = 1 mM; [bicarbonate] = 50 mM; P_{CH_4} = 1 atm; pH = 7; Temperature = 25 °C (adopted from (Leng et al., 2018)).

2.2.1.2 Methanogenesis

There are four main pathways for methane (CH_4) production: (i) acetoclastic methanogens utilize acetate to directly produce CH_4 and CO_2 ; (ii) hydrogenotrophic methanogens use H_2 or formate to reduce CO_2 to CH_4 ; (iii) methylotrophic methanogens metabolize methyl compounds to produce a small amount of CH_4 ; (iv) syntrophic partnerships of acetate-oxidizing bacteria and hydrogenotrophic methanogens convert acetate to CH_4 via the intermediates H_2 and CO_2 . In anaerobic wastewater treatment, acetate-based methanogenesis is responsible for almost 70% of the total methane production, and the rest mostly comes from H_2 and CO_2 (Venkiteshwaran et al., 2015). Acetate oxidation is thus potentially a very important process in anaerobic digestion. It has been observed once that only by increasing the P_{H_2} that an acetate-oxidizing system can be changed to a CO_2 -reducing system (Lee & Zinder, 1988).

In AD systems treating waste streams mostly containing easily biodegradable substances, methanogenesis is considered as the rate-limiting step that affects the overall process kinetics (Narihiro et al., 2016). Methanogens are relatively slow-growing microorganisms and have a limited range of available substrates (Y. Liu & Whitman, 2008). The typical CH_4 production reactions from major methanogenic substrates are listed in Table 2-5 (Y. Liu & Whitman, 2008; Thauer et al., 1977). The growth rates of hydrogenotrophic methanogens (0.05 to 4.07 d^{-1}) are normally faster than those of acetoclastic methanogen (0.08 to 0.7 d^{-1}) (Demirel & Scherer, 2008). There are various factors that influence the CH_4

Table 2-5. Reactions involved in propionate conversion to methane and responsible microbes along with standard Gibbs free energy.

Metabolism	Reactions involved	ΔG° (kJ/reaction)	Functional microbes	Reference
Hydrogenotrophic methanogenesis	$4 \text{ H}_2 + \text{HCO}_3^- + \text{H}^+ \rightarrow \text{CH}_4 + 3 \text{ H}_2\text{O}$	-135.6	Most methanogens	Thauer et al. (1977).
Acetoclastic methanogenesis	$\text{CH}_3\text{COO}^- + \text{H}^+ \rightarrow \text{HCO}_3^- + \text{CH}_4$	-30.96	<i>Methanosarcina</i> and <i>Methanotherix</i>	(Cai et al., 2016); A.-E. Rotaru, P. M. Shrestha, F. Liu, M. Shrestha, et al. (2014)
Methanogenesis from formate	$4 \text{ HCOO}^- + 4 \text{ H}^+ \rightarrow \text{CH}_4 + 3 \text{ CO}_2 + 2 \text{ H}_2\text{O}$	-144.5	Many of hydrogenotrophic methanogens	-

2.2.2 Interspecies electron transfer/flow in anaerobic digestion

Energy recovery in the form of methane with sewage is of great interest. (Li & Yu, 2011). Methanogenesis is accomplished by the syntrophic association between acetogenic bacteria and methanogens to achieve interspecies electron transfer (IET). IET from the electron donors (syntrophic bacteria) to electron acceptors (methanogens) determines whether organic matter degradation and methane production can be carried out in an efficient and orderly manner. This combination of different species is also necessary to break through the thermodynamic barrier to capture energy for growth (W. Liu et al., 2016). The syntrophic methane production mainly involves the two mechanisms of mediated interspecies electron transfer (MIET) and direct interspecies electron transfer (DIET).

2.2.2.1 Mediated interspecies electron transfer

Traditionally, IET was thought to be accomplished by syntrophs and methanogens through diffusive electron carriers. One of the extracellular electron carriers in syntrophic methanogenic associations that has received the most attention is H₂. *Methanoculleus*, *Methanospirillum*, *Methanoregula*, *Methanosphaerula*, *Methanobacterium*, *Methanobrevibacter*, and *Methanothermobacter* are the most common hydrogenotrophic methanogens in AD systems (Cai et al., 2016). Other than H₂, formate is another important electron carrier and can be detected in most methanogenesis systems. A co-culture study of *Desulfovibrio vulgaris* and *Methanobacterium formicicum* proved that more than 90% of methane production was mediated via interspecies formate transfer (Thiele & Zeikus,

1988). The solubility, transfer speed and diffusion distance of formate is higher than those of H₂ in syntrophic propionate and butyrate degradation proved by a flux analysis by F. A. de Bok, C. M. Plugge, and A. J. Stams (2004). Therefore, it is proposed that formate may be even more important than H₂ as extracellular electron carrier for syntrophic propionate oxidation. To ensure propionate oxidation is energetically feasible, the concentrations of H₂ and formate should maintain at extremely low level. Therefore, a close diffusion distance of the carriers is required to keep fast metabolic rates and high propionate conversion rates. In aggregated granules, the close proximity between microbes allows more efficient transfer of the interspecies electron carriers than random in cell-cell associations, contributing to the high conversion rates (F. A. de Bok et al., 2004).

2.2.2.2 Direct interspecies electron transfer

As discussed previously, the form of MIET is constrained by the physical distance between syntrophs and methanogens, and the diffusion rate of electron carriers, creating a metabolic bottleneck (Leng et al., 2018). However, there is growing evidence of an alternative direct interspecies electron transfer (DIET), which could overcome this bottleneck and enhance methane production rate (Cruz Viggi et al., 2014; F. Liu et al., 2012). It was observed that methanogens can directly accept electrons through direct electron transfer for methane production (A.-E. Rotaru, P. M. Shrestha, F. Liu, B. Markovaite, et al., 2014; Summers et al., 2010). More importantly, in methanogenic systems, DIET outcompetes MIET (via H₂ and formate) because of the higher electron transfer efficiency by electric

current and the lower loss of intermediates (Leng et al., 2018). It is an essential mechanism for electron transfer in natural methanogenic aggregates (Morita et al., 2011a) as well as in the engineered methanogenic aggregates predominated by *Geobacter daltonii* (25% of bacteria) and *Methanotherix concilii* (90% of archaea) (Morita et al., 2011b). In addition, DIET greatly contributed to IET in methanogenic system supplemented with electrically conductive particles such as magnetite (Fe_3O_4) (Cruz Viggli et al., 2014). DIET proceeds via electrically conductive pili or c-type cytochromes between syntrophs and methanogens. Such DIET was observed between *Geobacter*, the electron producer, and *Methanotherix* or *Methanosarcina*, the electron receiver, and produce methane from ethanol, (A.-E. Rotaru, P. M. Shrestha, F. Liu, B. Markovaite, et al., 2014). As shown in Fig. 2-6, a co-cultures study found that *Methanotherix harudinacea* accepts electrons generated by *G. metallireducens* from ethanol oxidation ($8\text{H}^+ + 8\text{e}^- + \text{CO}_2 \rightarrow \text{CH}_4 + 2\text{H}_2\text{O}$) via DIET for the reduction of carbon dioxide to methane (A. E. Rotaru et al., 2014).

DIET occurs in the presence of exoelectrogens, which are capable of shuttling electrons exogenously to methanogens through conductive pili or surfaces (F. Liu et al., 2012; Shrestha et al., 2013). There are two well-recognized mechanisms for DIET in methanogenic systems. The first is to direct electron transfer to the receptor via c-type cytochrome on the cell membrane (Leang, Qian, Mester, & Lovley, 2010); In the conductive aggregate for syntrophic ethanol-oxidization system, DIET was observed to be mediated by *G. sulfurreducens* c-type cytochrome (Summers et al.,

2010). Also, it was reported that a decrease in the concentration of cytochrome inhibited extracellular electron transport of *G. sulfurreducens*, further verified the necessity of cytochromes in DIET (Estevez-Canales et al., 2015). The second mechanism is electron transfer via pili or other cell appendages (Lovley, 2011). *G. sulfurreducens* pili are highly conductive and can act as biological nanowires to transfer electrons from the surface of the cell to extracellular insoluble Fe(III) oxides (Reguera et al., 2005). Also, the proteinaceous filaments on the pili of *G. sulfurreducens* can serve as a molecular conductor for long-range extracellular electron transfer (Malvankar, Yalcin, Tuominen, & Lovley, 2014). *Methanotherix* are obligate acetoclastic methanogens that are known to use only acetate or acetate plus electrons obtained via DIET (Venkiteshwaran et al., 2015). DIET raises the intriguing possibility that the organism gets additional energy with electrons transferred via DIET (Shrestha et al., 2013). Most interestingly, while *Methanotherix* is unable to perform hydrogenotrophic methanogenesis using CO₂ due to the absence of a hydrogen uptake mechanism (Berg et al., 2010), it can form syntrophic association, termed ‘electric syntrophy’, with *Geobacter* to achieve methane production, in a similar fashion to hydrogenotrophic methanogenesis, through DIET-dependent CO₂ reduction (Kato, Hashimoto, & Watanabe, 2012a; Morita et al., 2011a).

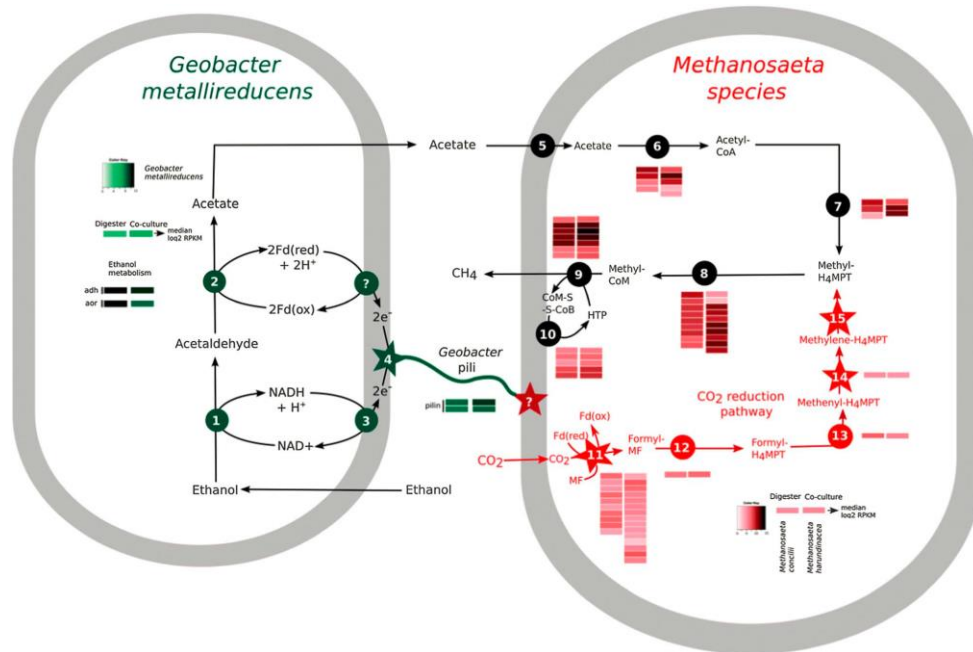


Figure 2-6. DIET-based metabolism in digester samples and defined co-cultures of *Geobacter metallireducens* and *Methanoxithrix harundinacea* as revealed by metatranscriptomics (adopted from (A. E. Rotaru et al., 2014)).

2.2.2.3 GAC enhancement

DIET can occur as electrical current through biotic (e.g., pili) and abiotic (e.g., conductive mineral and carbon particles) electrical conduits (Kouzuma, Kato, & Watanabe, 2015). In a lot of methanogenic setups, GAC addition was originally conceived to serve as a mechanical scouring agent along membrane for reducing membrane fouling and a carrier for microbial attachment. Recently, there have been many reports on the promotion of methane production via enhancing DIET during syntrophic methanogenesis by the addition of conductive materials, such as GAC (A.-E. Rotaru, P. M. Shrestha, F. Liu, B. Markovaite, et al., 2014), and (semi)conducting iron oxide minerals (F. Liu et al., 2012). It was reported that a *pilA*-defective strain of *G. metallireducens* was unable to initiate

syntrophic growth with *M. barkeri*, while syntrophic metabolism is restored by adding granular activated carbon (GAC). The restoration indicated that the conductive material could replace the pili and allow the DIET to happen.

2.2.3 The RHP pathway

Recently, a ribulose-1,5-bisphosphate carboxylase/oxygenase (RuBisCO)-mediated CO₂ fixation pathway was discovered in many methanogen species including *Methanotherix*, which could reduce CO₂ into various carbon intermediates for important metabolic pathways, such as gluconeogenesis and glycolysis (Kono et al., 2017). This newly-discovered pathway, as shown in Fig. 2-7, termed “reductive hexulose-phosphate (RHP) pathway”, is analogous to the Calvin–Benson cycle in plant photosynthesis, raising our hypothesis that it could be electron-driven (i.e., DIET). Additionally, this carbon fixation pathway has the potential to link with methanogenesis via a formaldehyde intermediate, leading to our speculation of a third methanogenesis route in *Methanotherix*.

summarizes physical properties and price comparison of different bio-products. SCCs, specifically acetate, can be used to produce MCCs, which the energy density is relatively higher. Moreover, fermentation processes usually require high water content and their products are commonly soluble in water, e.g. ethanol, resulting in high energy consumption for distillation and extraction from fermentation broth. MCCs are better alternatives because the longer hydrophobic carbon chain makes extraction from fermentation broth less energy-intensive (Matthew T. Agler et al., 2012). Upgrading diluted ethanol into MCCs would circumvent energy intensive distillation process, making this bioprocess energy-efficient and cost-effective. Therefore, the properties of low solubility and high energy density make MCCs superior bio-products to SCCs (Steinbusch et al., 2011). Currently, caproate is commercially produced via various petrochemical methods. A market would likely to develop if efficient and economical bioprocessing for MCCs production is developed.

Table 2-6. Physical Properties and price comparison of different bio-products.

Compound	Specific density/energy (MJ/kg)	Energy density (MJ/L)	Solubility in water g L ⁻¹ at 25 °C	Density g/cm ³ at 25 °C
Ethanol	23.4 - 26.8	18.4 - 21.2	Miscible	0.789
Butanol	36	29.2	73	0.81
Biodiesel	37.8	33.3 - 35.7	Slightly miscible	0.88

Acetic acid	14 - 15	14 - 15	Miscible	1.049
Caproate	30 - 31	27.5 - 28.5	10.82	0.929

* Resources: “Kirk-Othmer Encyclopedia of Chemical Technology, 3rd ed., 1978”, “Kirk-Othmer Encyclopedia of Chemical Technology, 4th ed, 1993”, “Research and Markets: N-Caproic acid (Hexanoic acid) (CAS 142-62-1) Market Research Report, 2012”



Figure 2-8. Examples of commercial applications of caproate.

(Adopted from “Global Industry Perspective, Comprehensive Analysis, Size, Share, Growth, Segment, Trends and Forecast, 2014 – 2020”, Dec. 2015, Code: MRS – 39802).

2.3.2 Ethanol-acetate fermentation for caproate production

Production of butyrate and caproate from acetate and ethanol has been known for decades with pure culture of *Clostridium kluyveri* (Bornstein & Barker, 1948), while caproate production in mixed culture fermentations was discovered more recently. Mixed-culture carboxylates chain elongation

upgrades short-chain carboxylates (SCCs) and ethanol into medium chain carboxylates (MCCs), mainly caproate as product, with higher energy density and better separation property (M. T. Agler, Wrenn, Zinder, & Angenent, 2011). In the mix-culture CE processes, *C. kluyveri* was also identified to be the predominant, as well as the main functional chain elongating microorganism (Matthew T. Agler et al., 2012; Steinbusch et al., 2011). Specifically, *Clostridium kluyveri* was found to be able to produce caproate from ethanol with acetate via the reverse β -oxidation pathway (Barker, Kamen, & Bornstein, 1945; Seedorf, Fricke, Veith, Bruggemann, Liesegang, Strittmatter, et al., 2008). The chain elongation (CE) process was reported to be an efficient fermentation with an MCCs selectivity of higher than 80% (Matthew T. Agler et al., 2012; T. I. Grootscholten et al., 2013). Recent studies demonstrated that caproate can be produced from miscellaneous low-grade organic wastes in both lab- (Matthew T. Agler et al., 2012; Ge et al., 2015; T. I. M. Grootscholten et al., 2013a; Grootscholten et al., 2014) and pilot-scale (Angenent et al., 2016) systems at high rates and specificities, suggesting great application potential of chain elongation bio-process. Previous studies have successfully separate caproate from fermentation broth using *in-situ* membranes (Xiong, Richard, & Kumar, 2015) or membrane electrolysis (Xu, Guzman, Andersen, Rabaey, & Angenent, 2015).

In chain elongation process, both the substrates, SCCs and diluted ethanol, can be derived from waste materials, such as yeast fermentation beer (Matthew T. Agler et al., 2012), lignocellulosic materials (M. T. Agler et al.,

2011; Sarkar, Ghosh, Bannerjee, & Aikat, 2012), municipal solid waste (Grootscholten et al., 2014) and acidified food waste. These waste streams are ideal candidates due to their readily degradable organics-rich contents. In addition, their property of high water-content circumvents the necessity of additional water consumption that is problematic in bio-ethanol industry with food crops. Moreover, ethanol use as feed for caproate production has been identified as the predominant cause of environmental impact in a life cycle assessment study, and thus it was suggested to use lignocellulosic ethanol (LE) as an alternative feedstock (W. S. Chen, Strik, Buisman, & Kroeze, 2017).

2.3.2.1 Enhancement approaches for caproate production - configuration and operation

To further improve the CE process, approaches like a new reactor system, upflow anaerobic filter, and reducing the hydraulic retention time for high productivity of MCFA were successfully applied (T. I. Grootscholten et al., 2013; T. I. M. Grootscholten et al., 2013b). High production rates of MCCs have been achieved with high selectivity (>90%) by an improved chain elongation reactor design using a synthetic medium containing VFAs and ethanol (Grootscholten et al., 2012).

2.3.2.2 Enhancement approaches for caproate production - substrates

In particular, to support the growth of the MCFA producing bacteria and improve productivity of MCFAs, yeast extract was commonly added as a supplement in the CE process (W. S. Chen, Ye, Steinbusch, Strik, &

Buisman, 2016; T. I. Grootsholten et al., 2013; Grootsholten et al., 2012; T. I. M. Grootsholten et al., 2013b; Kucek, Spirito, & Angenent, 2016). Furthermore, it was pointed that yeast extract might also contribute to the butyrate formation and is unlikely the source of caproate production (W. S. Chen et al., 2016). The increased yeast extract concentration improved the MCFA production rate was speculated to stimulates growth of bacteria (T. I. M. Grootsholten et al., 2013b). Similarly, in a CE process using yeast-fermentation beer as feedstock, the yeast cells were hypothesized to be converted to acetate or butyrate, therefore facilitated the MCFA production (Ge et al., 2015).

Moreover, it has been recently reported that caproate production via CE was reinforced by adding biochar in the system, mostly because biochar facilitated electron transfer and formation of a stable microorganism community structure due to its conductivity and the partitioning by biochar (Y. H. Liu, He, Shao, Zhang, & Lu, 2017). Similar reinforcement effect of electrically conductive particles, such as granular activated carbon (GAC), iron-oxide minerals, or even magnetite nanoparticles, on anaerobic digestion (AD) has been reported widely (Kato et al., 2012a; Kato, Hashimoto, & Watanabe, 2012b; F. H. Liu et al., 2012), because the conductive particles promoted the direct interspecies electron transfer and stimulated aggregate of functional microorganisms in AD (Kato et al., 2012a; F. H. Liu et al., 2012). However, it still remains mysterious that whether such prevalent improvement of fermentation performance induced by conductive particles can be also employed in the CE process.

2.3.3 Caproate formation microbiomes and biological pathways

2.3.3.1 Caproate-producing microorganisms

Caproate is a unique product of several microbial species, such as *Eubacterium alactolyticus*, *E. bifforme*, *E. limosum* and *E. pyruvativorans*, as well as *Clostridium kluyveri*, *Peptococcus niger* and *Megasphaera elsdenii*. Among these caproate-producing bacteria, the spore-forming *C. kluyveri* has a strong capability to resist heat or chemical treatment. Additionally, the fermentative H₂-producing environments would favor the growth of *C. kluyveri*, rather than other species. Previous studies identified that *C. kluyveri* was the functional and predominated microbial group in chain elongation process (Kucek et al., 2016; Steinbusch et al., 2011).

2.3.3.2 Caproate production via the chain elongating reverse β -oxidation pathway

The major known pathway for caproate production is through chain elongation via the reversed β -oxidation pathway. It can elongate short chain carboxylates with two carbons derived from a reduced molecule, such as ethanol, into medium-chain carboxylates, leading to more energy-dense and insoluble products. As shown in Fig. 2-9, The reverse β -oxidation pathway is a cyclic process and adds an acetyl-CoA molecule derived from ethanol or lactate to a carboxylate, elongating its carbon chain length with C₂ at one time. The metabolism starts with ethanol oxidation to acetate. Accordingly, acetate is activated to acetyl CoA and is elongated in a cyclic pathway to butyrate using NADH and FADH₂. Similarly, butyrate can be

elongated via butyl-CoA in a similar cycle to caproate. In this metabolism of the pure culture, ethanol is used as the electron donor. An example of chain elongation bacteria is *Clostridium kluyveri*, and it was identified ubiquitously in environmental metagenomic studies (Seedorf, Fricke, Veith, Bruggemann, Liesegang, Strittmatter, et al., 2008). The first required environmental condition for chain elongation is the presence of energy-rich, reduced compounds, such as ethanol, to provide energy, reducing equivalents, and acetyl-CoA microbial pathways. A reduced enough condition is also a crucial factor to ensure that reversed β -oxidation can outcompete the oxidation of reduced molecules, such as electron donors and products, maintaining a well-functioned CE bioprocess and high rate of caproate production (Steinbusch et al., 2011). Table 2-7 lists the detailed steps and reactions involved in the reverse β -oxidation pathways, which are shown in Fig. 2-9 graphically.

Table 2-7. Metabolic stoichiometry in butyrate and caproate formation by *Clostridium kluyveri* (adopted from (Ding et al. 2010)).

NO.	Step	Reaction equations
A	Ethanol dehydrogenation	ethanol + 2NAD ⁺ + CoA = acetyl-CoA + 2(NADH + H ⁺)
A1		ethanol + 2NAD ⁺ = acetaldehyde-CoA + (NADH + H ⁺)
A2		acetaldehyde + NAD ⁺ + CoA = acetyl-CoA + (NADH + H ⁺)
B	ATP formation via SLP	acetyl-CoA + ADP + Pi = acetate ⁻ + ATP + CoA + H ⁺
		acetyl-CoA + Pi = acetate + Pi + CoA
		acetyl-Pi + ADP = acetate ⁻ + ATP + H ⁺
C1	Ferredoxin reduction	(NADH + H ⁺) + Fd _{ox} = NAD ⁺ + Fd _{red} ²⁻
C2	Hydrogen formation	Fd _{red} ²⁻ + H ⁺ = Fd _{ox} + H ₂
C3	NADH ₂ regeneration and ATP formation via ETP	Fd _{red} ²⁻ + NAD ⁺ + H ⁺ = Fd _{ox} + (NADH + H ⁺) + ΔμH ⁺
D		Additional ATP is concurrently synthesized by ETP (ΔμH ⁺)
		overall reaction = D2 + D2 + D3 + D4
		2Acetyl-CoA + (NAD(P)H + H ⁺) + 2(NADH + H ⁺) + Fd _{ox} = Butyryl-CoA + CoA + NAD(P) ⁺ + 2NAD ⁺ + Fd _{red} ²⁻ + H ₂ O
D1	Butyryl-CoA	2Acetyl-CoA = Acetoacetyl-CoA + CoA
D2		Acetoacetyl-CoA + (NAD(P)H + H ⁺) = 3-Hydroxybutyryl-CoA + NAD(P) ⁺

D3		$3\text{-Hydroxybutyryl-CoA} = \text{Crotonyl-CoA} + \text{H}_2\text{O}$
D4		$2(\text{NADH} + \text{H}^+) + \text{Crotonyl-CoA} + \text{Fd}_{\text{ox}} = \text{Butyryl-CoA} + 2\text{NAD}^+ + \text{Fd}_{\text{red}}^{2-}$
E	Butyrate formation	$\text{Butyryl-CoA} + \text{acetate}^- = \text{butyrate}^- + \text{Acetyl-CoA}$
F	Caproate formation	$\text{Caproyl-CoA} + \text{acetate}^- = \text{Caproate}^- + \text{Acetyl-CoA}$

Table 2-8. Possible reactions for butyrate and caproate formation (revised from (Ding, Tan, & Wang, 2010)).

NO.	Reactions	Combinations	References	Remark
1	$2\text{CH}_3(\text{CH}_2)_2\text{COO}^- = \text{CH}_3(\text{CH}_2)_4\text{COO}^- + \text{CH}_3\text{COO}^-$		(Yu & Mu, 2006)	Unlike to occur
2	$\text{CH}_3(\text{CH}_2)_2\text{COO}^- + \text{CH}_3\text{COO}^- + 2\text{H}_2 + \text{H}^+ =$ $\text{CH}_3(\text{CH}_2)_4\text{COO}^- + 2\text{H}_2\text{O}$			H_2 is used as eletron and proton donor
3	$\text{CH}_3(\text{CH}_2)_2\text{COO}^- + 2\text{CO}_2 + 6\text{H}_2 = \text{CH}_3(\text{CH}_2)_4\text{COO}^- + 4\text{H}_2\text{O}$			
4	$3\text{CH}_3\text{CH}_2\text{OH} + 4\text{H}_2 + 2\text{H}^+ = \text{CH}_3(\text{CH}_2)_4\text{COO}^- + 4\text{H}_2\text{O}$			
5	$2\text{CH}_3\text{CH}_2\text{OH} + \text{CH}_3\text{COO}^- = \text{CH}_3(\text{CH}_2)_4\text{COO}^- + 2\text{H}_2\text{O}$			Incomplete expression
6	$(k+1) \text{CH}_3\text{CH}_2\text{OH} + (k-1) \text{CH}_3\text{COO}^- = k \text{CH}_3(\text{CH}_2)_2\text{COO}^-$ $+ \text{H}^+ + 2\text{H}_2 + (k-1) \text{H}_2\text{O}$	Eq. 1 + k * Eq. 2	(Schoberth & Gottschalk, 1969)	<i>C. kluyveri</i> produces butyrate only from ethanol and acetate
7	$(k+1) \text{CH}_3\text{CH}_2\text{OH} + (k/2-1) \text{CH}_3\text{COO}^- = k/2$ $\text{CH}_3(\text{CH}_2)_2\text{COO}^- + \text{H}^+ + 2\text{H}_2 + (k-1) \text{H}_2\text{O}$	Eq. 1 + $k/2$ * Eq. 4		Butyrate is considered as an intermediate product
8	$(k+1) \text{CH}_3\text{CH}_2\text{OH} + (k/2-1) \text{CH}_3\text{COO}^- = k/2$ $\text{CH}_3(\text{CH}_2)_2\text{COO}^- + \text{CH}_3\text{COO}^- + \text{H}^+ + 2\text{H}_2 + (k-1) \text{H}_2\text{O}$	Eq. 1 + k * Eq. 3	(Ding et al., 2010)	<i>C. kluyveri</i> produces butyrate only from ethanol and butyrate

2.3.4 Challenges and opportunities

A lack of mechanistic understanding leads to a general perception that engineered systems with complex reactor microbiomes are somewhat inefficient and unpredictable. This resulted in the absence of wide-spread attempts to develop engineered systems that can produce carboxylates, even though microbiomes in anaerobic digesters have been producing gaseous methane successfully at industrial scales with stable, predictable, and functionally redundant community structures. The limited understanding of the microbial interactions, metabolic potential of mixed populations and the mechanism of enhancement/stimulation of performance in the CE process required for further investigation. A deeper mechanistic understanding of the CE process with complex reactor microbiomes would benefit for shaping stable and functional community structures, therefore provides clues for the design and operation of an efficient and predictable engineered system.

3. Chapter 3 Materials and Methodology

3.1 Inoculum and medium for CE fermentation

The inoculum of CE fermentation was anaerobic digesting (AD) sludge collected from the Shek Wu Hui (STW) Sewage Treatment Works in Sheung Shui, Hong Kong. It is a secondary sewage treatment works treating non-saline wastewater collected from Sheung Shui and Fanling areas. Specifically, the sludge used in our study was collected from the sludge digester, as indicated in Fig. 3-1.



Figure 3-1. Source of the inoculum sludge used in our study (Drainage Services Department, Hong Kong).

The fermentation medium contained minerals, trace metals, reducing agent, methanogenesis inhibitor and redox indicator, as described in detail in Table 3-1. In addition, sodium acetate and ethanol were supplied as substrates. Absolute ethanol was added as the ethanol source in most of the fermentation experiment except for one experiment. In particular, lignocellulosic ethanol (LE) produced from Momentary pine slurry via simultaneous saccharification and fermentation (SSF) (Dong, Wang, Zhang,

& Leu, 2017) was collected and supplied as ethanol source in one of the batch fermentation tests. The brief procedures for its production were: wood chips were firstly pretreated with bisulfite and sulfate, then $\text{Ca}(\text{OH})_2$ was added to adjust the pH to 5.5. 10g/L of yeast extract and 20 g/L of peptone were added to ferment the treated slurry for ethanol production. The obtained lignocellulosic ethanol yielded an ethanol concentration of 1000 mM.

Table 3-1. Composition of synthetic medium for fermentation.

Description	Composition	Concentration
Mineral	KH_2PO_4	0.20 g/L
	NH_4Cl	0.50 g/L
	NaCl	1.00 g/L
	$\text{MgCl}_2 \cdot 6\text{H}_2\text{O}$	0.40 g/L
	KCl	0.50 g/L
	$\text{CaCl}_2 \cdot 2\text{H}_2\text{O}$	0.15 g/L
	NaHCO_3	2.52 g/L
Trace metal	$\text{Fe}_2\text{Cl} \cdot 4\text{H}_2\text{O}$	1.50 mg/L
	H_3BO_3	0.30 mg/L
	$\text{CoCl}_2 \cdot 4\text{H}_2\text{O}$	0.20 mg/L
	ZnCl_2	0.05 mg/L
	$\text{MnCl}_2 \cdot 4\text{H}_2\text{O}$	0.03 mg/L
	$\text{Na}_2\text{MoO}_4 \cdot 2\text{H}_2\text{O}$	0.03 mg/L
	$\text{NiCl}_2 \cdot 6\text{H}_2\text{O}$	0.02 mg/L
	$\text{CuCl}_2 \cdot 2\text{H}_2\text{O}$	0.01 mg/L
Reducing	L-cysteine	0.5 g/L
Methanogenesis	2-bromoethanosulfonic acid	10 g/L
Redox indicator	Resazurin	(0.1% w/v)

3.2 CE fermentation experiment in batch

Four batch experiments were conducted to evaluate the chain elongation fermentation. The initial concentrations of ethanol and acetate were consistent in the four experiments and fixed at 150 mM and 50 mM, respectively. The control experiment, named “EtOH”, used absolute ethanol as an ethanol source. The second experiment named “LE” was supplied with lignocellulosic ethanol as ethanol source. The feedstock, lignocellulosic ethanol broth, was produced in a pre-fermentation process supplemented with 10 g/L of yeast extract (Dong et al., 2017) and resulted in residues of yeast extract and cellulose in the produced broth. The other two batch experiments using absolute ethanol, named “YE” and “CL”, were fed with extra supplement of yeast extract (5 g/L) and carboxymethyl cellulose sodium (2 g/L), respectively, to evaluate their influences on chain elongation process.

The batch fermentation tests were conducted in 100-mL serum bottles anaerobically. Each serum bottle was filled with 30 mL of fermentation broth. pH was adjusted to 7 using phosphate buffer saline (PBS) solution. The serum bottles were purged with nitrogen (N₂) gas for 5 min to provide anaerobic condition, and then sealed with rubber inlets and capped with aluminum crimp caps. Thereafter, 5 ml (14% v/working volume) of well-mixed AD sludge was injected to each bottle as inoculum. The headspace of the serum bottles was vacuumed and flushed with N₂ gas until the redox indicator turned colorless and with a final pressure of 1 atm. The serum bottles were incubated under 37 °C in a rotating shaker at 100 rpm. All

experiments were performed in duplicate. The gas and liquid samples were periodically withdrawn for chemical analyses. The volume of gas production was determined with a 50 mL disposable syringe. Liquid sample was centrifuged at 10,000 rpm for 5 min, and the supernatant was filtered with 0.22 μm PTFE filter for composition analysis.

3.3 CE fermentation in semi-continuous reactor

Three semi-continuous fermentations were conducted in 1-L fermenters anaerobically. The nutrient medium contained minerals, trace metals, a reducing agent, a methanogenesis inhibitor and a redox indicator, as described in Table 3-1. In addition, sodium acetate and absolute ethanol were supplied as substrates. 10% (v/v) AD sludge was added to each fermenter as inoculum. Each reactor was filled with 0.5 L of fermentation broth, and pH was adjusted and maintained to 7 using phosphate buffer saline (PBS) solution. Specifically, extra 5 g/L of casamino acids (CAS: 65072-00-6, Fisher BioReagentsTM) were supplied into the reactor named “AA”, and 100 ml/L of granular activated carbon (GAC) particles (size 1.5-2 mm) were added to the reactor named “GAC”. There was no extra supplement into the control reactor, “Control”. The reactors were purged with nitrogen (N_2) gas for 15 min and sealed afterwards to provide an anaerobic condition. Thereafter, 50 ml (10% v/v) of well-mixed wet sludge was inoculated to each reactor. The headspaces of the reactors were vacuumed and flushed with N_2 gas until the redox indicator turned colorless and with a final pressure of 1 atm. The reactors were incubated under 37 °C at an agitation speed of 100 rpm. The liquid samples were

periodically withdrawn for chemical analyses. The volume of gas production was determined with a 50 mL disposable syringe. Liquid sample was centrifuged at 10,000 rpm for 5 min, and the supernatant was filtered with 0.22 μm PTFE filter for composition analysis. The semi-continuous fermentation was operated for 7 days per cycle. During each cycle, 100-mL suspension was extracted and the same volume of substrate medium was supplemented. The pressure of headspace was adjusted to 1 atm by exhausting gas. The hydraulic retention time (HRT) was controlled at 35 days. Sampling was conducted on Day 0 (influent sampling), Day 3, and Day 7 (effluent sampling) of each cycle.

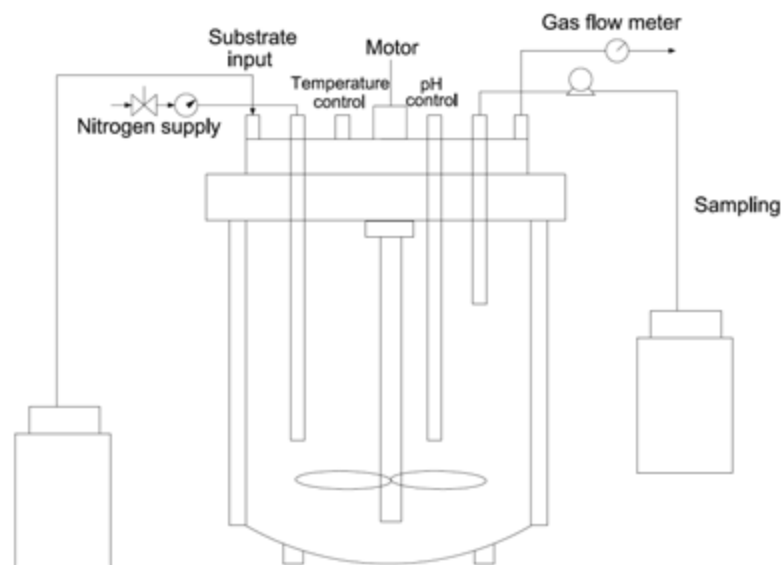


Figure 3-2. Schematic diagram of the semi-continuous fermentation system.

3.4 Analytical procedures

A 200 μL of gas sample was analyzed with gas chromatography (Agilent 6850 Series II single channel, CA, USA) equipped with a thermal conductivity detector (TCD) using helium as a carrier gas. A carbon molecular sieve type stationary phase column (TDX-01, JingKeRuiDa Technology, Beijing, China) installed in the gas chromatography was used to determine the composition of hydrogen, carbon dioxide and methane. The operation conditions were 120°C for injector temperature, 100°C for oven temperature, 150°C for detector temperature, 20 psi front inlet pressure for pressure control, 15 mL/min for front detector reference flow rate, 5 mL/min for front detector makeup flow rate, and 41.7 mL/min for total detected flow rate. The species of alcohols and fatty acids in the liquid filtrate were determined with high performance liquid chromatography (HPLC, SHIMADZU Prominence, MD, USA) equipped with a refractive index detector (RID) and a column (Bio-Rad Aminex HPX-87H column, CA, USA). The operation conditions were 5 mM H_2SO_4 as mobile phase, 0.6 mL/min for pump flow rate, 50°C for detector temperature, and 65°C for oven temperature.



Figure 3-3. The HPLC system (SHIMADZU) used for quantification of the target compounds and GC system (Agilent) used for quantification of the target gases.

3.5 DNA extraction and high-throughput sequencing

Genomic DNA extraction was conducted on the samples centrifuged at 16000 g for 10 min using a commercial kit (PowerSoil™ DNA Isolation Sample Kit, MoBio Laboratories, Inc., Carlsbad, CA), following the instructions of the manufacturer. The quantity and quality of the DNA was assessed with a NanoDrop® 2000c UV-Vis spectrophotometer (Thermo Scientific, USA).

3.5.1 SAF-CMBR systems

In the SAF-CMBR system using GAC as fluidizing medium, the samples for microbial analysis were taken on day 162, at which extremely short HRT less than 1.5 h was applied, from the bulk liquid and fluidized GAC

particles, in both AFBR and AFCMBR. Biomass on the GAC particles was obtained via grind and sonication.

In the SAF-CMBR system using both GAC and PET as fluidizing medium in two parallel reactors, the samples for microbial analysis were taken on day 135, from the bulk liquid and fluidized biofilm carriers, in the two AFCMBRs and the AFBR, respectively. Biomass on the GAC particles and PET beads were collected via grind and sonication.

Library preparation and high throughput sequencing on Illumina MiSeq platform was performed at BGI (Shenzhen, China). A 16S rRNA amplicon sequencing was conducted using primers 515F-806R, amplifying the V4 region (Albertsen, Karst, Ziegler, Kirkegaard, & Nielsen, 2015) of the 16S rRNA gene.

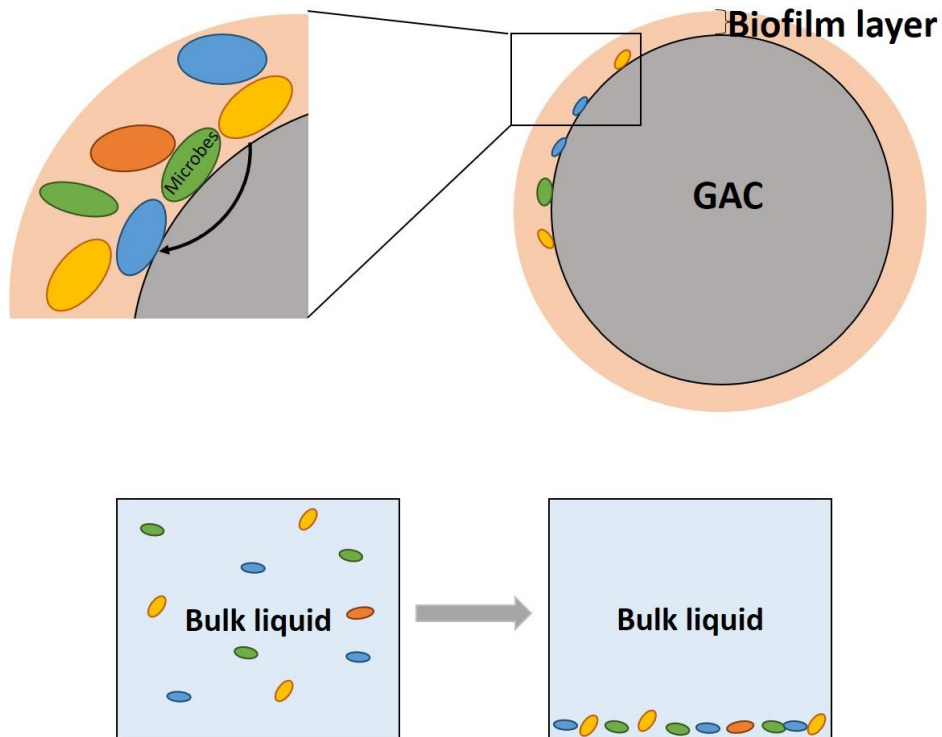


Figure 3-4. Illustration of samples collection.

3.5.2 CE batch fermentation

The samples were taken from the serum bottles at the end of fermentation for DNA extraction. Library preparation and high throughput sequencing on Illumina MiSeq platform was performed at BGI (Shenzhen, China). A primer pair 341F-806R (Kozich, Westcott, Baxter, Highlander, & Schloss, 2013), amplifying the V3-V4 region of the 16S rRNA gene (Takahashi, Tomita, Nishioka, Hisada, & Nishijima, 2014), was used for PCR amplification.

3.5.3 CE fermentation reactors

Biomass-containing bulk samples were collected and centrifuged at 10,000 rpm at 4 °C for 5 min, and the sediment were preserved and stored at -20

°C before DNA extraction from each reactor on Day 0, Day 10, Day 14, Day 21, Day 30, Day 45 and Day 51. 16S rRNA genes library construction and high throughput sequencing on Illumina MiSeq platform was performed at BGI (Shenzhen, China). A primer pair 341F-806R (Kozich et al., 2013), amplifying the V3-V4 region of the 16S rRNA gene (Takahashi et al., 2014), was used for PCR amplification. On Day 14, a sample extracted from reactor AA was collected for shotgun metagenomic sequencing. The sequencing was performed on an Hiseq 4000 platform at BGI (Shenzhen, China), generating paired-end (PE) reads with a read length of 150 base pairs (bp). About 35.6 Gbp (AA) and 41.8 Gbp (GAC) of metagenomic data was generated for each DNA sample.

A sample was extracted and preserved for metatranscriptomic sequencing from the fermentation reactor “AA” on Day 51 when its conditions reached steady phase. The sample was mixed and submerged with *RNAlater* solution (ThermoFisher, USA) in a volume ratio of 1:1 immediately after sample collection and frozen at -20 °C overnight. Then the samples were delivered for mRNA extraction, metatranscriptomic library construction and metatranscriptomic sequencing on Illumina Hiseq 4000 platform at BGI (Shenzhen, China). rRNA was removed with kit after total RNA was collected from. Fragmentation buffer was added for interrupting mRNA to short fragments. Paired-end (PE) with read length of 150 bp and 28.8 Gbp of metatranscriptomics data per sample was generated.

3.6 Genomic analysis

3.6.1 16S rDNA gene-based analysis

A modified version of the standard operation procedure for MiSeq data (Kozich et al., 2013) in Mothur v.1.38.1 (Schloss et al., 2009) was used to assemble and screen paired-end raw sequences. The qualified sequences were aligned and filtered against the SILVA reference database (release 128) to ensure that the derived sequences were from the amplified region. UCHIME algorithm was used for chimeric sequences detecting and removing (Edgar, Haas, Clemente, Quince, & Knight, 2011). Taxonomic classification at different taxonomic levels (from phylum to genus) was performed with the aforementioned SILVA database using the Bayesian Classifier (Wang, Garrity, Tiedje, & Cole, 2007). Clustering sequences into operational taxonomic units (OTUs) with 97% identity threshold was performed to categorize bacteria groups. One representative sequence for each OTU was extracted using the Ribosomal Database Project (RDP) classification method by using *get.oturep* command, and the representative sequences with relative abundance higher than 1% were compared with NCBI (National Center for Biotechnology Information) GenBank nucleotide database to assign putative taxa by BLAST (Basic Local Alignment Search Tool) (Madden, Tatusov, & Zhang, 1996). Sample diversity was evaluated based on OTUs using Mothur. The potential correlations between the bacterial community composition and various environmental variables (EV) was investigated by Canonical Correspondence Analysis (CCA). The R Studio version 3.2.3. software (<http://www.r-project.org>) (R Development Core Team, 2013) was used for statistical analysis. The packages ggplot2 (Wickham, 2009) , grid (Murrell,

2012) and vegan (Oksanen *et al.*, 2013) were used for microbial community analysis and plotting.

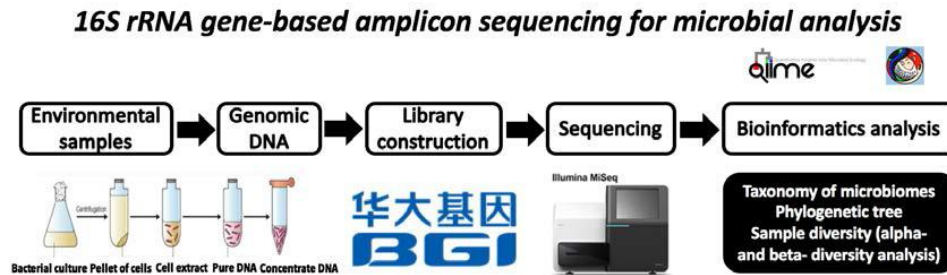


Figure 3-5. Flowchart of 16S rRNA gene-based amplicon sequencing for microbial analysis.

3.6.2 Metagenomic analysis

For metagenomics analysis, the raw reads were first trimmed with a minimum quality cutoff of 3, and further screened to be at least 78 bp in length, having an average quality score >30 and containing less than 3 ambiguous nucleotides (N's) using trimmomatic (Bolger, Lohse, & Usadel, 2014). Then, digital normalization was performed to remove redundant sequences with khmer scripts (k-mer size 20). Afterwards, paired-end reads were *de novo* assembled into long sequence contigs using St. Petersburg genome assembler (SPAdes, version 3.9.0) based on de Bruijn graph with default settings (“-k 19,33,47,61,75 --careful”) (Bankevich et al., 2012; Nurk et al., 2013). Meanwhile, a parallel hybrid assembly was performed on the trimmed reads sequenced on Illumina HiSeq platform together with the trimmed reads sequenced on the PacBio Sequel Platform using the same parameters. Next, MaxBin was used for binning the assembled contigs into taxonomic bins based on an Expectation-Maximization

algorithm (Y. W. Wu, Tang, Tringe, Simmons, & Singer, 2014). Then, CheckM was performed to assess the quality of draft genomes using a broader set of marker genes specific to the position of a genome within a reference genome tree and information about the collocation of these genes (Parks, Imelfort, Skennerton, Hugenholtz, & Tyson, 2015). The recovered genome bins were phylogenetically identified by comparing with reference genomes using PhyloPhlAn (Segata, Bornigen, Morgan, & Huttenhower, 2013). Prokka (version 1.11) (Seemann, 2014) was used to annotate protein coding genes. Then gene functions were further characterized and functional pathways were reconstructed with BlastKOALA (Kanehisa, Sato, & Morishima, 2016).

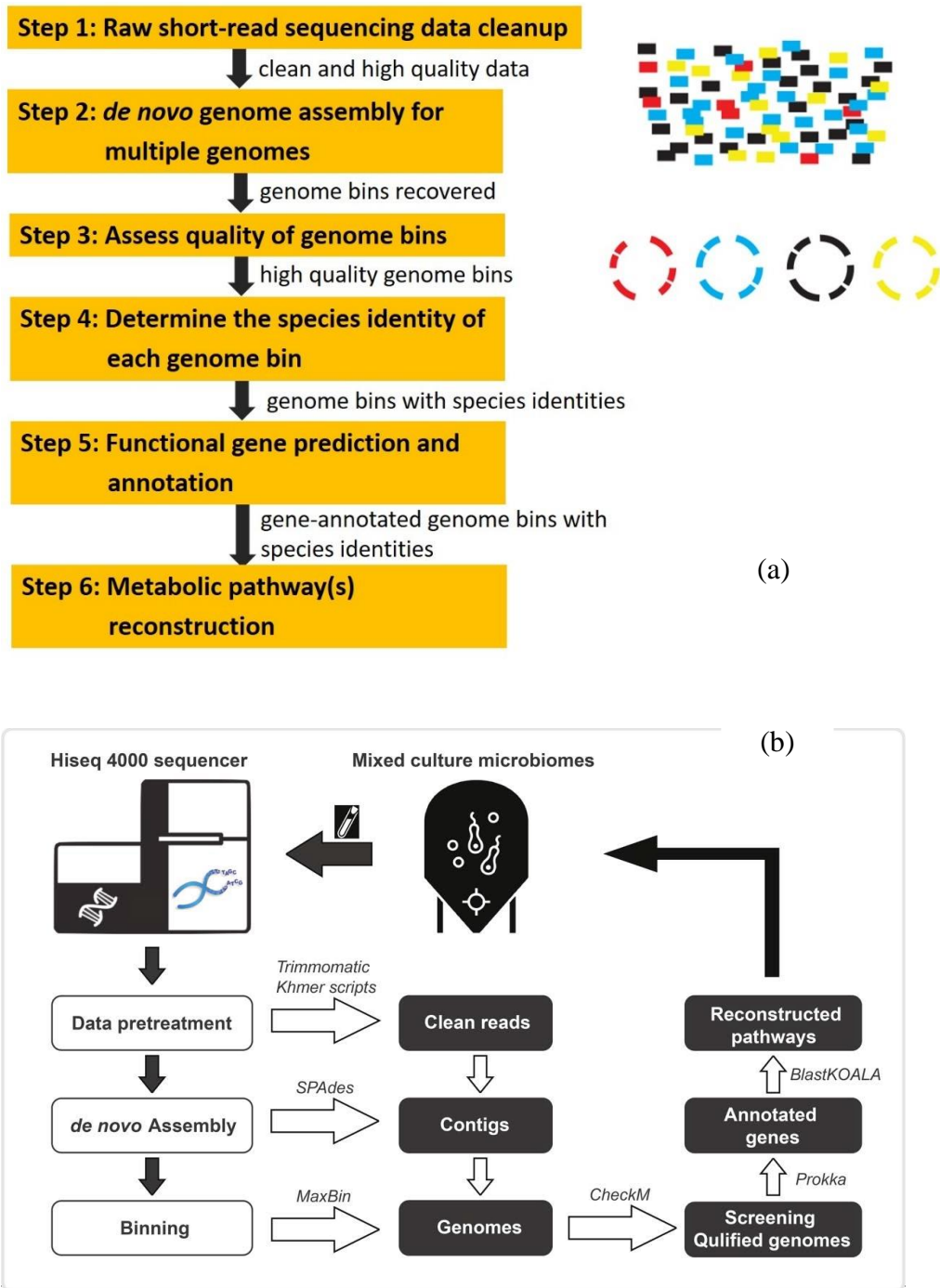


Figure 3-6. Flowchart of (a) metagenomics analysis pipeline and (b) software used in the analysis.

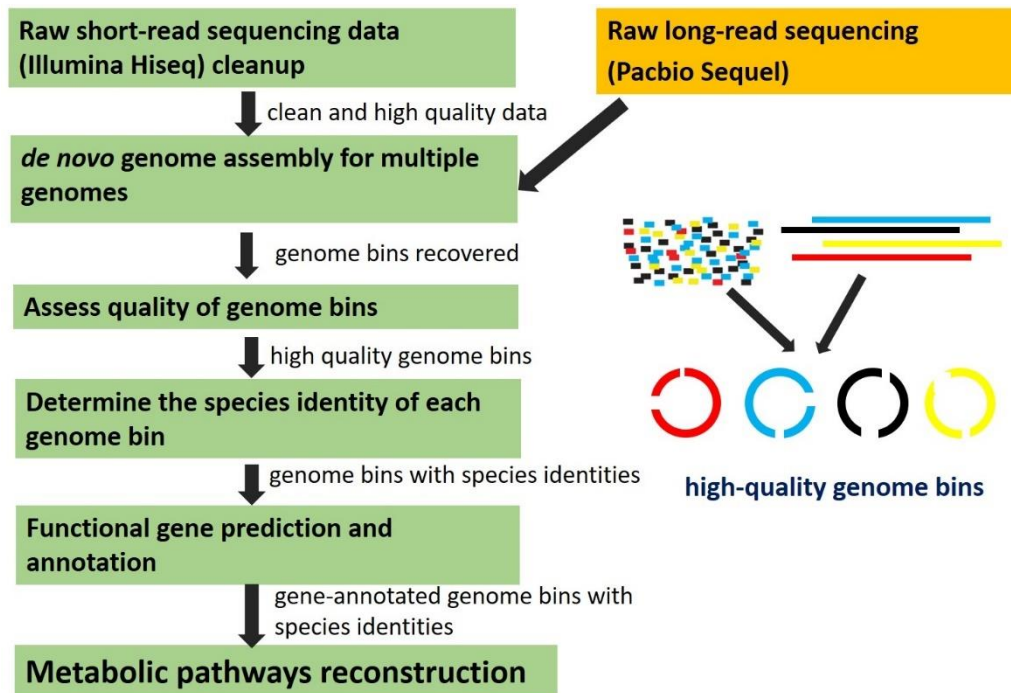


Figure 3-7. Illustration of metagenomics analysis pipeline via hybrid *de novo* assembly.

3.6.3 Metatranscriptomic analysis

For metatranscriptomics analysis, the raw reads were first trimmed with a minimum quality cutoff of 3, and further screened to be at least 50 bp in length, having an average quality score >30 and containing less than 3 ambiguous nucleotides (N's) using trimmomatic (Bolger et al., 2014). Assembly was performed on the paired-end trimmed reads using Trinity (Grabherr et al., 2011). Afterward, Sequence Expression AnaLyzer (Seal) in the BBTools suite was used to map the assembled metatranscriptomic file against the recovered high-quality genome bins generated from metagenomic analysis pipeline under “ambig modes” (Bushnell). Genes expression level was evaluated based on generated Reads Per Kilobase Million (*RPKM*) and calculated as \log_2 *RPKM* values.

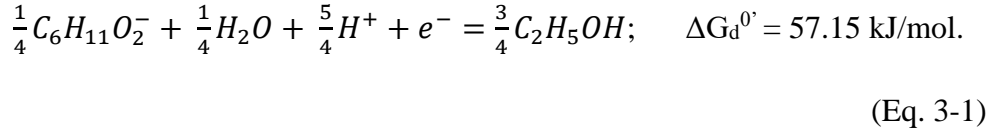
3.7 Microbial kinetics calculation

In the initial stage of fermentation (time < 10 days), growth rate of bacteria that utilizes ethanol as the electron donor and converts into caproate was estimated. The approaches for developing the overall reaction for caproate production and cell growth were modified from Thermodynamic Electron Equivalents Model (TEEM) developed by Rittmann & McCarty (Rittmann & McCarty, 2001). Half-reactions for electron donor (ethanol) and acceptor (acetate) were developed to establish redox reaction for energy harvesting. Then cell synthesis reaction with ethanol as electron donor was included to complete the stoichiometry of biological caproate production. When utilizing the electron-donor substrate, a portion of the electron is transferred to electron acceptor for cell maintenance (f_e), and the rest is used for cell synthesis (f_s). Energy transfer efficiency (ϵ) determines the portions of electron flow by considering energy released by the energy reaction and energy required to supply cell synthesis. By combining proper proportions of the energy reaction and synthesis reaction, an overall reaction for cell growth to estimate microbial kinetics was obtained. Afterward, true yield (Y) was obtained based on stoichiometry of the overall reaction. At 20°C, the maximum electron flow to energy reaction, \hat{q}_e , is about 1 e⁻ eq/gVSS-d. The maximum specific rate of substrate utilization \hat{q} can be computed from $\hat{q} = \hat{q}_e / f_e$.

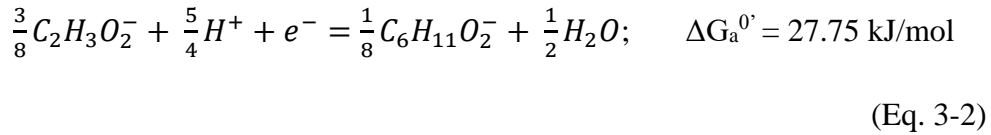
Half reactions for an electron donor (R_d) and an electron acceptor (R_a) were integrated to produce an energy reaction (R_e) with its associated Gibbs free

energy (ΔG_r). Half reactions for electron donor and cell synthesis (R_c) can be combined to produce the synthesis reaction (R_s), from which the Gibbs free energy for synthesis (ΔG_s) is derived. All reactions described in the calculation were written on one-electron-equivalent basis.

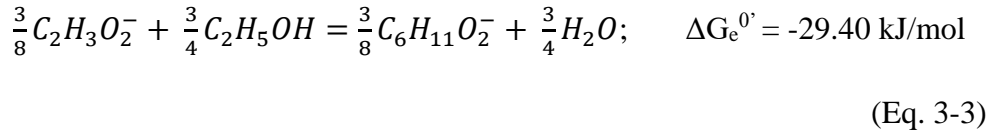
Half-reaction for electron donor ethanol (R_d):



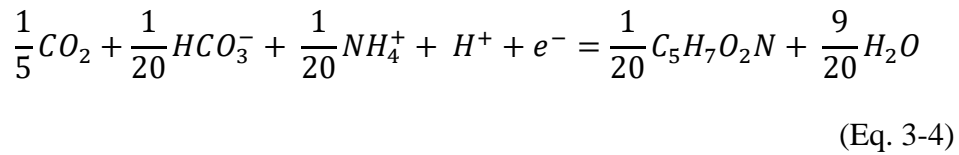
Half-reaction for electron donor acetate (R_a):



Energy reaction becomes $R_e = R_a - R_d$, written as:



The synthesis reaction becomes $R_s = R_c - R_d$. Cell synthesis equation (R_c):



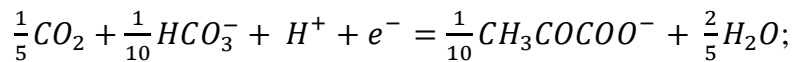
An overall reaction R for cell growth is obtained by combining proper proportion of the energy reaction and synthesis reaction. It is the summation of $f_s R_s$ and $f_e R_e$, expressed as $R = f_e R_a + f_s R_c - R_d$. The initial portions of electrons transferred to electron acceptor to provide energy and into microbial cells are assigned as f_e^0 and f_s^0 , respectively. The cell decay was assumed to be negligible in batch reactor, therefore $f_s^0 = f_s$

and $f_e^0 = f_e$ can be employed. Their values can be computed by $f_s^0 = \frac{1}{1+A}$, and $f_e^0 = 1 - f_s^0$. The proportions depend upon the energy transfer efficiency (ϵ) and is represented by A, a value that is obtained by consideration of the energy released by the energy reaction and equivalents of electron donor required to supply energy to synthesize an equivalent of cells. It is defined that A equivalents of electron donor must be oxidized to supply the amount of energy required to synthesize an equivalent of cells. The energy released by this oxidation is $A\Delta G_r$, where ΔG_r is the free energy released per equivalent of donor oxidized for energy generation. An energy balance must be maintained, therefore resulted in:

$$A \epsilon \Delta G_r + \Delta G_s = 0 \quad (\text{Eq. 3-5})$$

ΔG_r is determined based on the half reaction reduction potentials of the electron acceptor (ΔG_a) and the electron donor (ΔG_d) (Madden et al.), and their respective stoichiometric coefficients, ν_i . In our case, $\Delta G_r^0 = \Delta G_a^0 - \Delta G_d^0 = -29.40$ kJ/mol. The standard Gibbs free energy of each reaction was calculated using the equation: $\Delta G = \sum \Delta G_f^0 \text{ products} - \sum \Delta G_f^0 \text{ reactants}$, and the values of standard Gibbs free energy used in this study referred to Amend's table (Amend & Shock, 2001).

The half-reaction for pyruvate is:



$$\Delta G_e^0 = 35.09 \text{ kJ/mol.}$$

(Eq. 3-6)

The energy required to convert the carbon source to pyruvate is ΔG_p , and $\Delta G_p = 35.09 - \Delta G_c^0 = 35.09 - 57.15 = -22.06$ kJ/mol. The energy required

converting pyruvate carbon to cellular carbon ΔG_{pc} is based on an estimated value of 3.33 kJ per gram cells (McCarty, 1971), and $\Delta G_{pc} = 3.33 \cdot 5.65 = 18.8$ kJ/ e^- eq for the case with ammonium as nitrogen source. The energy requirement for cell synthesis becomes:

$$\Delta G_s = \frac{\Delta G_p}{\varepsilon^n} + \frac{\Delta G_{pc}}{\varepsilon} \quad (\text{Eq. 3-7})$$

If ΔG_p for some electron donors is negative, meaning energy is obtain by its conversion to pyruvate, and for this case, $n = -1$, and vice versa.

Then A can be solved by:

$$A = -\frac{\frac{\Delta G_p}{\varepsilon^n} + \frac{\Delta G_{pc}}{\varepsilon}}{\varepsilon \Delta G_r} \quad (\text{Eq. 3-8})$$

the transfer efficiency ε , is usually in the range of 0.55 to 0.7. In this case, a value of 0.6 was assumed. Therefore:

$$A = -\frac{\frac{-22.06}{0.6^{-1}} + \frac{18.8}{0.6}}{0.6 * (-29.40)} = 1.026 \quad (\text{Eq. 3-9})$$

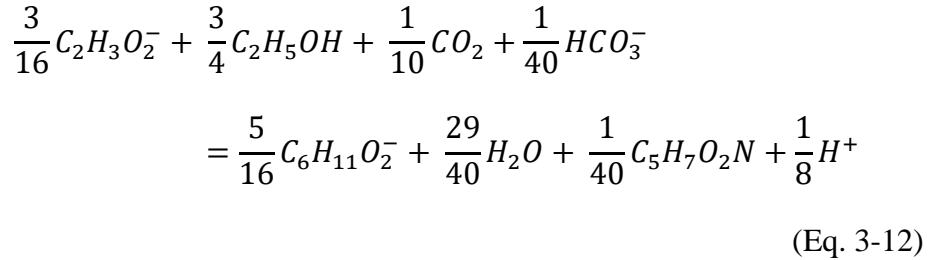
$$f_s^0 = \frac{1}{1 + A} = 0.494 \quad (\text{Eq. 3-10})$$

$$f_e^0 = 1 - f_s^0 = 0.506 \quad (\text{Eq. 3-11})$$

$f_s^0 \approx 0.5$ & $f_e^0 \approx 0.5$ were applied in the following calculation. Since the bacteria of interest utilizes ethanol as electron donor and acetate as electron

acceptor for energy production as well as for biomass synthesis, the energy reaction and cell synthesis reaction were supposed to be the same for all experimental groups, resulting in the same f_s^0 and f_e^0 .

Whole equation R is written as:



The true yield (Y) was obtained based on stoichiometry of the overall reaction:

$$Y = \frac{\frac{1}{40} * 113 \text{ g cell/mol}}{\frac{3}{4} * 46 \text{ g ethanol/mol}} = 0.082 \text{ g cell/g ethanol}$$

(Eq. 3-13)

At 20°C, the maximum flow to the energy reaction, \hat{q}_e , is about 1 e⁻ eq/gVSS-d.

$$\hat{q}_e = 1 \frac{e^- \text{ eq}}{gVSS - d} = \frac{\frac{3}{4} \text{ mol ethanol} * 116 \frac{g}{mol}}{gVSS - d} = 34.5 \frac{g \text{ ethanol}}{g VSS - d}$$

(Eq. 3-14)

The maximum specific rate of substrate utilization \hat{q} can be computed from

$$\hat{q} = \hat{q}_e / f_e^0:$$

$$\hat{q} = \hat{q}_e / f_e^0 = 69 \frac{g \text{ ethanol}}{g VSS - d}$$

(Eq. 3-15)

The influence of temperature on \hat{q} can be approximated by $\hat{q}_T = \hat{q}_{20}(1.07)^{T-20}$. At 37°C:

$$\hat{q}_T = \hat{q}_{20}(1.07)^{T-20} = 69 * (1.07)^{37-20} \frac{g \text{ ethanol}}{g \text{ VSS} - d} = 218 \frac{g \text{ ethanol}}{g \text{ VSS} - d}$$

(Eq. 3-16)

Electron donor, ethanol, was the rate-limiting substrate in this case. Other bacterial requirements, such as electron acceptor and nutrients, were supplied with high enough concentration, and were assumed to impose no limitations on the bacterial growth. The growth rate of organisms was assumed to follow the Monod kinetics, and decay was negligible. For batch growth in which organism decay is a small factor while the microorganisms are growing rapidly, also, only growth rate of the initial stage (<10 day) was discussed (growing phase), therefore this is a satisfactory assumption. The fermentation was operated in a batch mode. Mass balance for substrate is written as:

$$\frac{dS}{dt} = -\frac{\hat{q} S}{K + S} X_a$$

(Eq. 3-17)

Mass balance for microorganisms is expressed as:

$$\frac{dX_a}{dt} = \left(\hat{q} \frac{YS}{K + S} - b \right) X_a$$

(Eq. 3-18)

and $X_a = X_a^0 + Y(S^0 - S)$.

If re-write the equation of Eq. 3.18, the below equation is obtained:

$$\frac{dS}{dt} = -\frac{\hat{q} S}{K + S} [X_a^0 + Y(S^0 - S)]$$

(Eq. 3-19)

After integration:

$$t = \frac{1}{\hat{q}} \left\{ \left(\frac{K}{X_a^0 + YS^0} + \frac{1}{Y} \right) \ln(X_a^0 + YS^0 - YS) - \left(\frac{K}{X_a^0 + YS^0} \right) \ln \left(\frac{SX_a^0}{S^0} \right) - \frac{1}{Y} \ln X_a^0 \right\}$$

(Eq. 3-20)

Therefore, in batch reactor, based on mass balance of substrate and the relationship between biomass and substrate utilization, $X_a = X_a^0 + Y(S^0 - S)$, the integrated equation can be rearranged as:

$$\hat{q} = \frac{1}{t} \left\{ \left(\frac{K}{X_a^0 + YS^0} + \frac{1}{Y} \right) \ln(X_a^0 + YS^0 - YS) - \left(\frac{K}{X_a^0 + YS^0} \right) \ln \left(\frac{SX_a^0}{S^0} \right) - \frac{1}{Y} \ln X_a^0 \right\}$$

(Eq. 3-21)

where t is time (T); K is concentration giving one-half the maximum rate ($M_S L^{-3}$); X_a and X_a^0 are concentration of active biomass in the end and initial stage of batch experiment, respectively ($M_X L^{-3}$); S is concentration of the rate-limiting substrate ($M_S L^{-3}$); superscript 0 represents the initial state.

The most variable parameter, K , was highly affected by environmental conditions and hypothesized to vary in different experimental groups, also keep changing as the fermentation process proceed. The initial concentration of limiting-substrate, S^0 , and its concentration at time t , S , were known. The value of K was computed according to the four

experiments at certain time using Eq. 3-21, together with concentration of ethanol, to further estimate growth rate μ with the Monod equation:

For all the batch experiments, $X_a^0 = 50$ mg VSS/L was fixed for all experimental groups. Parameters Y and \hat{q} , estimated from microbial energetics and stoichiometry, remained consistent for all experimental groups, because their determining factors, bacterial type and temperature, were invariable in this case. The most variable parameter, K , was highly affected by environmental conditions and hypothesized to vary in different experimental groups, also keep changing as the fermentation process proceed. The initial concentration of limiting-substrate, S^0 , and its concentration at time t , S , were knowns. Accordingly, the value of K was computed according to the four experiments at certain time using Eq. 3-21. Afterwards, by combining the detected concentration of limiting substrate - ethanol, growth rate μ can be estimated with Monod equation.

$$\mu = Y \frac{\hat{q} S}{K + S}$$

(Eq. 3-22)

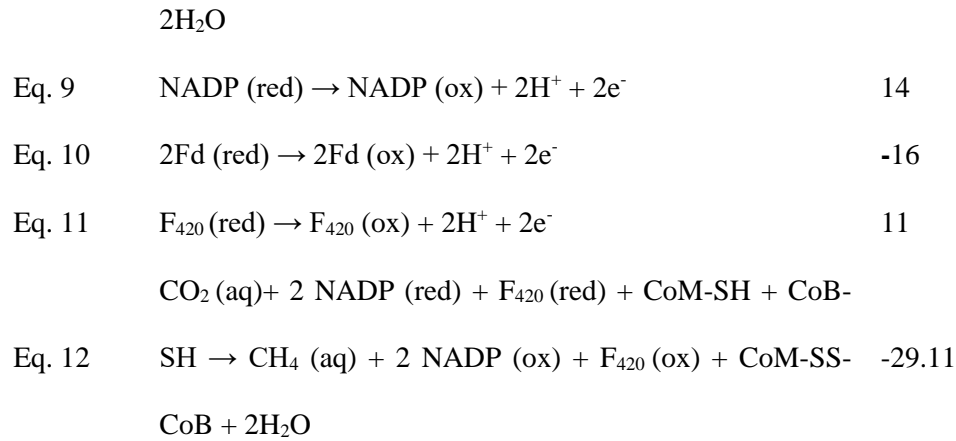
3.8 Thermodynamics calculation of biochemical reactions

To estimate ΔG^0 of two reactions reducing CO_2 into methane, the reactions of each step were written and the corresponded ΔG^0 of each step reactions were calculated (at 298 K, pH 7.0 and all compounds at 1 molar activity) (Table 3-2) (Thauer, Kaster, Seedorf, Buckel, & Hedderich, 2008). Summing up Eq.1 – Eq.7 resulted in an overall reaction of classical CO_2

reduction, Eq. 8, and $\Delta G^{0'}$ of the reaction was obtained by summing up the values from Eq.1 to Eq.7. Considering the differences of electron carriers involved in classical CO₂ reduction pathway and RHP pathway, the overall reaction of RHP pathway was modified based on the classical CO₂ reduction reaction by including the involved electron carriers and excluding the uninvolved ones. Specifically, Eq. 9 - Eq. 11 in Table 3-2 are half reactions of electron carriers, and the reaction of CO₂ reduction via RHP pathway, Eq. 12 = Eq. 8 + 2 * Eq. 9 - Eq. 10 - Eq. 11, was obtained subsequently.

Table 3-2. The step reactions involved in classical CO₂ reduction, half reactions of electron carriers and their standard Gibbs free energy changes ($\Delta G^{0'}$) at 298 K, pH 7.0 and all compounds at 1 molar activity.

Reaction number	Reaction	$\Delta G^{0'}$ (kJ/mol)
Eq. 1	$\text{CO}_2 (\text{aq}) + \text{MFR} + 2 \text{Fd}_{\text{red}}^{2-} + 2 \text{H}^+ \rightarrow \text{CHO-MFR} + 2 \text{Fd}_{\text{ox}} + \text{H}_2\text{O}$	-8.16
Eq. 2	$\text{CHO-MFR} + \text{H}_4\text{MPT} \rightarrow \text{CHO-H}_4\text{MPT} + \text{MFR}$	-5
Eq. 3	$\text{CHO-H}_4\text{MPT} + \text{H}^+ \rightarrow \text{CH}\equiv\text{H}_4\text{MPT}^+ + \text{H}_2\text{O}$	-5
Eq. 4	$\text{CH}\equiv\text{H}_4\text{MPT}^+ + \text{F}_{420}\text{H}_2 \rightarrow \text{CH}_2=\text{H}_4\text{MPT} + \text{F}_{420} + \text{H}^+$	6
Eq. 5	$\text{CH}_2=\text{H}_4\text{MPT} + \text{F}_{420}\text{H}_2 \rightarrow \text{CH}_3-\text{H}_4\text{MPT} + \text{F}_{420}$	-6
Eq. 6	$\text{CH}_3-\text{H}_4\text{MPT} + \text{HS-CoM} \rightarrow \text{CH}_3-\text{S-CoM} + \text{H}_4\text{MPT}$	-30
Eq. 7	$\text{CH}_3-\text{S-CoM} + \text{HS-CoB} \rightarrow \text{CH}_4 (\text{aq}) + \text{CoM-S-S-CoB}$	-13.95
Eq. 8	$\text{CO}_2 (\text{aq}) + 2 \text{Fd} (\text{red}) + 2 \text{F}_{420} (\text{red}) + \text{CoM-SH} + \text{CoB-SH} \rightarrow \text{CH}_4 (\text{aq}) + 2 \text{Fd} (\text{ox}) + 2 \text{F}_{420} (\text{ox}) + \text{CoM-SS-CoB} +$	-62.11



3.8.1 MATLAB programs for thermodynamics calculation

The code below is designed to calculate the Gibbs free energy change of three reactions, acetoclastic methanogenesis, CO_2 reduction to methane, and CO_2 fixation via RHP pathway, as function of acetate concentration and partial pressure ratio of CH_4/CO_2 . As described in detail in Section 5.2.5.

```
# Step1: To calculate the contribution from different PCH4 and PCO2
CH4=[0.00064, 0.00076, 0.00089, 0.00102];
#aqueous concentrations of methane under PCH4 at 50%, 60%, 70% and 80%
CO2=[0.01498, 0.01199, 0.00899, 0.00599];
#aqueous concentrations of carbon dioxide under PCO2 at 50%, 40%, 30%
and 20%
R = 0.008314;
#gas constant
T= 298.15;
#temperature
for i=1:4
```

```
k(i)=R x T x ln ((CH4(i))*(CO2(i))); k(i) = R x T x ln((CH4(i)) x
(CO2(i))
```

```
end
```

```
#Step 2: To calculate  $\Delta G^0$  for acetoclastic methanogenesis at different
acetate concentrations and different  $P_{CH4}$  and  $P_{CO2}$ 
```

```
acetate=[0.00003,0.0003,0.003, 0.03, 0.3, 3];
```

```
#acetate concentrations
```

```
 $\Delta G^0_1$ =zeros((length(acetate), length(k)));
```

```
for j=1:length(k)
```

```
for h=1:length(acetate)
```

```
 $\Delta G^0_1$  (h,j)= (-24.84) + k(j) - R x T x ln(acetate(h))
```

```
end
```

```
end
```

```
#Step 3: To calculate  $\Delta G^0$  for the combined acetoclastic methanogenesis
and CO2 reduction pathway at different acetate concentrations and different
```

```
 $P_{CH4}$ 
```

```
 $\Delta G^0_2$ =zeros((length(acetate), length(CH4)));
```

```
for j=1:length(CH4)
```

```
for h=1:length(acetate)
```

```
 $\Delta G^0_2$  (h,j)= (-62.1 - 24.84) + R x T x ln((CH4(j)) x (CH4(j))) -
R x T x ln(acetate(h))
```

```
# $\Delta G^0$  for the combined acetoclastic methanogenesis and electron-dependent
CO2 reduction reaction
```

```
end
```

```

end
ΔG03=zeros((length(acetate), length(CH4)));
for j=1:length(CH4)
for h=1:length(acetate)
ΔG03 (h,j)= (-29.1 - 24.84) + R × T × ln((CH4(j)) × (CH4(j))) -
R × T × ln(acetate(h))
#ΔG0 for the combined acetoclastic methanogenesis and RHP pathway
end
end
end

```

4. Chapter 4 Microbial communities of two methanogenic SAF-CMBR system using conductive GAC and non-conductive PET beads as biofilm carriers

4.1 Overview

In anaerobic membrane bioreactors for wastewater treatment, granular activated carbon (GAC) particles are often added and fluidized by bulk recirculation through the membrane reactor to control membrane fouling. The GAC particles can provide not only high specific surface area for biofilm formation but also mechanical cleaning to reduce fouling on membrane (Kim et al., 2011). Besides, an alternative cost-effective material, polyethylene terephthalate (PET) beads are used in the anaerobic digestion systems as biofilm carriers (Marti-Herrero et al., 2014). While it is expected that GAC particles play a critical role in promoting interspecies electron transfer in anaerobic environment due to their conductive properties (F. Liu et al., 2012; J. X. Zhang et al., 2017; S. Zhang et al., 2017). The effects of these fluidized media on membrane fouling and energy consumption in the anaerobic fluidized membrane bioreactor (AFMBR) were evaluated previously (Aslam, McCarty, Bae, & Kim, 2014). Besides, different biofilm carriers would affect the AFMBR systems in all kinds of respects, such as microbial distribution, biofilm development, or even organic removal.

To evaluate the effects of different biofilm carriers, specifically GAC particles and PET beads, on the systems, two novel staged anaerobic fluidized bed ceramic membrane bioreactor (SAF-CMBR) systems for low-

strength wastewater treatment were operated under similar operation conditions. Their performance, in terms of organic removal, microbial distribution and biofilm development in the two systems treating low-strength wastewater are assessed (Aslam, Yang, Lee, & Kim, 2018) (Aslam, Yang, Lee, & Kim, 2018, unpublished work). As shown in Fig. 4-1, the first system is an SAF-CMBR with GAC as biofilm carrier, and the anaerobic fluidized bed bioreactor (AFBR) was followed by an anaerobic fluidized bed ceramic membrane bioreactor (AFCMBR). Another SAF-CMBR uses different fluidized biofilm carriers. As shown in Fig. 4-2, followed the AFBR, two AFCMBRs were operated in parallel and used GAC and PET beads, respectively, as fluidized biofilm carriers for a comparative study. During the long-term operation of the two SAF CMBR systems, the feed to the AFBR consisted mainly of an equal chemical oxygen demand (COD) mixture of sodium acetate and sodium propionate with a total COD concentration of 250 mg/L. A 0.096 g/L of NH_4Cl and 10 mL/L of anaerobic digester supernatant taken from a local wastewater facility were also added as sources of nutrients (Aslam et al., 2018; Kim et al., 2011).

In this chapter, the microbial communities of the two systems are compared. In the first SAF-CMBR system with GAC as carries, microbial communities developed in both GAC particles and bulk suspensions in the membrane reactor were analyzed. It was revealed that anaerobic treatment was achieved mainly by microbial communities grown on the GAC particles fluidized in which propionate-degrading syntrophs,

acetoclastic/DIET-dependent CO₂ reduction methanogens *Methanothrix* and exoelectrogenic *Geobacter* are dominated. The similar microbial composition was observed in the reactors fluidized with GAC in the second SAF-CMBR system. While the microorganisms responsible for propionate metabolization to methane were rarely enriched in the reactor with PET beads as carries in the same SAF-CMBR system.

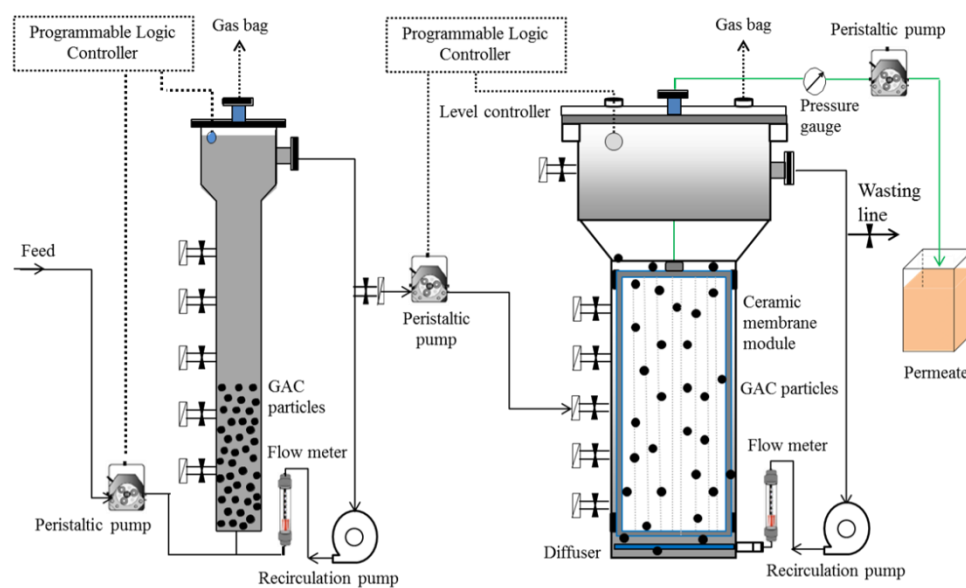


Figure 4-1. Schematic diagram of the staged anaerobic fluidized bed ceramic membrane bioreactor (SAF-CMBR) system (adopted from (Aslam et al., 2018)).

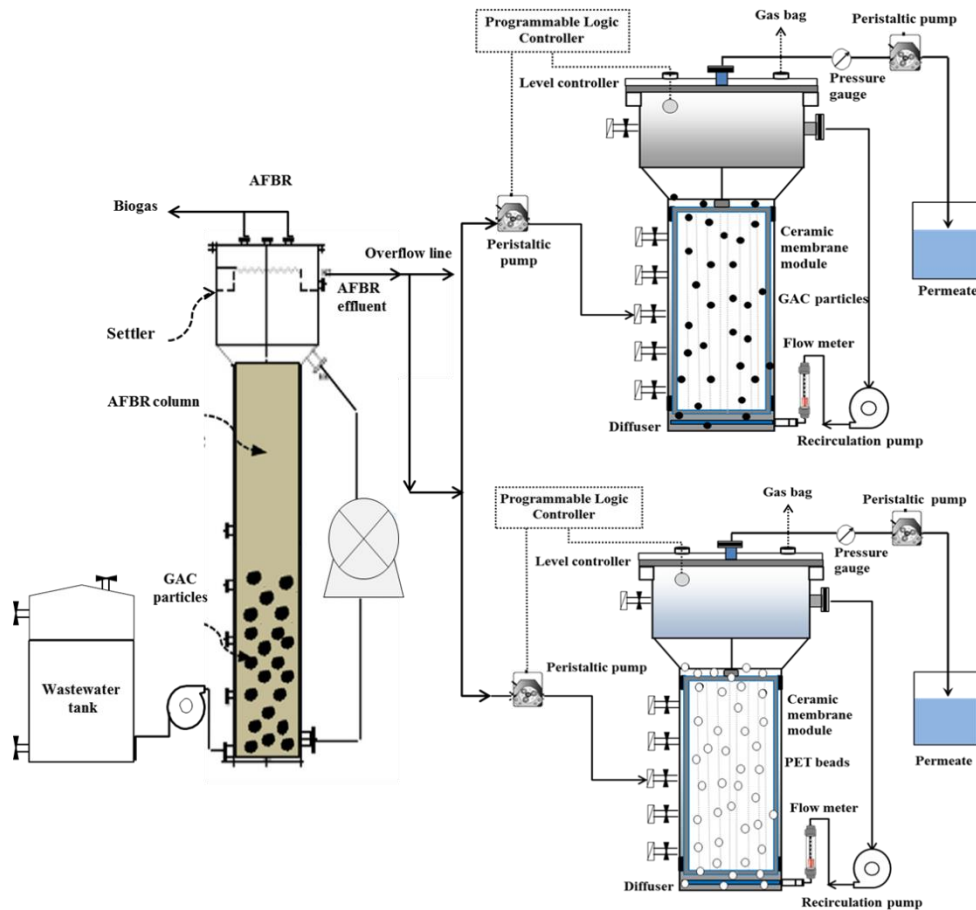


Figure 4-2. Schematic diagram of the staged anaerobic fluidized bed ceramic membrane bioreactor (SAF-CMBR) system with different biofilm carriers (GAC and PET beads) (adopted from an unpublished work (Aslam et al., 2018)).

4.2 Results and discussion

4.2.1 Microbial community of the SAF-CMBR with GAC as carrier

As shown in Fig. 4-1, in the SAF-CMBR system, an anaerobic fluidized bed bioreactor (AFBR) was followed by an anaerobic fluidized bed ceramic membrane bioreactor (AFCMBR) with GAC as biofilm carrier. Biofilm layer attached on the fluidized GAC particles and biomass suspended in the bulk liquid were collected from both AFBR and AFCMBR reactors for characterizing microbial community on day 162, at which extremely short HRT less than 1.5 h was applied. Beta diversity analysis revealed that the two microbial communities on GAC particles were similar and noticeably different from those of the bulk liquid (Fig. 4-3). At phylum level, Proteobacteria, Bacteroidetes and Firmicutes were identified with high abundances in both bulk and GAC samples (Fig. 4-4), and this is similar to the observation of other two-stage AFBR system (B. Wu et al., 2017). The predominant group, Proteobacteria, especially in the bulk samples, are associated with the development of biofilms on the fluidized GAC particles (B. Wu et al., 2017). Similarly, it was proposed in the previous study that Firmicutes enriched in anaerobic membrane bioreactor (AnMBR) accelerates biofouling (Gao et al., 2010; Ma, Wang, Zou, Feng, & Wu, 2013). While the archaeal population, Euryarchaeota, was identified to be dominant in the two GAC communities only (29.3% in AFBR GAC and 38.9% in AFCMBR GAC), suggesting that methane production was attributed to the microbes attached on GAC particles.

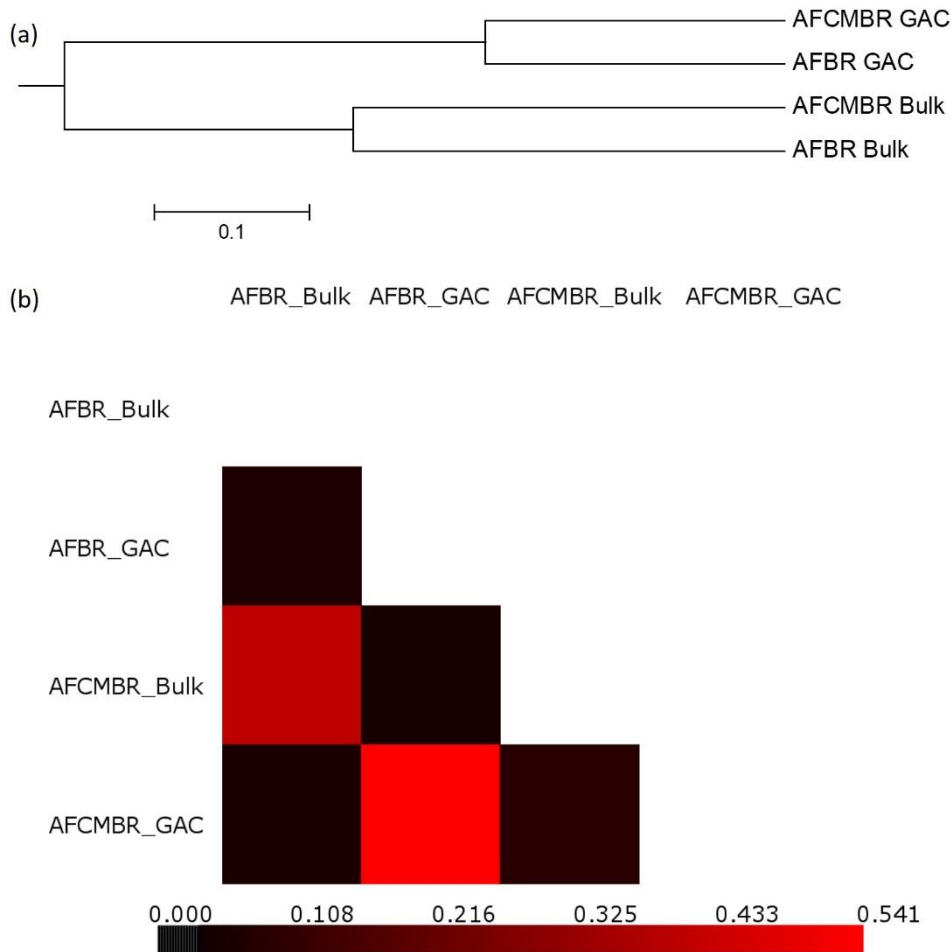


Figure 4-3. Beta diversity analysis (a) Dendrograms describing the similarity of the microbial communities of the samples to each other; (b) Braycurtis heat map at distance 0.03.

As shown in Fig. 4-4, at phylum level, the bulk communities were highly dominated by *Pseudomonas*, which produce exopolysaccharides associated with biofilm formation. While the functional groups of microorganisms responsible for methane production, syntrophic bacteria and methanogens, were low in abundances in the bulk suspension. The methanogenic group mainly consisted of four genera in the system, *Methanotherix* (*Methanosaeta*), *Methanoregula*, *Methanolinea* and *Methanobacterium*.

Particularly, *Methanothrix* were highly enriched in two GAC samples (21.0% and 23.4% of the total microbial population in AFBR and AFCMBR, respectively), and such dominance was also observed in other AFMBR system (LaBarge et al., 2016). *Methanothrix* is acetoclastic methanogen with a high affinity for acetate and have the potential to accomplish CO₂ reduction pathway (K. S. Smith & Ingram-Smith, 2007). Acetate contained in the feed and produced from syntrophic propionate oxidizing bacteria (SPOB) greatly contributed to the dominance of *Methanothrix*. Syntrophic bacteria accounted for a large proportion of the microbial population in two GAC samples, and the top two abundant groups, *Syntrophobacter* and *Smithella*, are both SPOB who grow on propionate in syntrophic association with hydrogenotrophic methanogens and produce acetate and hydrogen gas. *Syntrophobacter* degrade propionate using methylmalonyl-CoA (MMC) pathway adopted by most SPOB (Müller, Worm, Schink, Stams, & Plugge, 2010). While *Smithella* use a distinctly different pathway which degrade propionate via butyrate and result in higher acetate and lower hydrogen production compared to MMC pathway (Frank AM de Bok et al., 2001). Based on thermodynamic and energetic estimation (J. Dolfing, 2013), propionate degradation via the *Smithella* pathway would be exergonic under wider range of conditions and less sensitive toward H₂ than MMC pathway. *Geobacter* and sulfate reducing bacteria (SRB), *Desulfobulbus* enriched on GAC particles can transfer electrons exocellularly, even without mediators (Holmes, Bond, & Lovley, 2004; F. Liu et al., 2012). High electrical conductivity of GAC particles was hypothesized to stimulate direct interspecies electron transfer (DIET)

between *Geobacter* and methanogens and enhanced methane production indirectly (F. Liu et al., 2012). It was revealed that *Geobacter* can donate electrons to *Methanotherix* species to support CO₂ reduction via DIET (Holmes et al., 2017; S. Zhang et al., 2017), which facilitates energy recovery in the form of methane from the system.

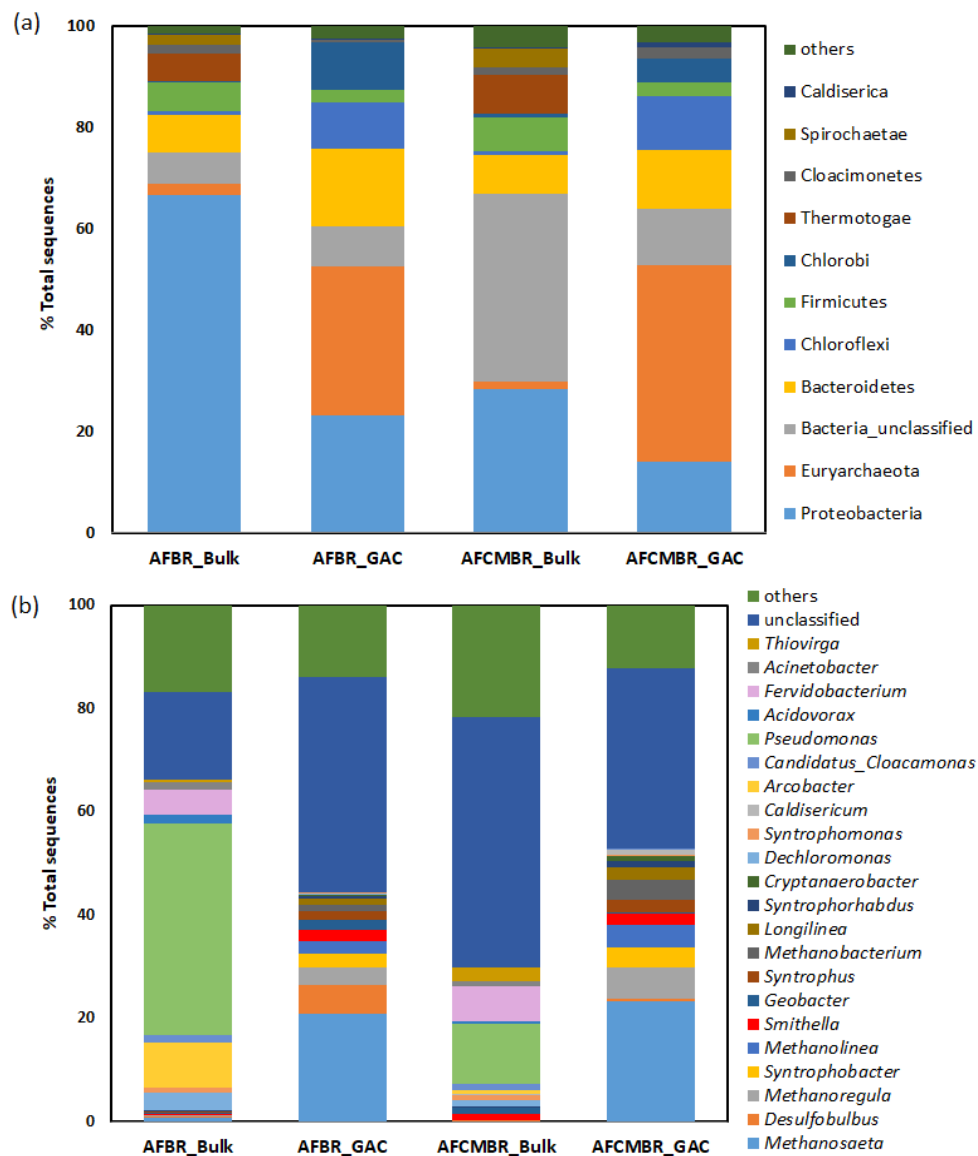


Figure 4-4. Taxonomic classification of the communities displaying both bacteria and archaea developed on fluidized GAC and bulk suspension (collected on day 162); (a) at phylum level; (b) at genus level.

* Phylum or genus occurred at abundance more than 1 % in at least one sample was annotated whereas rests were grouped as “others”.

4.2.2 Microbial community of the SAF-CMBR with different biofilm carriers: PET beads and GAC

The SAF-CMBR uses different fluidized biofilm carriers, as shown in Fig. 4-2. Following an AFBR with GAC as carrier, two AFCMBRs were operated in parallel and used GAC and PET beads, respectively, as fluidized biofilm carriers. In the three reactors, biomass suspended in the bulk, as well as biofilm layer attached on the fluidized carriers, GAC particles and PET beads, were collected for microbial community characterization on the Day 135 of operation. However, since there was no inner-pores for microbes to attach in the PET beads, effective fluidization washed off most of the attached biomass on them. Therefore, genomic DNA was not collected successfully on the PET beads due to limited biofilm attached. For the other five samples, it was found that microbial communities on the two GAC particles share high similarity while differed greatly from the three of bulk liquid based on the Beta diversity analysis (Fig 4-5). The taxonomic distribution in Fig. 4-6 shows the five microbial communities at phylum level (Fig. 4-6a) and genus level (Fig. 4-6b). Generally, Proteobacteria and Bacteroidetes were the most predominated phyla in all these communities, and Proteobacteria is closely correlated to the growth of biofilms on the fluidized carriers (B. Wu et al., 2017). Whereas Euryarchaeota, mostly methanogens attributing to methane production, mainly predominated in the two GAC communities (18.54% of

the total microbial population in AFBR_GAC and 24.15% in AFCMBR_GAC) (Fig. 4-6a) and poorly enriched in the AFCMBR_PET reactor. It implied that the microorganisms aggregated on GAC particles contributed to methane production from the system. The similar microbial community patterns are also observed in the previous analysis of SAF-CMBR in section 4.2.1 and other studies (Aslam et al., 2018; Gao et al., 2010; Ma et al., 2013).

At genus level, microbial communities of the three bulk samples were distinctly predominated by the exopolysaccharide-producing bacteria *Pseudomonas*, which facilitated biofilm formation on the surface of carriers (Fig. 4-6b). Whereas in the communities of GAC samples, syntrophic propionate oxidizing bacteria (SPOB), *Syntrophobacter* and *Smithella*, acetoclastic methanogen, *Methanothrix* and exoelectrogenic bacteria, *Geobacter* predominated and formed a metabolic network with close interactions. Primarily, the SPOB, *Syntrophobacter* and *Smithella*, were responsible to degrade propionate into acetate (F. A. de Bok et al., 2001; Müller et al., 2010). Moreover, to accomplish the bioconversion from propionate to CH₄ and CO₂, SPOB need to grow under an obligate syntrophic association with the acetoclastic methanogen *Methanothrix*. On the other hand, the methanogenesis step would be promoted by the syntrophic cooperation with *Geobacter* via direct interspecies electron transfer (DIET) attributed to the electric conductivity of GAC (Holmes et al., 2004; F. Liu et al., 2012). The microbial communities developed on the GAC samples and their main microbial interactions were similar to the

finding discussed in Section 4.2.1. While the community developed in the AFCMBR with PET was distinctly different. The microbial groups responsible for methane production, SPOB and methanogens, were poorly enriched in the AFCMBR_PET. Instead, it was mainly predominated by *Pseudomonas* associated with biofilm formation and two groups of exoelectrogenic bacteria, *Geobacter* and *Arcobacter*. These two exoelectrogenic bacteria can transfer electrons to extracellular electron acceptors and feed on acetate as substrates (Fedorovich et al., 2009).

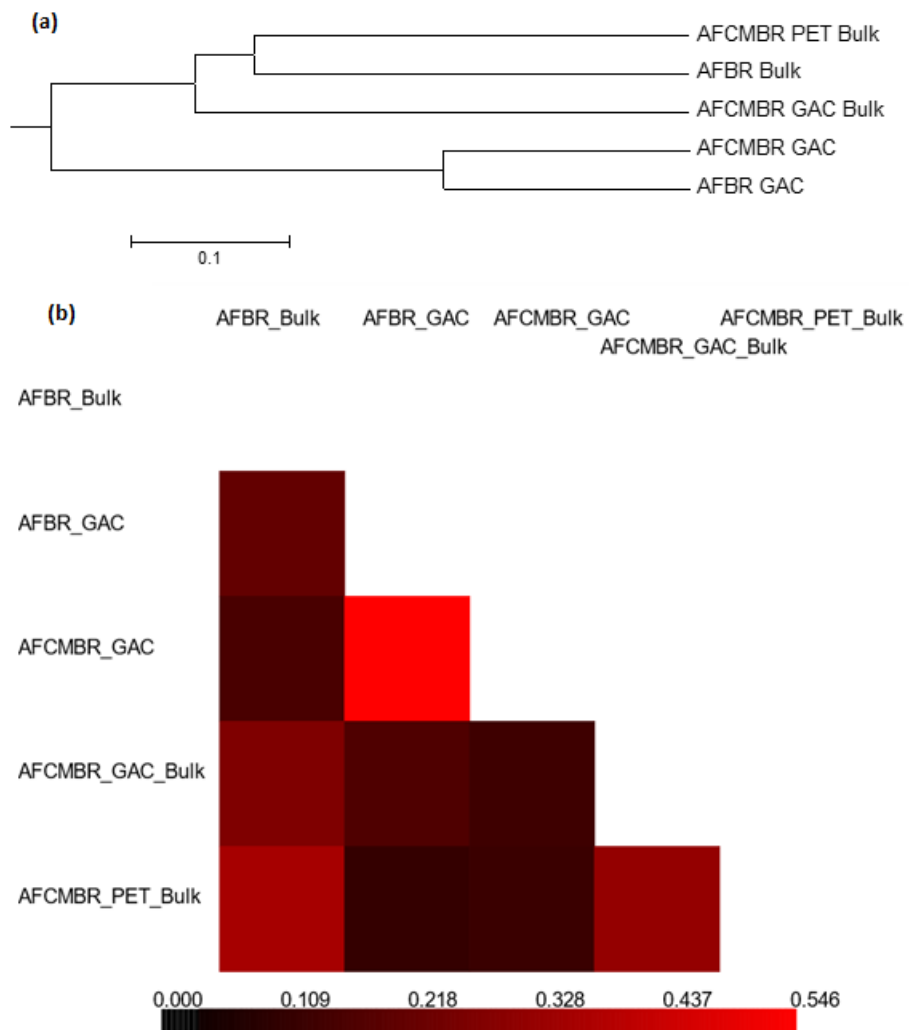


Figure 4-5. Beta diversity analysis (a) Dendrograms describing the similarity of the microbial communities of the samples to each other; (b) Thetayc heat map at distance 0.16.

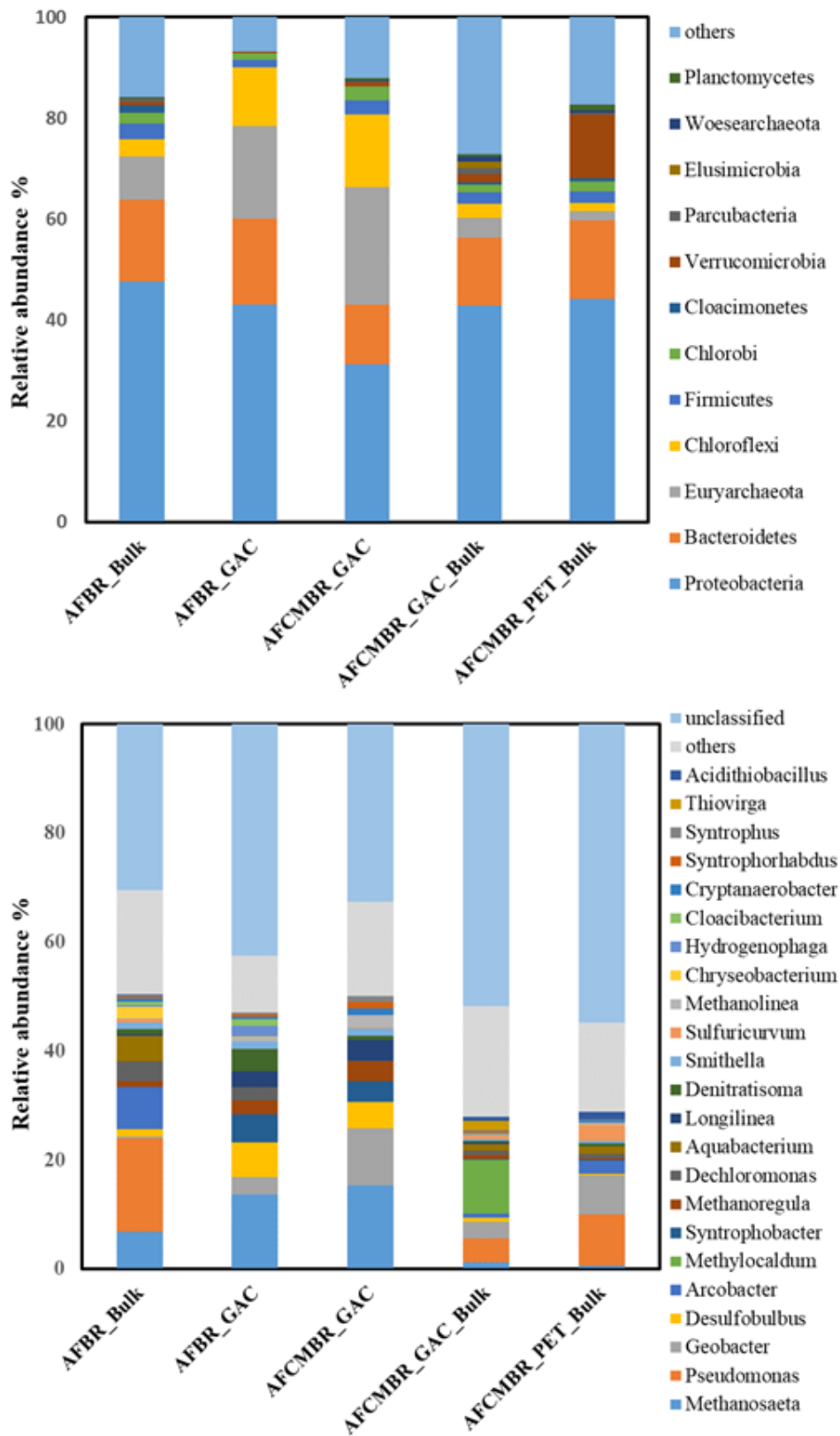


Figure 4-6. Taxonomic classification of the microbial communities displaying both bacteria and archaea developed on the biomass carriers and

bulk (collected on day 135): (a) at phylum level; (b) at genus level. Phylum or genus occurred at abundance more than 1 % in at least one sample was annotated whereas the rest were grouped as “others”.

4.3 Chapter summary

This chapter reports the microbial communities of two staged anaerobic fluidized bed ceramic membrane bioreactor (SAF-CMBR) systems using different fluidizing media, conductive GAC and non-conductive PET beads. The biomass suspended in the bulk and biofilm attached on the GAC/PET beads were taken, respectively. The result indicates that GAC is a more selective environment for microorganisms, particularly syntrophic propionate oxidizing bacteria (SPOB) and methanogens, than the bulk liquid for methane production. In both systems, and all the four reactors using GAC as fluidizing media, the microbial communities were predominated by SPOB (*Syntrophobacter* and *Smithella*), acetoclastic/DIET-dependent CO₂ reduction methanogens *Methanotherix* and exoelectrogenic bacteria, *Geobacter*. Although there were two AFCMBRs operated in parallel, the microbial community developed in the one with PET beads significantly differed from those in the reactors with GAC. The AFCMBR with PET beads was predominated by *Pseudomonas* associated with biofilm formation and two groups of exoelectrogenic and acetate-utilizing bacteria, *Geobacter* and *Arcobacter*. While the primary microbial groups responsible for methane production, SPOB and methanogens, were barely enriched.

5. Chapter 5 Metatranscriptomic evidence for classical and RuBisCO-mediated CO₂ reduction to methane facilitated by direct interspecies electron transfer in a methanogenic system

5.1 Overview

Methanogenesis is accomplished by the syntrophic microbial interactions via interspecies electron transfer (IET), which was traditionally considered to be accomplished through diffusive carriers (e.g. acetate, hydrogen and formate). The physical distance between microbes and the diffusion rate of electron carriers hinder this form of mediated IET (MIET) (Leng et al., 2018). While direct interspecies electron transfer (DIET) can overcome such bottleneck therefore enhancing energy methane production rate (Cruz Viggi et al., 2014; F. H. Liu et al., 2012). DIET is achieved by shuttling electrons exogenously from exoelectrogens to methanogens through conductive pili or surfaces (F. H. Liu et al., 2012; Shrestha et al., 2013). The addition of conductive materials, such as GAC, was recently found to be able to enhance DIET during syntrophic methanogenesis (A.-E. Rotaru, P. M. Shrestha, F. Liu, B. Markovaite, et al., 2014).

The examination of microbial community in the SAF-CMBR system with GAC as biofilm carrier, as discussed in Chapter 4, revealed that it is an ideal system for investigating syntrophic microbial interactions. On one hand, propionate- and acetate-fed (250 mg COD L⁻¹) are the key precursors of methanogenesis, driving IET in energy-limited methanogenic systems (F.

A. M. de Bok, C. M. Plugge, & A. J. M. Stams, 2004; P. L. McCarty, 2001; Müller et al., 2010). Importantly, we observed the co-dominance of syntrophic propionate oxidizing bacteria (SPOB), *Syntrophobacter* and *Smithella*, acetoclastic methanogen *Methanothrix*, and exoelectrogen *Geobacter* on the GAC particles, suggesting that GAC plays an electrically conductive material for promoting DIET in the SAF-CMBR (Aslam et al., 2018). Nevertheless, the metabolic interactions, possibly facilitated by DIET and particularly between *Methanothrix* and *Geobacter* have yet to be fully understood.

Competition may occur between *Methanothrix* and *Geobacter* as both species utilize acetate for methanogenesis and respiration, respectively (Patel & Sprott, 1990; Sung et al., 2006). However, synergetic interaction between these two microbes is also possible. Most interestingly, while *Methanothrix* is unable to perform hydrogentrophic methanogenesis using CO₂ due to the absence of a hydrogen uptake mechanism (Berg et al., 2010), it can form syntrophic association, termed ‘electric syntrophy’, with *Geobacter* to achieve methane production, in a similar fashion to hydrogentrophic methanogenesis, through DIET-dependent CO₂ reduction (Kato et al., 2012a; Morita et al., 2011a). On the other hand, Kono et al. (2017) recently have uncovered a ribulose-1,5-bisphosphate carboxylase/oxygenase (RuBisCO)-mediated CO₂ fixation pathway in many methanogen species including *Methanothrix*, which could reduce CO₂ into various carbon intermediates for important metabolic pathways, such as gluconeogenesis and glycolysis (Kono et al., 2017). This newly-

discovered pathway, termed “reductive hexulose-phosphate (RHP) pathway”, is analogous to the Calvin–Benson cycle in plant photosynthesis, raising our hypothesis that it could be electron-driven (i.e., DIET). Additionally, this carbon fixation pathway has the potential to link with methanogenesis via a formaldehyde intermediate, leading to our speculation of a third methanogenesis route in *Methanotherix*.

In this chapter, the interspecies interactions, particularly between *Geobacter* and *Methanotherix*, on GAC surfaces in the SAF-CMBR are examined. By employing a combinatorial approach of metagenomics and metatranscriptomics sequencing, we intend to decipher the microbial interactions on the GAC, aiming to disclose potential methane formation pathways, facilitated by MIET and DIET, and their metabolic link in *Methanotherix*. The efficient and stable operation of methanogenic bioreactors relies heavily on syntrophic-driven IET mechanisms. A deeper understanding of such interactions is therefore critical to ultimately tie ecology to improvements in engineering operation and design.

High quality metagenome bins representing the predominating microbes syntrophic propionate-oxidizing bacteria (SPOB), *Syntrophobacter fumaroxidans* and *Smithella sp.*, acetoclastic *Methanotherix concilii*, and exoelectrogenic *Geobacter lovleyi*, were successfully recovered. Metabolic pathway reconstructions and metatranscriptomics mapping revealed that *M. concilii* and *G. lovleyi* competed for acetate only at substrate-level. With the facilitation of DIET, *M. concilii* received electrons from *Geobacter* and

reduced CO₂ into methane via both the classical CO₂ reduction and the reductive hexulose-phosphate (RHP) pathway, which were both metabolically linked with the acetoclastic methanogenesis. Complete acetate reduction to methane attributed to high methane yield from the system. The high activity of the anabolic RHP pathway enables the catabolic methane formation or versa in *M. concilii*, facilitating its dominance and enhancing energy yield. Such tight interactions, probably induced by the conductive GAC, promote the overall efficiency of bioenergy processes.

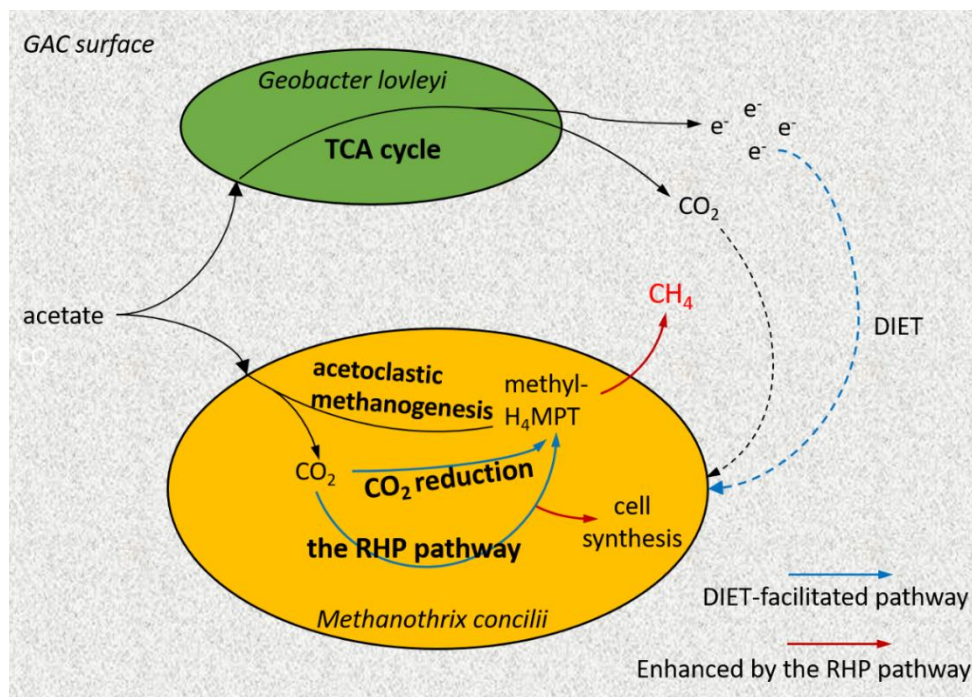


Figure 5-1. Metabolic interactions between *Methanotherx concilii* and *Geobacter lovleyi* in the SAF-CMBR system.

5.2 Results and discussion

5.2.1 Overview of the metagenome bin and metatranscriptomes

In total, around 313.8 million of 150 bp reads were obtained for the samples of AFBR GAC and AFCMBR GAC by paired-end sequencing on Illumina HiSeq platform (Table 5-1). Following read quality control and *de novo* assembly, a total of 543293 and 655739 contigs with N50 of 1890 bp and 1707 bp were retained for AFBR GAC and AFCMBR GAC, respectively (Table 5-1). Following by binning of the metagenomic sequencing reads, 56 (23 and 33) of draft genomes with high-quality (estimated > 90% completeness) were recovered from AFBR GAC and AFCMBR GAC. To further improve the quality of recovered genome bins, hybrid assembly was performed with the trimmed paired-end (PE) reads sequenced on Illumina Hiseq platform and the trimmed single-end (SE) reads sequenced on the PacBio Sequel Platform. *de novo* assembly and Maxbin binning yielded 85 (37 and 48) of genome bins with high completeness in AFBR_GAC and AFCMBR_GAC. These genome bins were phylogenetically identified by genomic comparison using PhyloPhlAn.

GAC microbial communities of both AFBR and AFCMBR in the SFA-CMBR were predominated by SPOB (*Syntrophobacter and Smithella*), acetoclastic methanogens (*Methanotherix*), and the exoelectrogen *Geobacter* (Aslam et al., 2018). To further examine the metabolic interactions between these species, high quality genome bins (with > 90% completeness) for these microbes were recovered through metagenomic short reads and hybrid assemblies (Table 5-2). These recovered genome bins are highly consistent with the abundant OTUs of the 16S rRNA gene analysis (Aslam

et al., 2018). Specifically, three high-quality bins with relatively high completeness, low contamination and low heterogeneity (Fig 5-2) were further annotated for pathways reconstruction. The three high-quality genome bins, AFBR_GAC_Bin72, AFCMBR_GAC_MaxBin.090 and AFBR_GAC_MaxBin.001, were phylogenetically identified to be closely related to the genomes of *Syntrophobacter fumaroxidans*, *Methanothrix concilii* and *Geobacter lovleyi*, respectively (Fig 5-3). The gene content of these reconstructed genome bins was annotated (Appendix I), thereby illuminating the potential functional properties of the microbial system.

The complete pathways for propionate degradation and acetate oxidation were recovered from the *S. fumaroxidans* MPOB (AFBR_GAC_Bin72) genome bin and *G. lovleyi* genome bin (AFBR_GAC_MaxBin.001), respectively. The acetoclastic methanogenesis, classical CO₂ reduction and RHP pathways were also fully recovered from the *M. concilii* genome bin (AFCMBR_GAC_MaxBin.090) (Fig. 5-4; Appendix I). After trimming and assembly of metatranscriptomic sequencing reads, the output file was inputted for mapping against the recovered genomes bins of interests. Specifically, the genome bins AFBR_GAC_Bin72 (*S. fumaroxidans* MPOB), AFCMBR_GAC_MaxBin.090 (*M. concilii* GP 6) and AFBR_GAC_MaxBin.001 (*G. lovleyi* SZ) were selected as the references since all the discussed pathways were well reconstructed in these three genomes. The assembled sequences for AFBR GAC were mapped against the three genomes bins to evaluate genes expression levels (Table S4) in AFBR_GAC_Bin72 and AFBR_GAC_MaxBin.001 which were

organically recovered from AFBR GAC sample. Meanwhile, the same analysis approach was applied to AFCMBR GAC metatranscriptomic sequences to assess genes expression levels (Appendix II) in bin of AFCMBR_GAC_MaxBin.090. Metatranscriptomics analysis confirmed that the genes involved in the aforementioned pathways were actively-transcribed.

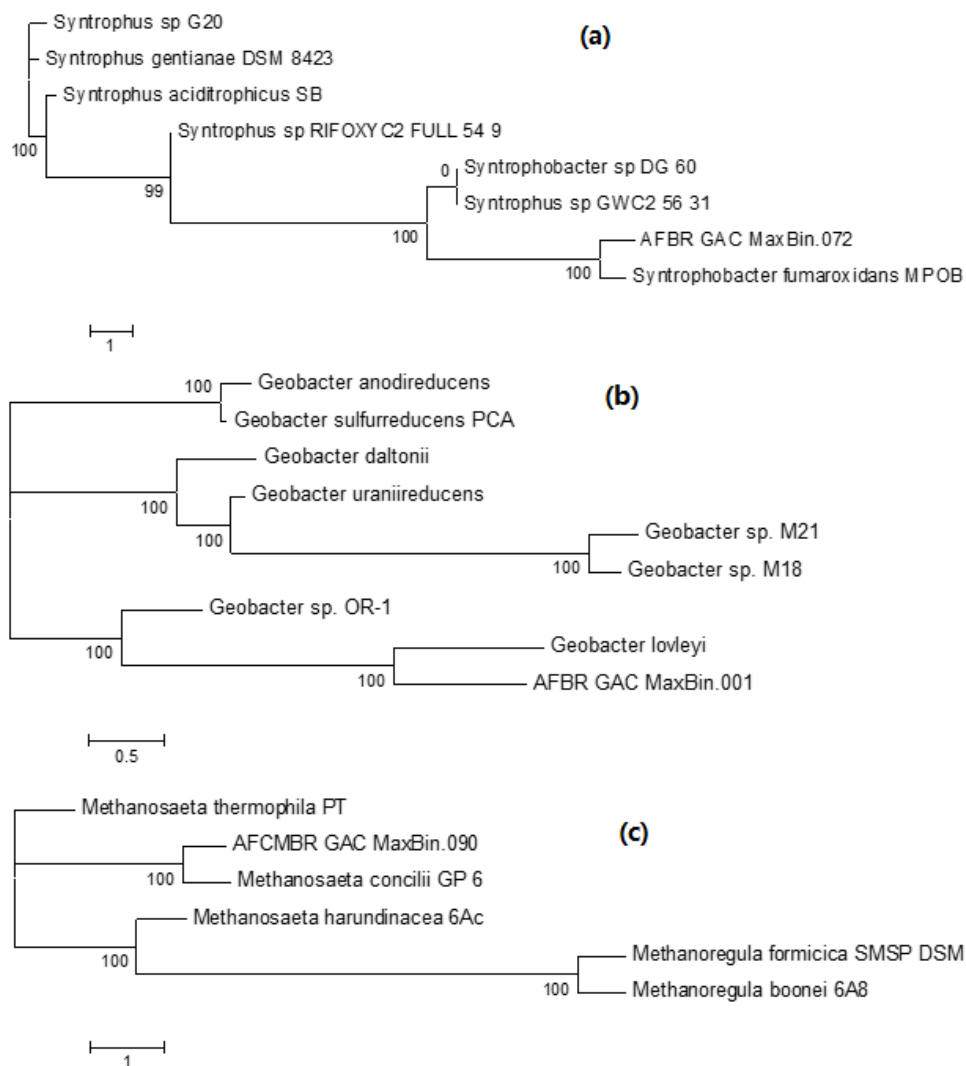


Figure 5-2. Phylogenetic tree of genome bins closely related to (a). *Syntrophobacter fumaroxidans*, (b). *Geobacter lovleyi* and (c). *Methanotherix concilii* using *PhyloPhlAn*.

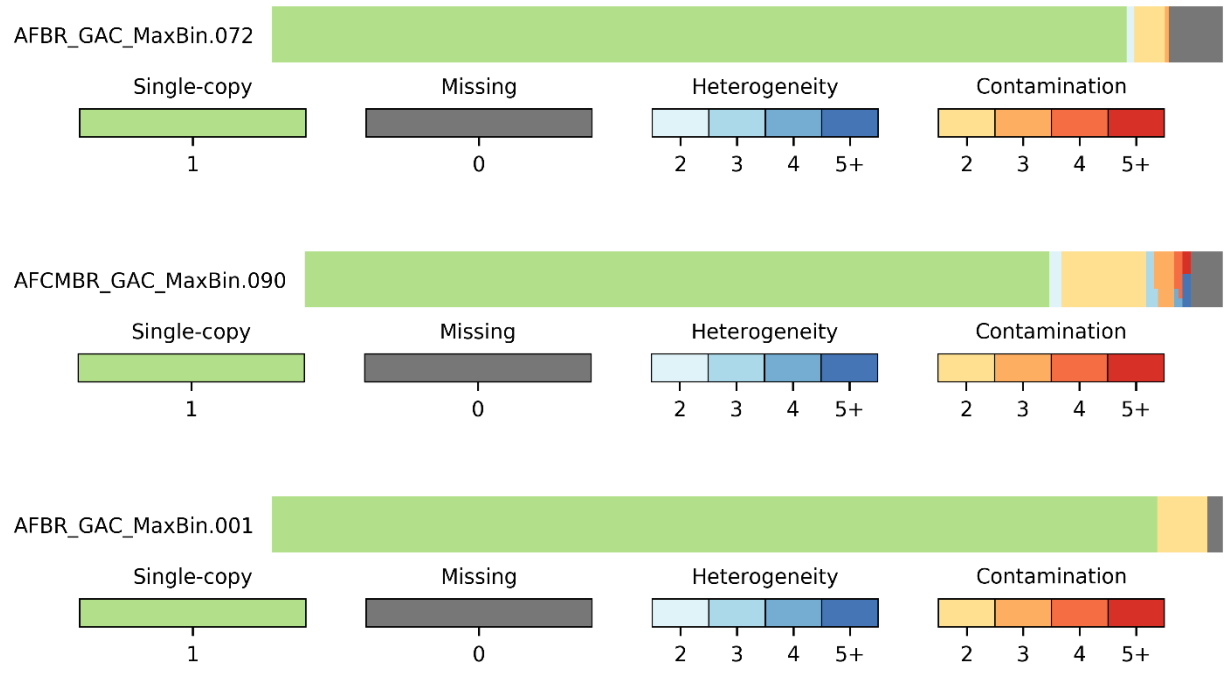


Figure 5-3. CheckM plot for the quality assessment of the genomes bins for further annotation and analysis.

Table 5-1. Summary of the 4 metagenomes.

Sample	Platform	Clean Reads	Total sequences (Gbp)	Average length (bp)	# of contigs after assembly	N50 after assembly
AFBR_GAC	Illumina HiSeq	157,411,554	53.8	150	543293	1890
AFBR_GAC hybrid ^a	Pacbio Sequel	1,066,949	11.87	5771	495970	2173
AFCMBR_GAC	Illumina HiSeq	156,430,090	53.54	150	655739	1707
AFCMBR_GAC hybrid ^a	Pacbio Sequel	507,843	5.34	5700	604865	1885

^ahybrid sample means that trimmed Illumina HiSeq reads and Pacbio Sequel reads were assembled together.

Table 5-2. High-quality recovered genome bins that are closely related to methanogens, syntrophs and *Geobacter*.

Bin name	Chromosome size, bp	GC content, %	Completeness^a, %	Contamination, %	Strain heterogeneity, %	Phylophlan
AFBR_GAC_Bin12	3700118	48.1	100 [69.27]	0.6	0	
AFCMBR_GAC_Bin40	3764333	48.4	100 [97.42]	29.84	16.88	
AFCMBR_GAC_Bin17	3647369	55.8	92.5 [95.51]	2.31	0	<i>Smithella sp.</i> F21
AFCMBR_GAC_MaxBin.006	3644658	48.4	100 [96.13]	13.87	3.57	
AFCMBR_GAC_MaxBin.051	3622302	58	100 [96.13]	9.44	13.64	
AFBR_GAC_Bin72	4370393	59.1	100 [81.29]	7.3	13.89	
AFCMBR_GAC_Bin25	4738005	60.2	97.5 [97.26]	18.04	4.17	<i>Syntrophobacter fumaroxidans</i>
AFBR_GAC_MaxBin.104	4482155	59.1	100% [95.32]	3.87	0	MPOB
AFBR_GAC_MaxBin.008	4909591	60.1	97.5% [99.19]	10.97	3.45	
AFCMBR_GAC_Bin24	3956411	52	95 [97.71]	26.47	27.59	<i>Methanotherix</i>

AFBR_GAC_MaxBin.122	1446900	53.7	95% [75.76]	1.96	33.33	<i>concilii</i> GP 6
AFCMBR_GAC_MaxBin.090	4095192	51.8	97.5% [95.59]	30.07	32.47	
AFCMBR_GAC_MaxBin.061	3035137	52.6	95% [93.57]	27.45	23.64	
AFCMBR_GAC_Bin.212	5221490	55.9	95 [83.04]	37.82	34.04	<i>Geobacter lovleyi</i>
AFBR_GAC_MaxBin.001	3296093	51.4	100% [98.35]	3.39	0	SZ
AFCMBR_GAC_Bin03	2080859	54.2	97.5 [92.37]	1.33	66.67	<i>Methanoregula</i>
AFCMBR_GAC_MaxBin.029	2321899	53.6	100% [97.25]	0.65	0	<i>formicica</i> SMSP DSM
AFCMBR_GAC_Bin21	2245848	54.8	95 [90.5]	16.97	23.81	<i>Methanolinea</i>
AFBR_Bulk_Bin.026	3639841	46.4	100 [99.49]	4.46	7.14	<i>tarda NOBI-1</i> <i>Syntrophomonas</i>
AFCMBR_GAC_MaxBin.071	3286932	64.2	100% [80.17]	36.14	7.22	<i>zehnderi</i> <i>Syntrophus sp</i>
GWC2						

^avalues in brackets were completeness of genome bins assessed with CheckM, and the ones outside brackets were completeness generated

by

Maxbin.

5.2.2 Propionate oxidation and acetoclastic methanogenesis

In our propionate and acetate-fed methanogenic system, propionate was first degraded into acetate and hydrogen, thereby acetate was adequately available as electron donor for further metabolization. *Syntrophobacter* degrade propionate into acetate using methylmalonyl-CoA (MMC) pathway adopted by most SPOB (Müller et al., 2010). While a unique syntrophic propionate oxidizer, *Smithella* was transcriptionally-active and it degrades propionate into acetate via butyrate using a distinctly different pathway, which the genes involved are still unclear so far (Frank AM de Bok et al., 2001). On the other hand, the MMC pathway was fully reconstructed in the *S. fumaroxidans* MPOB genome bin, and these genes were found to be highly expressed with log₂ RPKM values of 5.17 – 10.13 (Appendix I; Appendix II). Therefore, such acetate-rich environment was favorable for acetate-utilizing microbes, explaining the enrichment of exoelectrogenic *Geobacter* and methanogenic *Methanotherix*. Moreover, *G. lovleyi* is capable to use hydrogen as an alternate electron donor and exhibits lower hydrogen consumption threshold concentration than that of methanogen (Sung et al., 2006). The limited hydrogen produced from the propionate degradation pathways was too low to favor the growth of hydrogenotrophic methanogens in the system, while it could be utilized by *G. lovleyi* and further facilitated its dominance. This was reflected by the

observation that the abundance of hydrogenotrophic methanogens was relatively low and *G. lovleyi* dominated in the community.

Acetate, which acts as an electron diffusive carrier of MIET, is assimilated by acetoclastic methanogens for methane generation. The acetoclastic methanogenesis pathway, which splits acetate into a methyl group and an enzyme-bound CO then further reduced to methane (K. S. Smith & Ingram-Smith, 2007), was fully reconstructed in the *M. concilii* genome bin (Appendix I). The genes involved were also found to be highly expressed in the genome bin (\log_2 RPKM values of 5.45 – 11.96) (Appendix II; Fig. 5-4), indicating that *M. concilii* was metabolically active and contributed to the methane production via its acetoclastic methanogenesis pathway.

In propionate-fed syntrophic community, the metabolic activities of SPOB and methanogens are intimately dependent on each other (Kato & Watanabe, 2010). Collectively, these findings confirmed that a syntrophic interaction was present between GAC-dwelling acetoclastic methanogen *M. concilii* with SPOB, *S. fumaroxidans* MPOB and *Smithella. sp.*, to achieve the complete bioconversion of propionate to CH₄ and CO₂. Given that these microbes were selectively enriched on the GAC in the SFA-CMBR (Aslam et al., 2018), it is probably because that the GAC facilitated MIET by enabling the microbes to grow in proximity of each other.

5.2.3 Acetate oxidation and DIET-dependent CO₂ reduction

Pathway reconstruction in the draft genome bin related to *G. lovleyi* showed the capability of acetate utilization and CO₂ production via the tricarboxylic acid (TCA) cycle (Fig. 5-4; Appendix I). Gene expression patterns further confirmed that the acetate oxidation pathway was metabolically active in *G. lovleyi* (log₂ RPKM values of 4.53 – 8.30) (Fig. 5-4; Appendix II). The high abundance of gene transcripts was also observed when two *Geobacter* species were co-cultured together and acetate was available as an electron donor (Shrestha et al., 2013). Both the *G. lovleyi* acetate oxidation and *Methanothrix* acetoclastic methanogenesis pathway were found to be transcriptionally-active, indicating that they were competing for acetate at the substrate-level. While more importantly, they formed an electric syntrophic relationship and benefited each other via the IET. It was reported that the growth of *Geobacter spp.* was suppressed when methanogenesis was inhibited, suggesting that *Geobacter* grew under syntrophic or synergetic association with methanogens (Kato et al., 2012a). Methanogens are possibly “electron receivers” and serve as electron sinks of the dissipated electrons from *Geobacter*.

Attributed to the conductive GAC, the substrate-competing relationship turned to be a cooperative association via DIET-induced interactions.

Acetoclastic methanogenesis was not the only transcriptionally-active pathway detected in the *M. concilii* genome bin. The DIET-dependent CO₂ reduction methanogenesis pathway was also recovered (Fig. 5-4; Appendix I). The genes specifically associated with the CO₂ reduction pathway (*fwd*, *ptr*, *mch*, *mtd* and *mer*) were highly expressed at levels close to the acetoclastic methanogenesis pathway (log₂ RPKM values of 5.89 – 9.68) (Fig. 5-4; Appendix II). Unlike hydrogenotrophic methanogens, *Methanotherix* is incapable of performing CO₂ reduction to methane via MIET as it cannot uptake reducing equivalents (i.e., hydrogen) (Kosaka et al., 2006b; Shrestha et al., 2013; K. S. Smith & Ingram-Smith, 2007), suggesting that DIET-driven methanogenesis was prevalent within the GAC community of SFA-CMBR. This observation agrees with a finding that *Geobacter* species could transfer electrons to *Methanotherix* species to support CO₂ reduction via DIET (Holmes et al., 2017; S. Zhang et al., 2017). In other words, *G. lovleyi* and *M. concilii* also established a close “electric syntrophic” relationship for the generation of methane from CO₂. The sources of CO₂ could be extracellular (CO₂ released from propionate oxidation and TCA cycle in SPOB and *Geobacter*, respectively) and intracellular (CO₂ as a byproduct from acetoclastic methanogenesis). In *M. concilii*, the by-product of MIET facilitated pathway (acetoclastic methanogenesis), CO₂, was further utilized in the DIET facilitated pathways (CO₂ reduction). By coupling the MIET and DIET, *M. concilii*

could utilize the metabolite, CO₂, for additional energy capture. Accordingly, in this SFA-CMBR, such interspecies interactions facilitated DIET-dependent pathway and promoted the overall energy recovery in the form of methane.

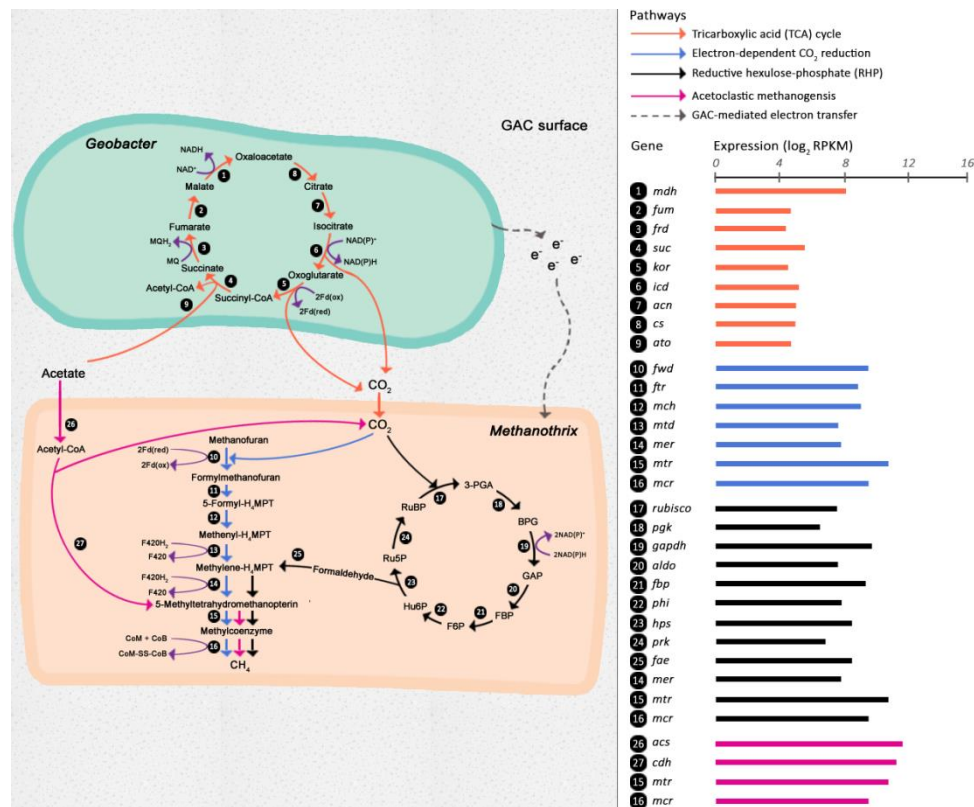


Figure 5-4. Annotated pathways of acetate oxidation, acetoclastic methanogenesis, classical CO₂ reduction and CO₂ reduction via RHP for methane production.

* Expression level of involved genes were evaluated as the log₂ RPKM values and represented by the bar chart. Ru5P, ribulose-5-phosphate; RuBP, ribulose-1,5-bisphosphate; 3-PGA, 3-phosphoglycerate; BPG, 1,3-

diphosphoglycerate; GAP, glyceraldehyde-3-phosphate; FBP, fructose-1,6-bisphosphate; F6P, fructose-6-phosphate; Hu6P, D-arabino-3-hexulose-6-phosphate; H₄MPT, tetrahydromethanopterin.

5.2.4 CO₂ reduction via the RHP pathway

Besides the classical CO₂ reduction, the RHP pathway for carbon fixation is expected to be widely distributed in methanogenic archaea and the genes in such pathway are conserved in *M. concilii* (Kono et al., 2017). Indeed, the complete RHP pathway was identified in the *M. concilii* genome bin (Fig. 5-4; Appendix I). All the genes involved in the RHP pathway were at equally high expression levels as compared to the acetoclastic and classical DIET-dependent CO₂ methanogenesis one with log₂ RPKM values ranging between 6.05 and 9.79 (Fig. 5-4; Appendix II). This provides the first definitive proof that the entire RHP pathway is metabolically active in *M. concilii*. The RHP pathway, similar to the Calvin–Benson cycle, includes three phases: carbon fixation, carbon reduction, and ribulose-1,5-bisphosphate (RuBP) regeneration (Kono et al., 2017). A study analyzing the RHP pathway *in vivo* for *Methanospirillum hungatei* showed that a small proportion of carbons fixed by RuBisCO were recycled for RuBP regeneration in the RHP pathway, and a great amount were supplied to gluconeogenesis and glycolysis (Kono et al., 2017). Also, it was proposed that the archaea invested much smaller of energy in the RHP pathway

compared with the investment of plants in the Calvin–Benson cycle (Kono et al., 2017). By accomplishing this carbon fixation pathway with relatively low-energy investment, *M. concilii* could proceed further cell synthesis, therefore facilitated the dominance of *M. concilii* in the community and strengthened their overall activities. Hence, it is very likely that the RHP pathway plays an important role in anabolism in *M. concilii*.

A question raises if the RHP pathway in *M. concilii* mediates methane production. The formaldehyde intermediate has been speculated to act as a metabolic link between the RHP pathway and methanogenesis in methanogens (Kono et al., 2017). Accordingly, formaldehyde released from the RHP cycle can be condensed with tetrahydromethanopterin to form methyl-H₄MPT, which is a key methanogenic precursor also central to both the methanogenesis and classical CO₂ reduction pathways (Fig. 5-4). Four copies of the 5,6,7,8-tetrahydromethanopterin hydrolyase gene (*fae*), which perform formaldehyde condensation, were successfully recovered from the *M. concilii* genome bin (Fig. 5-4; Appendix I). The high expression levels of *fae* (log₂ RPKM values of 7.54 – 8.66) strongly suggest the involvement of the RHP pathway likely associated with methanogenesis. Moreover, similar to the classical DIET-dependent CO₂ methanogenesis, the RHP carbon fixation pathway is also an electron-consuming process. This raises

the possibility that the RHP pathway could be relying on external electrons received from *G. lovleyi* through DIET.

5.2.5 Thermodynamics estimation of the CO₂ reduction pathways

Since all MIET and DIET pathways were active, this meant that they were all concurrently happening. Therefore, the thermodynamics of each pathway was explored. To estimate ΔG^0 of two reactions reducing CO₂ to methane, the reactions of each step were written and the corresponded ΔG^0 of each step reactions were calculated (at 298 K, pH 7.0 and all compounds at 1 molar activity) (Table 5-3) (Thauer et al., 2008). Summing up Eq.1 – Eq.7 resulted in an overall reaction of classical CO₂ reduction, Eq. 8, and ΔG^0 of the reaction was obtained by summing up the values from Eq.1 to Eq.7. Considering the differences of electron carriers involved in classical CO₂ reduction pathway and RHP pathway, the overall reaction of RHP pathway was modified based on the classical CO₂ reduction reaction by including the involved electron carriers and excluding the uninvolved ones. Specifically, Eq. 9 - Eq. 11 in Table S5 are half reactions of electron carriers, and the reaction of CO₂ reduction via RHP pathway, Eq. 12 = Eq. 8 + 2 * Eq. 9 – Eq. 10 - Eq. 11, was obtained subsequently.

Table 5-4 summarizes the reactions of acetoclastic methanogenesis (Eq. 1), CO₂ reduction to methane (Eq. 2), CO₂ fixation via RHP pathway (Eq. 3).

At biological conditions (298 K and pH 7.0), the standard Gibbs free energy changes (ΔG^0) of Eq. 1 – Eq. 3 were calculated. Given that the intracellular-produced CO_2 from acetoclastic methanogenesis could serve as a substrate for CO_2 reduction in *M. concilii*, a concurrent MIET and DIET activity could result in a complete acetate reduction to methane (2 mole of methane formation per 1 mole acetate consumption). This is reflected in the summation of acetoclastic methanogenesis with classical CO_2 reduction (Eq. 4) and RHP pathway (Eq. 5). As shown in Table 5-4, all these discussed reactions were thermodynamically favorable under standard biological conditions since all the ΔG^0 values were far below zero. Additionally, the energy released/yielded from the classical CO_2 reduction ($-86.95 \text{ kJ mol}^{-1}$) and the RHP pathway ($-53.95 \text{ kJ mol}^{-1}$) are significant and higher than that from acetoclastic methanogenesis, when there is an incoming electron supply for *M. concilii*, presumably from *G. lovleyi* via DIET. With facilitation of DIET, methanogens proceeded the CO_2 reduction and yielded more energy comparing with the condition without external electrons available. The yielded energy in *M. concilii* results in more methane formation, therefore improving the overall energy recovery efficiency of the AFCMBR.

Table 5-3. The step reactions involved in classical CO₂ reduction, half reactions of electron carriers and their standard Gibbs free energy changes (ΔG^0).

Reaction number	Reaction	ΔG^0 (kJ/mol)
Eq. 1	$\text{CO}_2 \text{ (aq)} + \text{MFR} + 2 \text{ Fd}_{\text{red}}^{2-} + 2 \text{ H}^+ \rightarrow \text{CHO-MFR} + 2 \text{ Fd}_{\text{ox}} + \text{H}_2\text{O}$	-8.16
Eq. 2	$\text{CHO-MFR} + \text{H}_4\text{MPT} \rightarrow \text{CHO-H}_4\text{MPT} + \text{MFR}$	-5
Eq. 3	$\text{CHO-H}_4\text{MPT} + \text{H}^+ \rightarrow \text{CH}\equiv\text{H}_4\text{MPT}^+ + \text{H}_2\text{O}$	-5
Eq. 4	$\text{CH}\equiv\text{H}_4\text{MPT}^+ + \text{F}_{420}\text{H}_2 \rightarrow \text{CH}_2=\text{H}_4\text{MPT} + \text{F}_{420} + \text{H}^+$	6
Eq. 5	$\text{CH}_2=\text{H}_4\text{MPT} + \text{F}_{420}\text{H}_2 \rightarrow \text{CH}_3-\text{H}_4\text{MPT} + \text{F}_{420}$	-6
Eq. 6	$\text{CH}_3-\text{H}_4\text{MPT} + \text{HS-CoM} \rightarrow \text{CH}_3-\text{S-CoM} + \text{H}^+$	-30
Eq. 7	$\text{CH}_3-\text{S-CoM} + \text{HS-CoB} \rightarrow \text{CH}_4 \text{ (aq)} + \text{CoM-S-S-CoB}$	-13.95
Eq. 8	$\text{CO}_2 \text{ (aq)} + 2 \text{ Fd (red)} + 2 \text{ F}_{420} \text{ (red)} + \text{CoM-SH} + \text{CoB-SH} \rightarrow \text{CH}_4 \text{ (aq)} + 2 \text{ Fd (ox)} + 2 \text{ F}_{420} \text{ (ox)} + \text{CoM-SS-CoB} + 2\text{H}_2\text{O}$	-62.11
Eq. 9	$\text{NADP (red)} \rightarrow \text{NADP (ox)} + 2\text{H}^+ + 2\text{e}^-$	14
Eq. 10	$2\text{Fd (red)} \rightarrow 2\text{Fd (ox)} + 2\text{H}^+ + 2\text{e}^-$	-16
Eq. 11	$\text{F}_{420} \text{ (red)} \rightarrow \text{F}_{420} \text{ (ox)} + 2\text{H}^+ + 2\text{e}^-$	11
Eq. 12	$\text{CO}_2 \text{ (aq)} + 2 \text{ NADP (red)} + \text{F}_{420} \text{ (red)} + \text{CoM-SH} + \text{CoB-SH} \rightarrow \text{CH}_4 \text{ (aq)} + 2 \text{ NADP (ox)} + \text{F}_{420} \text{ (ox)} + \text{CoM-SS-CoB} + 2\text{H}_2\text{O}$	-29.11

The standard free energy change (ΔG^0) was calculated at 298 K, pH 7.0 and all compounds at 1 molar activity. F₄₂₀, coenzyme F₄₂₀; Fd, ferredoxin;

H₄MPT, tetrahydrosarcinapterin; HS-CoB, coenzyme B; HS-CoM, coenzyme M; MFR, methanofuran; MP, methanophenazine.

Table 5-4. Reactions of methane production in the system and the corresponded standard Gibbs free energy.

Number	Description of reaction	Reaction	$\Delta G^{0'}$ (kJ mol⁻¹)
Eq. 1	Acetate methanogenesis	$\text{CH}_3\text{COOH (aq)} \rightarrow \text{CH}_4 \text{ (aq)} + \text{CO}_2 \text{ (aq)}$	-24.84
Eq. 2	Classical CO ₂ reduction	$\text{CO}_2 \text{ (aq)} + 2 \text{ Fd (red)} + 2 \text{ F}_{420} \text{ (red)} + \text{CoM-SH} + \text{CoB-SH} \rightarrow \text{CH}_4$	-62.11
Eq. 3	CO ₂ reduction via the RHP	$\text{CO}_2 \text{ (aq)} + 2 \text{ NADP (red)} + \text{F}_{420} \text{ (red)} + \text{CoM-SH} + \text{CoB-SH} \rightarrow$	-29.11
Eq. 4	Complete acetate	$\text{CH}_3\text{COOH (aq)} + 2 \text{ Fd (red)} + 2 \text{ F}_{420} \text{ (red)} + \text{CoM-SH} + \text{CoB-SH} \rightarrow$	-86.95
Eq. 5	Complete acetate	$\text{CH}_3\text{COOH (aq)} + 2 \text{ NADP (red)} + \text{F}_{420} \text{ (red)} + \text{CoM-SH} + \text{CoB-SH}$	-53.95

The standard free energy change ($\Delta G^{0'}$) was calculated from the standard free energies of formation at 298 K, pH at 7.0 with CO₂ and CH₄ in the aqueous state and all compounds at 1 molar activity.

To further evaluate thermodynamic feasibility of these reactions in the AFCMBR, the transformed Gibbs free energy values ($\Delta G'$) at 298 K and pH 7 were estimated within an acetate concentration range of 0.03 mM – 4 mM and a CH_4/CO_2 partial pressure ratio of 1 – 4, which mimics the actual conditions prevalent in the AFCMBR and other anaerobic digestion systems. Fig. 5-5a displays the variation of $\Delta G'$ for acetoclastic methanogenesis, indicating that the reaction can proceed even under very low acetate concentration. The energy gain from acetoclastic methanogenesis gently decreases as the acetate concentration decreases, while its effects on $\Delta G'$ became more obvious at extremely low acetate concentration. In comparison, within the set range, changes of partial pressure ratio of CH_4 to CO_2 exerted insignificant influence on the energy gain. On the other hand, as shown in 5-5b, both the complete acetate reduction reactions were highly driven, and both of their energy gains (-60 to -80 and -90 to -110 kJ mol^{-1}) were higher than that of acetoclastic methanogenesis alone without further CO_2 reduction (-30 to -40 kJ mol^{-1}). Therefore, when there are electrons available via DIET for *M. concilii*, the thermodynamic driving force for further CO_2 reduction and/or the complete acetate reduction into methane is favorable. Notably, the energy gain from the complete acetate reaction via classical CO_2 reduction is higher compared to the one via the RHP pathway, due to the differences of each metabolism involved intrinsically. Similar to the acetoclastic methanogenesis, $\Delta G'$ of the two complete acetate reduction reactions were hardly affected by the partial pressure ratio of CH_4/CO_2 , and their energy gains gently enhances as the acetate concentration increases. Overall, all

the three reactions were thermodynamically feasible under this SFA-CMBR even at very low substrate concentrations.

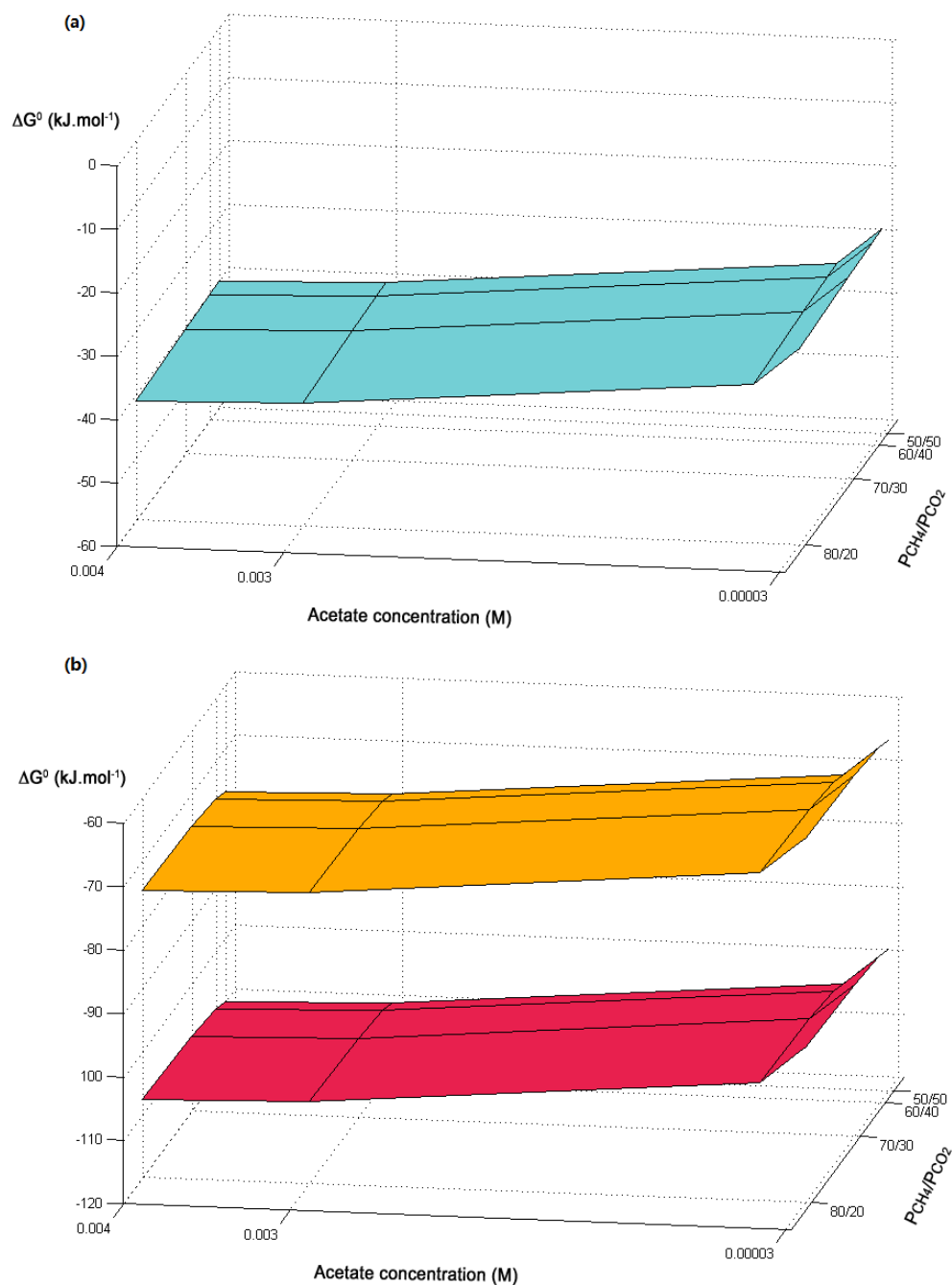


Figure 5-5. Transformed Gibbs free energy values ($\Delta G'_{298\text{K}}$) in KJ/mol at pH of 7 and pressure of 1 atm as a function of acetate concentration and partial pressure ratio of CH_4/CO_2 for (a) Eq. 1: acetoclastic methanogenesis

(b) Eq. 4 (complete acetate reduction via classical CO₂ reduction) and Eq. 5 (complete acetate reduction via RHP pathway). The red curve represents Eq. 4, and the red orange one represents Eq. 5.

5.3 Chapter summary

In the energy-efficient SFA-CMBR with GAC fluidization fed with low-strength wastewater, metagenomic and metatranscriptomic analyses confirmed that propionate was degraded into acetate by the SPOB. The acetate-rich system favored the synergic growth of *M. concilii* and *G. lovleyi*. Acetate was further degraded into CO₂ and methane by *M. concilii* via acetoclastic methanogenesis pathway, meanwhile *G. lovleyi* also competed for acetate as substrate to oxidize into CO₂ via the TCA cycle. Furthermore, with the facilitation of DIET, *M. concilii* received electrons from *Geobacter* and reduced CO₂ into methane via both the classical CO₂ reduction and RHP pathway. These two pathways were metabolically linked with the acetoclastic methanogenesis via the intermediate methyl-H₄MPT. Therefore, acetate could be completely reduced to methane (2 mole methane formation per 1 mole acetate consumption) and contributed to high methane yield from the system. Additionally, it is plausible that the high activity of the anabolic RHP pathway enables the catabolic methane formation or versa in *M. concilii*, facilitating its dominance and enhancing methane yield. Further thermodynamics calculation verified the feasibility of the acetoclastic methanogenesis and classical and RHP CO₂ reduction pathway under such system conditions. With these two CO₂ reduction pathways facilitated by DIET, the energy gain from the complete acetate

reduction was higher than acetoclastic methanogenesis alone without further CO₂ reduction. Unveiling such microbial interactions involving DIET help to elucidate microbial behavior and provide strategies for the further improvement of bioenergy processes.

6. Chapter 6 Upgrading lignocellulosic ethanol for caproate production via chain elongation fermentation

6.1 Overview

Mixed-culture carboxylates chain elongation (CE) upgrades short-chain carboxylates (SCCs) and diluted ethanol into medium chain carboxylates (MCCs) with higher energy density and better separation property (M. T. Agler et al., 2011). In this chain elongation process, ethanol use as feed for caproate production has been identified as the predominant cause of environmental impact in a life cycle assessment study, and thus it was suggested to use lignocellulosic ethanol (LE) as an alternative feedstock (W. S. Chen et al., 2017). By integrating lignocellulosic ethanol with this low-energy anaerobic fermentation process, the energy intensive ethanol distillation process is circumvented. Moreover, the process upgrades the feedstock into a product with higher energy density and better separation property. Meanwhile, in anaerobic fermentation, yeast extracts/protein-rich feedstocks were found to improve fermentation performance (Y. Chen, Jiang, Yuan, Zhou, & Gu, 2007; Feng, Chen, & Zheng, 2009; Morgan-Sagastume et al., 2011), and cellulose can serve as an additional substrate. Cellulose addition for caproate production from ethanol was observed by co-cultures of *Clostridium kluyveri*, chain elongating bacteria, with ruminal cellulolytic bacteria (Weimer, Nerdahl, & Brandl, 2015). However, few attentions have been paid on the effect of cellulose and yeast extract on chain elongation in terms of kinetics and microbial community structures.

In this chapter, caproate production using the waste-based lignocellulosic ethanol (LE) as feedstock via chain elongation fermentation is examined. Additionally, the effects of yeast extract and cellulose contained in the LE for caproate formation are discussed. Specifically, extra yeast extract and cellulose were supplied separately to assess fermentation performance associated with microbial community and kinetics. To this end, 16S rRNA sequencing was conducted to inspect microbial interactions; the Thermodynamic Electron Equivalents Model (TEEM) and Monod equation were performed to reveal the correlations between fermentation performance and its kinetics. The results show that using LE as feedstock shortens the lag phase of caproate production and enhances fermentation kinetics. Specifically, supplement of yeast extract (YE) and cellulose, contained in LE, were identified to be capable to improve the fermentation performance. In this regard, potential of using LE as the feedstock can be evaluated, suggesting it is promising to upgrade the wastes-based medium into a more valuable bio-fuel precursor. Moreover, the study provides clues for improvement of the process, especially in terms of shortening the retention time, which is crucial parameter to an efficient and compact reactor in application.

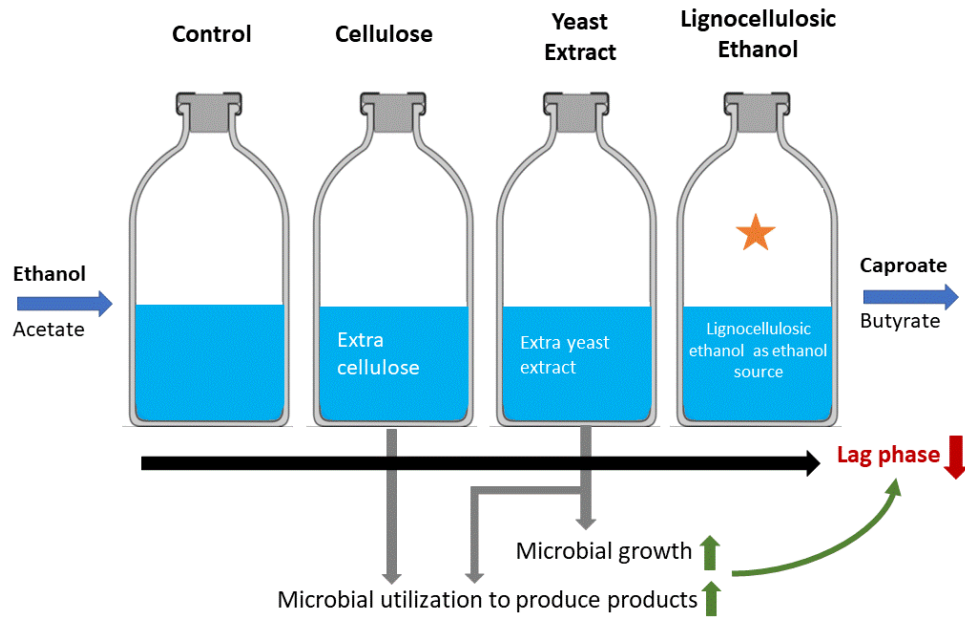


Figure 6-1. Illustration of the batch experiment and improvement of fermentation performance.

6.2 Results and discussion

6.2.1 Caproate yield and lag phase

Fig. 6-2 shows concentration profile of substrates and main products in the fermentation. In all experiments, 150 mM of ethanol was completely consumed during the period of fermentation, and formation of butyrate and caproate always associated with consumption of ethanol. Sharp decrease of ethanol accompanied with rapid accumulation of butyrate and caproate, Day 15-20 in EtOH, Day 5-10 in CL, Day 0-5 in LE and Day 5-10 in YE, as displayed in Fig. 6-2. It was also observed that caproate production lagged or concurred with formation of butyrate, suggesting that the chain elongation accomplishes via reverse β -oxidation pathway that 2-carbon acetate is first elongated into 4-carbon butyrate, then further into 6-carbon

caproate (Seedorf, Fricke, Veith, Bruggemann, Liesegang, Strittmatter, et al., 2008). Based on the potential stoichiometric relationship (Leng et al., 2017), the concentration ratio of produced caproate to butyrate should be 2.1 ± 0.7 under this experimental condition, and the obtained ratios were 2.1 (EtOH), 1.9 (CL), 0.7 (YE) and 1.5 (LE). Obviously, YE yielded a small value of ratio, and this was due to rapid consumption of ethanol in the first 5 days of fermentation. After consumption of ethanol, its deficiency resulted in a thermodynamic bottleneck limiting further conversion from butyrate to caproate, causing low level of caproate production and accumulation of butyrate

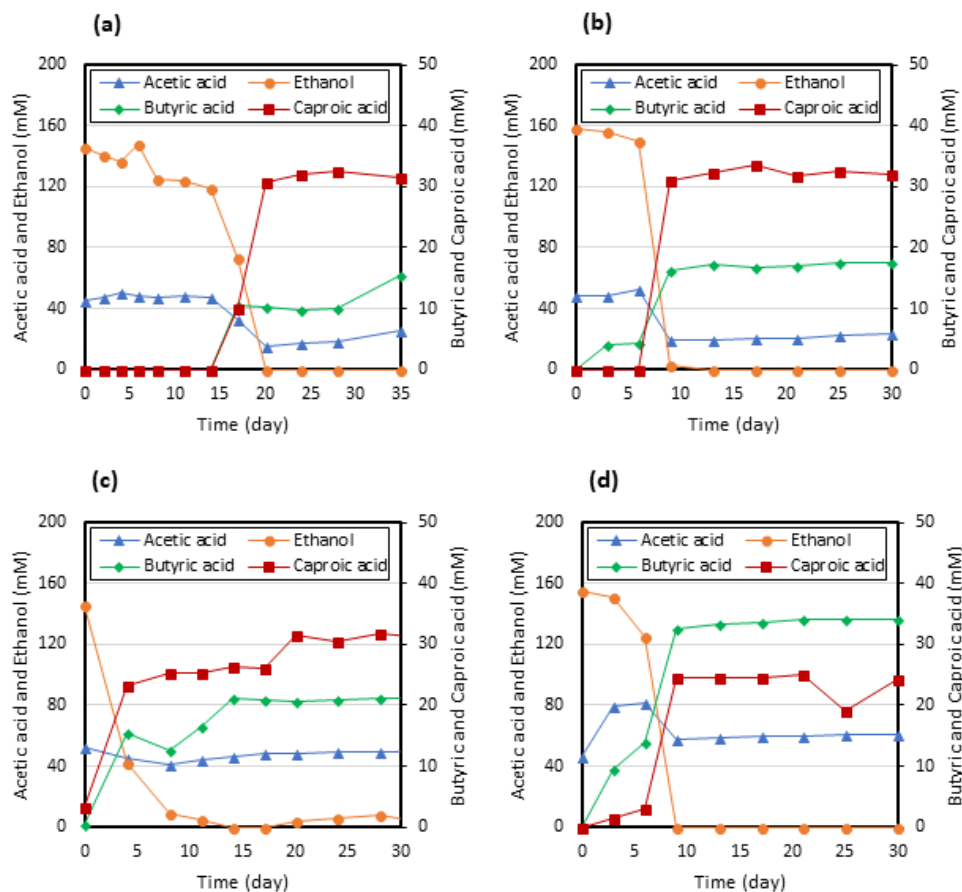


Figure 6-2. Profile of concentrations of substrates and products during the fermentation cycle in group (a) EtOH; (b) CL; (c) LE; (d) YE.

Table 6-1 summarizes caproate and butyrate yields, carbon conversion ratio, and lag phase of four batch experiments. Caproate yields were comparable in the order of CL (33.6 mM) > EtOH (32.6 mM) > LE (31.7 mM) > YE (25.2 mM), while the butyrate yield differed greatly in the order of YE (34.2 mM) > LE (21.2 mM) > CL (17.4 mM) > EtOH (15.4 mM). Carbon conversion ratios, calculated as the percentage of carbons converted into butyrate and caproate over the carbons initially in the forms of ethanol and acetate, were in the order of YE (71.5%) > LE (69.4%) > EtOH (65.6%) \approx CL (65.2%). Although the CL yielded the highest concentration of caproate, its carbon conversion ratio was the lowest. This suggests that a portion of products were potentially metabolized from cellulose, instead of directly elongating from acetate in the feedstock. Conversely, the YE yielded the lowest concentration of caproate while the highest carbon conversion ratio. In addition, the butyrate concentration in YE was lower than the others. Presumably, yeast extract could boost the uptake of substrates by enhancing microbial activities (Seedorf, Fricke, Veith, Bruggemann, Liesegang, Strittmatter, et al., 2008), therefore resulting in a high butyrate yield. While the lowest caproate yield was due to fast consumption and scarcity of ethanol, thus limited the further elongation from butyrate into caproate.

Table 6-1. Summary of concentrations of products, carbon conversion percentages and lag phase of caproate production in the four experimental groups.

	Caporate ^a (mM)	Butyrate ^a (mM)	Carbon Conversion ^b (%)	Initiation of Caproate Formation ^c
EtOH (Control)	32.6 ± 0.8	15.4 ± 0.55	65.6	Day 17
CL	33.6 ± 2.2	17.4 ± 1.5	65.2	Day 9
YE	25.2 ± 0.9	34.2 ± 1.9	71.5	Day 6
LE	31.7 ± 1.1	21.2 ± 0.9	69.4	Day 4

^aThe final stable concentration during the whole fermentation period.

^bPercentage of the carbons converted to butyrate and caproate over the carbons initially in the forms of ethanol and acetate.

^cThe first sampling day that caproate was detected.

The “lag phase” for caproate formation varied greatly among the experiments in the order of LE (Day 4) < YE (Day 6) < CL (Day 9) < EtOH (Day 17). Compared to the control one (EtOH), CL and YE had shorter lag phases, suggesting that cellulose and yeast extract could boost the caproate formation. This enhancement by cellulose was possibly contributed by cellulolytic bacteria, which metabolize cellulose into butyrate, or even caproate, in the initial stage of fermentation (Kenealy,

Cao, & Weimer, 1995). Yeast extract contains nitrogen source and essential nutrients, and thus it stimulated bacterial growth and boosted the activities of microorganisms (Feng et al., 2009; Ge et al., 2015; Morgan-Sagastume et al., 2011). The increased ethanol uptake and chain elongation activities resulted in high butyrate and caproate yields. The LE had the shortest lag phase compared with other three experiments. This was speculated to be the effects attributed to both yeast extract and cellulose contained in the feedstock. The enhancement on the kinetics of caproate and other product yields reflected that LE is an excellent candidate as a substrate for improving performance of chain elongation process.

6.2.2 Bacterial community characterization

The samples for microbial community structure analysis were taken from each chain elongation system at the end of fermentation cycle. 16s rRNA sequencing was performed to examine the variations of microbial community structures, and to identify the dominant bacterial populations and their correlation with the essential environmental factors among four groups. A sequence-based rarefaction analysis was performed to test for efficient OTU coverage. The reads and coverage obtained for bacteria communities for each sample are shown in Table 6-2. The coverage value of samples exceeded 88.3%, indicating that the sequencing depth was sufficient to represent the full diversity of the system.

Table 6-2. The reads and coverage obtained for bacteria communities.

	Clean reads	Sequences postprocessing	Normalized sequences	OTUs	Good's coverage
EtOH	169,277	42,267	25,124	5,237	89.4
CL	52,500	25,124	25,124	4,000	88.3
YE	52,500	26,761	25,124	3,248	91.3
LE	239,251	67,013	25,124	3,812	94.3

Table 6-3 summarizes the indices related to alpha-diversity to assess the internal complexity of individual microbial community. The listed indices, Shannon diversity, Richness and Evenness are positively related to community diversity, richness and evenness, respectively. EtOH yields the highest values among all experiments. Result shows that community of EtOH was the most diverse one, followed by CL, YE and LE. Noticeably, the decreasing trend of alpha-diversity indices values correlates with an enhancement in the caproate production kinetics, i.e. a shorter lag phase. This implies that an assorted feedstock containing potential substrates or essential growth nutrients is likely to facilitate condensation of microbial community compositions by enriching certain microbial groups adapting to the conditions well. In addition, both the values of evenness and richness indices in YE and LE were obviously lower than in EtOH and CL, suggesting that yeast extract could potentially facilitate to construct an enriched community structure. In contrast, the addition of cellulose did not significantly influence the biodiversity of community, indicating that the improvement of fermentation performance was possibly attributed to

metabolization of cellulose. Moreover, similarities and distances of the microbial communities between samples were delineated in Jackknife-supported UniFrac tree (Fig. 6-3). Result shows that the microbial communities of YE and CL were similar to each, whereas LE shared the lowest similarity with the other three groups (data not shown). Therefore, it was speculated that microbial community shifted significantly upon the complexity of feedstock compositions.

Table 6-3. Alpha-diversity indices of the four microbial communities at 3% cutoff.

	Shannon diversity	Chao1 richness	Shannon evenness
EtOH	5.62	16100	0.677
CL	5.34	14670	0.653
YE	4.68	10297	0.582
LE	3.69	6840	0.491

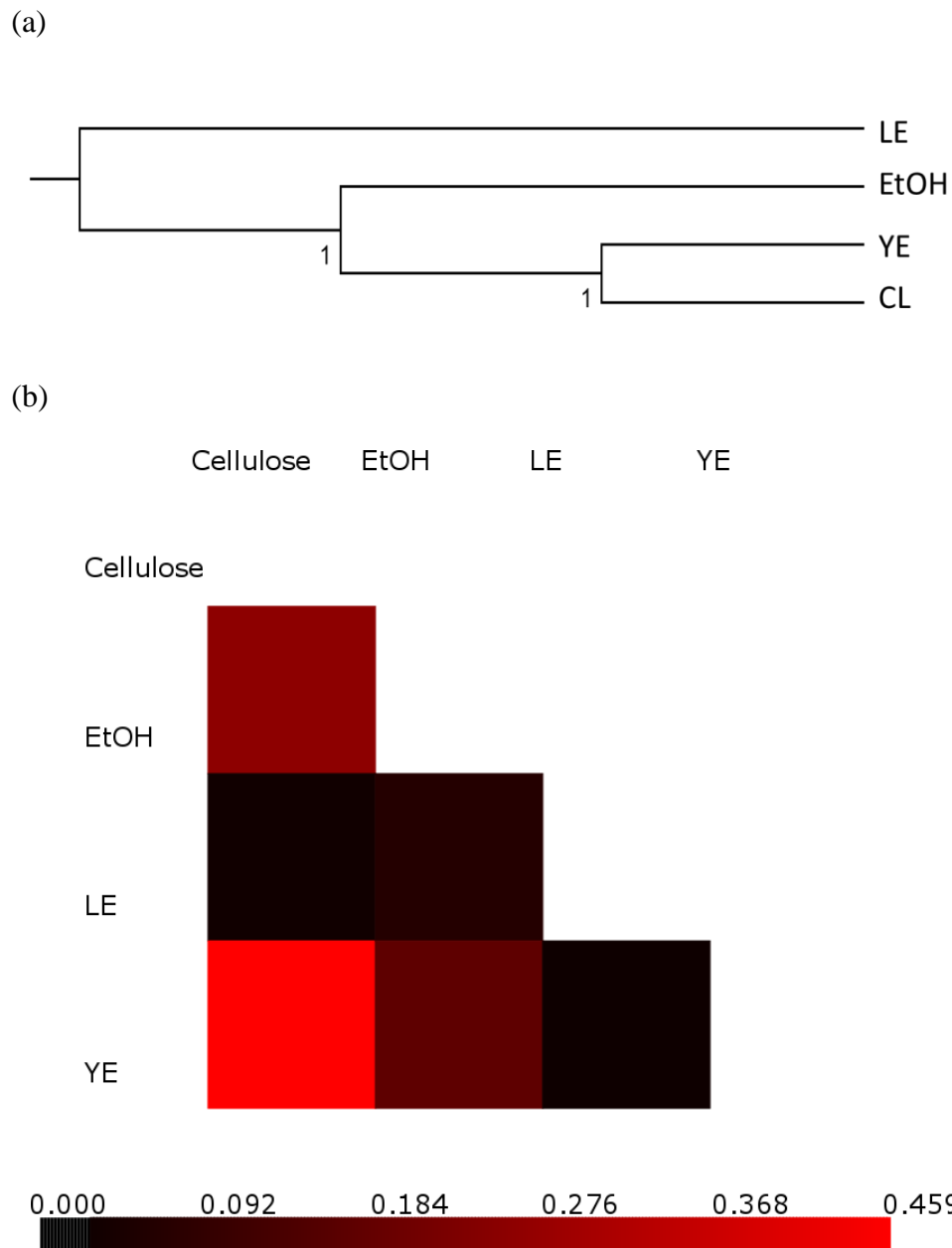


Figure 6-3. Beta-diversity analysis among groups with (a) UNIFRAC tree; (b) braycurtis heatmap.

Fig. 6-4 shows the phylogenetic classification of samples at phylum (Fig. 6-4a) and genus (Fig. 6-4b) levels, respectively. Generally, the bacterial communities were composed of 12 phyla, accounting for > 96% of the total sequences. Among them, the three phyla Firmicutes, Proteobacteria and

Bacteroidetes mainly dominated in LE (>98%), YE (83%) and CL (78%), whereas only 44% in the control group EtOH (Fig. 6-4a). The phylum's population distribution verifies the hypothesis mentioned above that a diverse feedstock composition is likely to enrich microbial populations.

Genera with relative abundance higher than 1% in each sample (a total of 25 genera) were displayed in Fig. 6-4b, and three genera, *Proteiniphilum* (1.1% - 18.7%), *Desulfovibrio* (1.1% - 20.1%) and *Brassicibacter* (1.6% - 4.2%), predominated in all the four batch experiments. The proteolytic and SCCs-producing *Proteiniphilum* dominated in the communities, especially in LE, with a high abundance of 18.7%. The sulfate reducing *Desulfovibrio* predominated notably in the community of LE (20.1%). The dominant of *Desulfovibrio* might be due to the addition of 2-bromoethanosulfonic acid (BESA) that could inhibit methanogenesis. In addition, the hydrolysis or metabolization of amino acids may release sulfate-related intermediates (Chiu & Lee, 2001; Ye, Quensen, Tiedje, & Boyd, 1999). The sugars- and peptides-utilizing *Brassicibacter* were prevailing in the four communities, especially in CL (4.2%). In both CL and YE, *Macellibacteroides* (13.4% and 29.9%), and *Peptoclostridium* (8.5% - 7.6%), were the first and second dominant genera, respectively. They were mainly responsible for hydrolysis of macromolecules and further converted into SCCs, such as acetate and butyrate (Galperin, Brover, Tolstoy, & Yutin, 2016; Jabari et al., 2012). The SCCs, specifically butyrate, are readily utilized for chain elongation together with ethanol, therefore promoting further caproate production. Additionally, the reductive metabolites, such as H₂ or formate,

help to maintain a reducing environment which is favorable to this bio-process (Steinbusch et al., 2011). In EtOH, 61% of sequences were categorized as unclassified genus or with abundance lower than 1%. No apparent dominance of particular genus was observed, and the bacterial population showed a relatively even distribution over the top 25 identified genera. Hereby, it was presumed that an enriched microbial community correlates to a synergetic network with relatively high efficiency in chain elongation system.

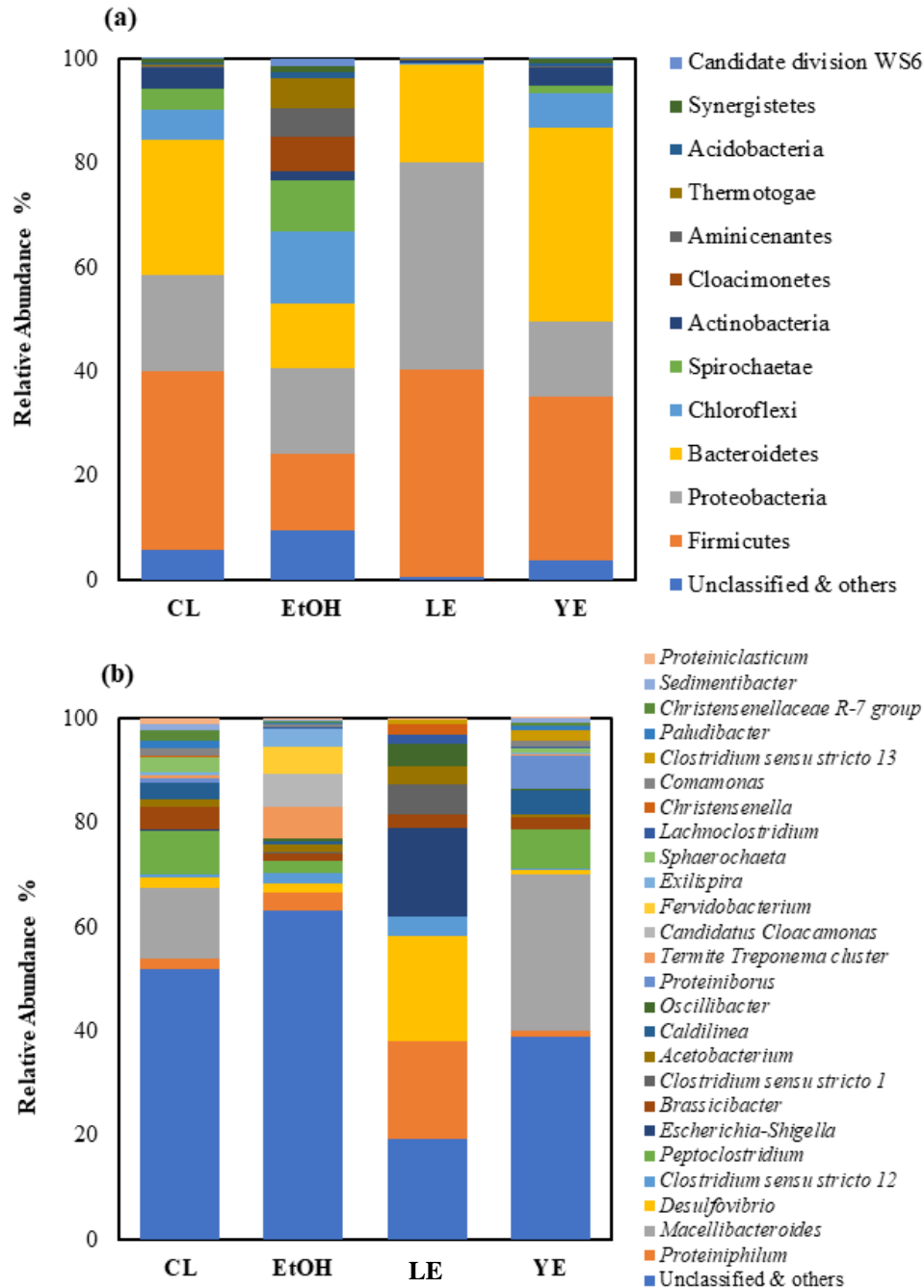


Figure 6-4. Taxonomic classification of bacterial communities of the four groups at (a) phylum and (b) genus levels. Relative abundance is defined as the number of reads affiliated with any given taxon divided by the total number of reads per sample. Phylogenetic groups with a relative abundance lower than 1% were classified as “others”.

Fig. 6-5 shows potential correlations between the bacterial populations and experimental variables (supplement of lignocellulosic ethanol, yeast extract or cellulose; concentrations of substrates, ethanol and acetate; concentrations of intermediate butyrate and product caproate). Canonical Correspondence Analysis (CCA) resolves that neither concentration of substrates nor products exerted significant effect on the microbial communities. The explanation is that the initial concentrations of ethanol and acetate were fixed as the same, and the concentrations of intermediate and product varied within a relatively small range. Furthermore, the control experiment (EtOH) was located with long distance from other three experiments and varied greatly in direction (Fig. 6-5). The distributions of the microbial communities in YE and CL were similar than that of LE, which was possibly contributed by the complexity of feedstock composition of lignocellulosic ethanol.

Results shown in Fig. 6-5 indicates that macromolecule-degrading *Proteiniborus* and *Macellibacteroides* were positively correlated to the supplement of yeast extract. Specifically, *Proteiniborus* are the protein-utilizing and hydrogen-producing bacteria, which could produce ethanol, acetic acid and hydrogen from yeast extract (Niu, Song, & Dong, 2008). In addition, macromolecule-utilizing *Peptoclostridium* was found to correlate with the addition of cellulose while *Clostridium sensu stricto* 1 and *Escherichia-Shigella* were observed because of the present of lignocellulosic ethanol providing energy and carbon sources. Particularly, the chain elongation intermediate, butyrate, is a genus-specific product

from fermentation of *Clostridium sensu stricto* 1. Additionally, the acetate or ethanol are also formed by this genus. Genera of *Clostridium sensu stricto* 12 and *Acetobacterium* were positively and remarkably correlated to the group of EtOH. The well-known caproate producing species *C. kluyveri*, belongs to *Clostridium sensu stricto* 12, indicating that ethanol is a crucial factor to this type of caproate producer. It also implied that *Acetobacterium* is prevalent bacteria in chain elongation system irrespective of substrate complexity, and they were predominantly producing acetic acid as a product.

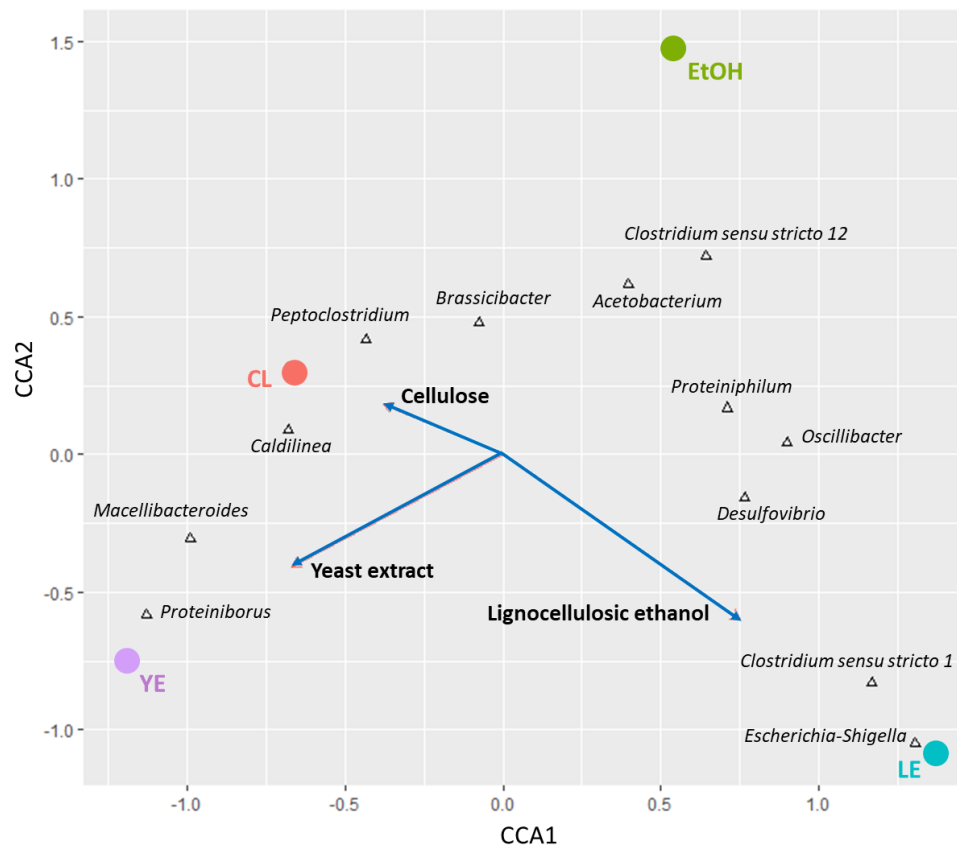


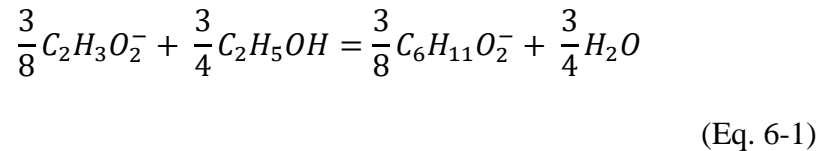
Figure 6-5. Canonical Correspondence Analysis (CCA) of microbial community patterns. The experimental variables (EVs), lignocellulosic ethanol, yeast extract and cellulose, are represented as arrows, whose direction explains most of the bacterial patterns and length indicates the magnitude of contribution of that EV in explaining variation in bacterial profiles. Dots represent the four experimental groups.

6.2.3 Microbial kinetics characterization

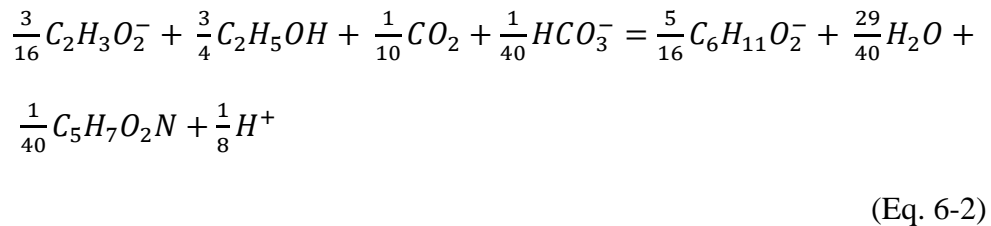
To better understand the performance of chain elongation for caproate formation in terms of kinetics, microbial kinetics of the chain elongating bacteria are estimated in our four experiments. A modified Thermodynamic Electron Equivalents Model (TEEM) was used to deduce the energetic and stoichiometric equations of caproate production (Rittmann & McCarty,

2001), then the growth rate of chain elongating bacteria was estimated by incorporating the Monod equation.

The energy reaction (R_e) for caproate production based on one electron flow is written as:



The reactions described here were written on one-electron-equivalent basis and the deduction procedure are described in Section 3.7 in detail. An overall reaction R for cell growth is obtained by combining proper proportion of the energy reaction and synthesis reaction. Accordingly, an overall equation including cell maintenance and cell synthesis was obtained:



According to the stoichiometry, the true yield (Y) was calculated as 0.08 g cells/g ethanol, and the maximum specific rate of substrate utilization \hat{q} was $218 \frac{g \text{ ethanol}}{g \text{ VSS-d}}$ at 37°C. Also, Y and \hat{q} were assumed to remain consistent because the caproate-producing bacteria and temperature were assumed unchanged in this case. Moreover, for all experimental groups, the concentration of active biomass initially, X_a^0 , was fixed at 50 mg VSS/L. Conversely, the value of concentration giving one-half the maximum rate ($M_5 L^{-3}$), K , highly affected by environmental conditions, was computed in separate group at different time. Lastly, together with

concentration of ethanol, growth rate μ was estimated using the Monod equation as described in Section 3.7.

Table 6-4 summarizes the estimated K and growth rate, μ , of the caproate-producing bacteria. The growth rate was determined in the initial stage of fermentation (< 10 days) because it was critical for evaluating the kinetics of caproate production. In Table 6-4, the values of μ for different electron donors were in the order of LE ($0.150 d^{-1}$) > YE ($0.136 d^{-1}$) > EtOH ($0.118 d^{-1}$) > CL ($0.047 d^{-1}$). Although the CL had the slowest growth rate in the initial stage, it was observed that the caproate formation initiated before Day 9. The explanation could be that the metabolization of cellulose results in butyrate, or even caproate production (Kenealy et al., 1995). Meanwhile, the value of K directly reflects the affinity of microorganisms to substrates, controlling the uptake efficiency of substrates. The compositions and viscosities of fermentation broth were different among all of experimental groups, resulting in different mass-transport resistances and substrate affinities for fermentation. In addition, K was affected by metabolic enzymes, which vary with different microbes.

According to the microbial community analysis, several OTUs with high abundance in the CL were closely related to *Macellibacteroides fermentans* (12.5%), *Sphaerochaeta globosa* (2.4%) and *Pseudoramibacter alactolyticus* (1.1%). These species were known to be capable of metabolizing glucose into butyrate, or even caproate (Jabari et al., 2012; Ritalahti et al., 2012; Willems & Collins, 1996). This metabolization is

recognized as a “shortcut” caproate process that reduces the lag phase in caproate formation. Compared with the EtOH, the YE increased both kinetics of caproate production and growth of caproate producing bacteria by shortening the lag phase and stimulating the cell synthesis, respectively. The possible explanation was that yeast extract provides nitrogen source, as well as other essential nutrients to support bacteria growth, and therefore stimulate bacteria activities for caproate production. From the perspective of energetics, the proportions of electron transferred to cell synthesis and microbial energy production from caproate formation were fixed. Thus, the overall electron uptake efficiency increased with the cell synthesis enhanced. Accordingly, yeast extract is speculated to promote the substrate uptake rate. As suggested by a previous study that proteinaceous materials could be metabolized by certain microorganisms into carboxylates (S. Y. Chen & Dong, 2005), this may potentially accelerate the chain elongation process, which is necessary for further study.

Table 6-4. Values of half-maximum rate concentration K and growth rate μ in the initial stage of fermentation ($t < 10$ days).

Group	K (mg/L)	μ (d^{-1})
LE	19,919 ^a (16,062 ~ 23,776) ^b	0.150 ^a (0.041 ~ 0.258) ^b
YE	131,365 ^a (73,952 ~ 188,777) ^b	0.136 ^a (0.085 ~ 0.187) ^b
EtOH	117,416 ^a (90,221 ~ 125,905) ^b	0.118 ^a (0.105 ~ 0.161) ^b
CL	191,465 ^a (211,041 ~ 340,260) ^b	0.047 ^a (0.014 ~ 0.076) ^b

^aMean value of parameters at different sampling points.

^bRange of parameter' values within $t < 10$ days.

6.3 Chapter summary

Fermentation performance shows that the lag phase of caproate production were shortened in experimental group LE (4 days), yeast extract (6 days), and cellulose (9 days) compared with the control group (17 days) without extra supplement. It suggests that LE is a promising feedstock for caproate production. Depletion of ethanol limited further elongation into caproate and resulted in comparable caproate yields, as well as carbon conversion ratios in four experimental groups. Microbial community and microbial kinetics analysis revealed that both yeast extract could be metabolized by protein-utilizing bacteria into short chain carboxylates (SCCs), which facilitated biological chain elongation. Important was found that yeast extract as nitrogen and other nutrient source stimulated the growth of caproate-producing bacteria. Apart from yeast extract, cellulose was utilized and further converted into SCCs, or even caproate, by cellulolytic bacteria. Together, caproate production was enhanced with high microbial activities and intermediates formation using LE. Via the energy-efficient chain elongation fermentation, LE was upgraded to a higher energy density product, caproate. Future study to optimize feedstock supplement and operation parameters is necessary to further improve the performance.

7. Chapter 7 Metagenomic insight into the microbial networks and metabolic mechanism in chain elongation for caproate production enhanced by casamino acids

7.1 Overview

Chain elongation (CE) process with mix-culture upgrades diluted ethanol and short chain carboxylates (SCCs) into medium chain carboxylates (MCCs). Approaches like modification of reactor configuration, adjustment of operation parameters were successfully applied to improve the productivity of MCCs in the process (T. I. Grootscholten et al., 2013; T. I. M. Grootscholten et al., 2013b). In particular, to support the growth of the MCCs producing bacteria and increase the productivity, yeast extract was commonly added as a supplement in the CE process (W. S. Chen et al., 2016; T. I. Grootscholten et al., 2013; Grootscholten et al., 2012; T. I. M. Grootscholten et al., 2013b; Kucek et al., 2016). Moreover, it was proposed that yeast extract might also contribute to the butyrate formation therefore facilitated the CE process indirectly (W. S. Chen et al., 2016). Specifically, the well-known caproate-producing bacteria, *Clostridium kluyveri*, produces caproate from ethanol with acetate (Barker et al., 1945; Seedorf, Fricke, Veith, Bruggemann, Liesegang, Strittmatter, et al., 2008) was identified to be the predominant and the main functional chain elongating microorganism in the mix-culture CE processes (Matthew T. Agler et al., 2012; Steinbusch et al., 2011). Yeast extract is also a common supplement used to stimulate growth and production rates of *C. kluyveri* (Gildemyn et al., 2017; Tomlinson & Barker, 1954). On the other hand, the addition of biochar was recently reported to be able to improve the CE process

presumably because biochar facilitates electron transfer and the formation of a stable microorganism community structure due to its conductivity and the partitioning by biochar (Y. H. Liu et al., 2017). Similarly, such reinforcement effect of electrically conductive particles, such as granular activated carbon (GAC) was reported widely in anaerobic digestion (AD) systems (Kato et al., 2012a, 2012b; F. H. Liu et al., 2012). This is attributed to the conductive particles which promote the direct interspecies electron transfer and stimulate aggregate of functional microorganisms in AD (Kato et al., 2012a; F. H. Liu et al., 2012).

In this chapter, the effects of casamino acids, as the main composition in the yeast extract, and the conductive GAC particles on the MCCs production in CE process are evaluated, respectively. The fermentation performance, composition of microbial communities and their changes over time in each experiment are examined. Meanwhile, metagenomics and meta-transcriptomics sequencing are applied to investigate the interspecies metabolic interactions and to estimate metabolic activities of the primary pathways. A deeper mechanistic understanding of the enhancement of fermentation performance and the associated microbial responses and their metabolic behavior in the mixed populations is necessary. CE process with complex reactor microbiomes would benefit from shaping a stable and functional community structure, therefore provides information for the design and operation of an efficient and predictable system.

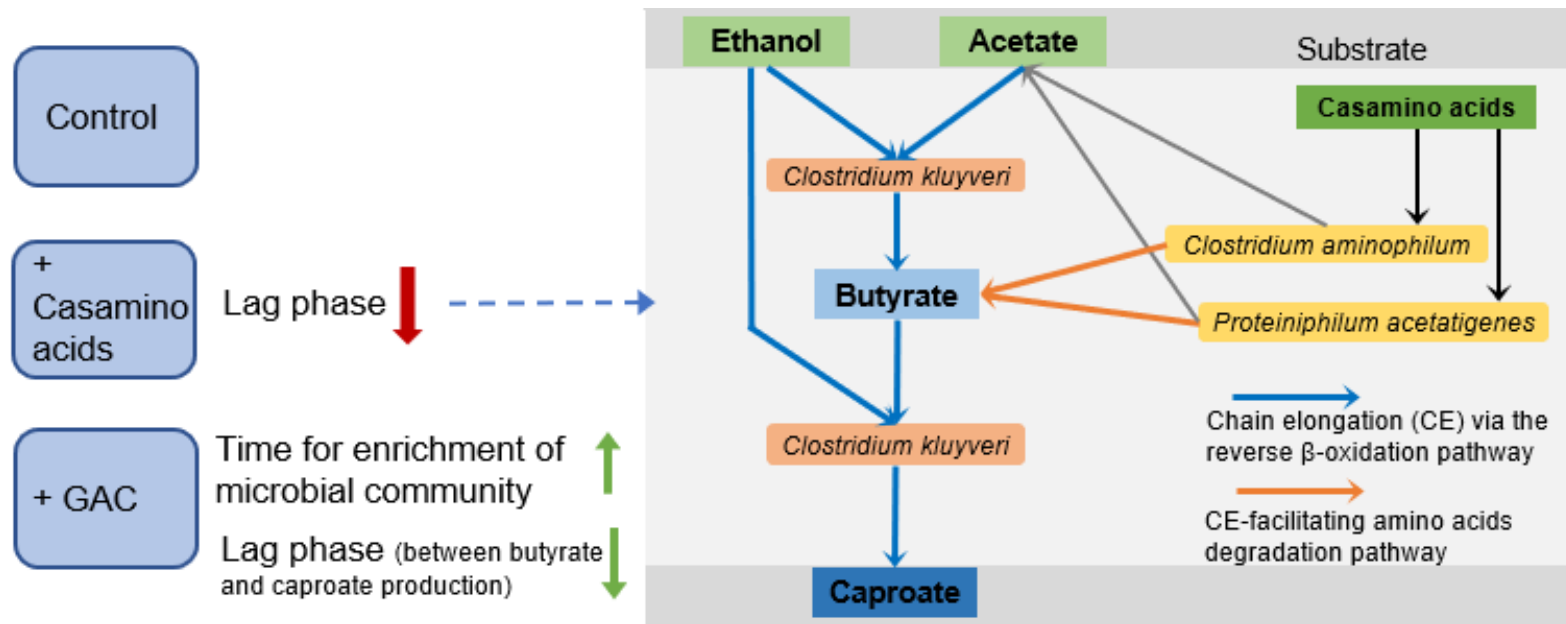


Figure 7-1. Experimental groups to enhance caproate production via chain elongation process, and the essential substrates flow in the experiment with extra supplement of casamino acids.

7.2 Results and discussion

7.2.1 Shortening the lag phase of caproate production

Three semi-continuous fermentations were conducted in 1-L fermenters anaerobically. The reactor “AA” was supplied with extra 5 g/L of casamino acids, meanwhile, 10% (v/v) of granular activated carbon (GAC) particles (size 1.5-2 mm) were added to the reactor named “GAC”. There was no extra supplement into the reactor “Control”. The details of reactor operation are provided in Section 3.3. In all the three reactors, the initial concentration of acetate and ethanol was 46 mM and 287 mM, respectively. As shown in Fig. 7-2, a significant increase in the concentration of butyrate was observed in the Control (44 mM) and AA (55 mM) on Day 7 days, indicating the formation of an effective microbial community for CE. Comparatively, although butyrate was produced within the first 20 days (max. of 20.5 mM) in the GAC, a high concentration of it was not detected until Day 30 (53 mM). This implied that the addition of GAC extended the time required for the butyrate production, presumably because microorganisms needed longer time to adapt and enrich on GAC particles than these without such interference. Furthermore, on Day 10, there was a notable increase in the concentration of caproate (35 mM). While concentration of caproate showed a slight increase on Day 21 and obviously increased on Day 30 in the Control. Thereby, its lag phase for caproate production (23 days) was prolonged by 20 days compared to the AA (3 days), suggesting that the addition of casamino acids greatly shortened the lag phase. Moreover, in the GAC, 12 days after the significant butyrate production, a high concentration of caproate was

observed. Accordingly, the reactor GAC resulted in a lag phase of 12 days, which was 11 days shorter than that of the Control. Although the microbial community required longer time for enrichment with the addition of GAC, once the community was well-enriched, the microbial interactions were more efficient than the Control. Figure 7-3 shows the concentration of electrons in the formed product in the three reactors during the whole fermentation. The concentration of inflow electron into the three reactors was the same, since they were supplied with substrates of the same concentrations. While the reactor AA yielded electron (in the forms of butyrate, caproate and butanol) with higher efficiency than the other two reactors. Presumably, the extra casamino acids added not only stimulated microbial growth, but also indirectly involved in the chain elongation process, attributing to efficient substrates utilization and product formation. Comparatively, the reactor with GAC was even less efficient than the Control, while the product yield surpassed after Day 54. Such lag phase of products formation caused by GAC was probably because that GAC disorganized the original microbial aggregates and the microorganisms would accommodate and form a well-functional structure gradually.

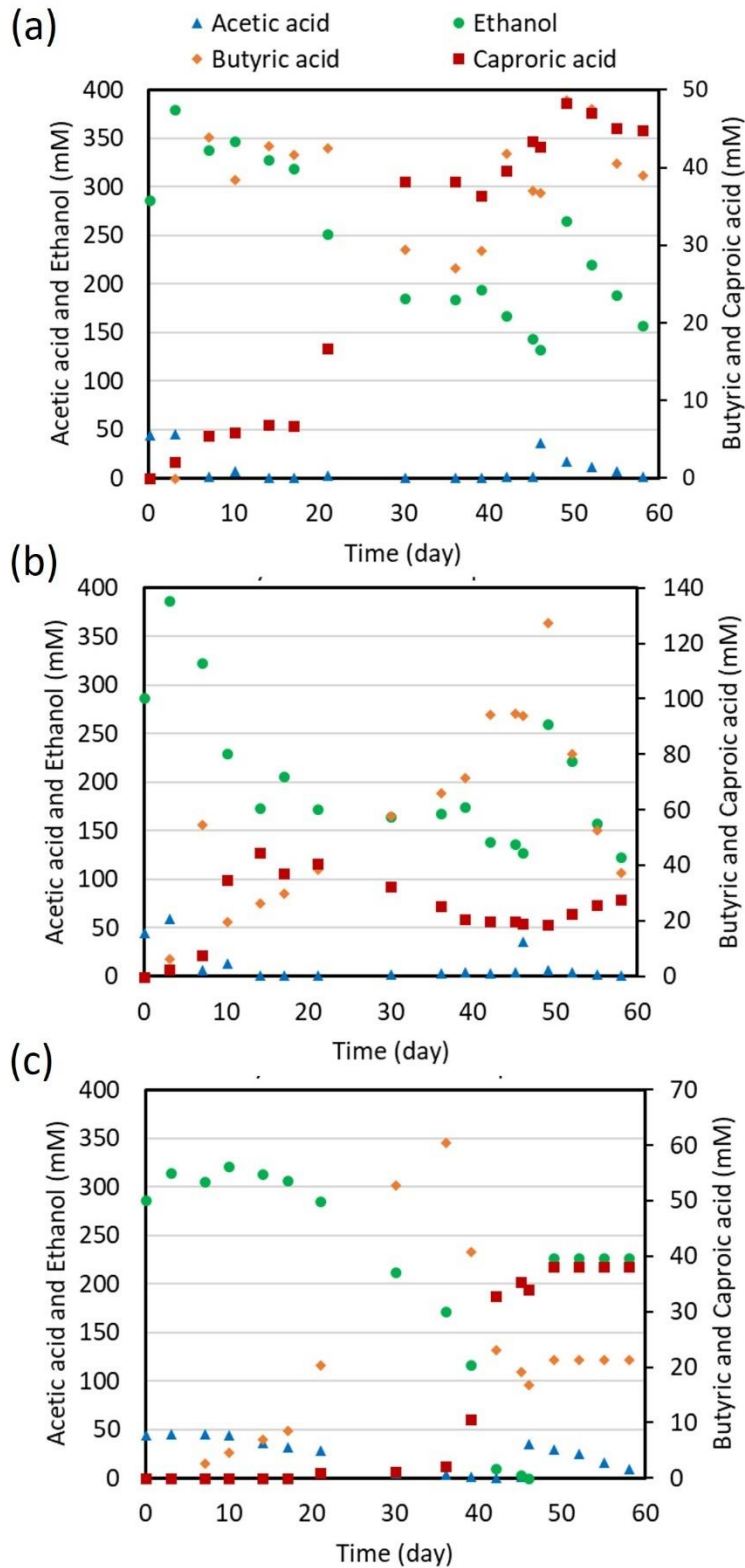


Figure 7-2. The concentration of substrates and products in the three CE reactors: (a) Control; (b) AA and (c) GAC.

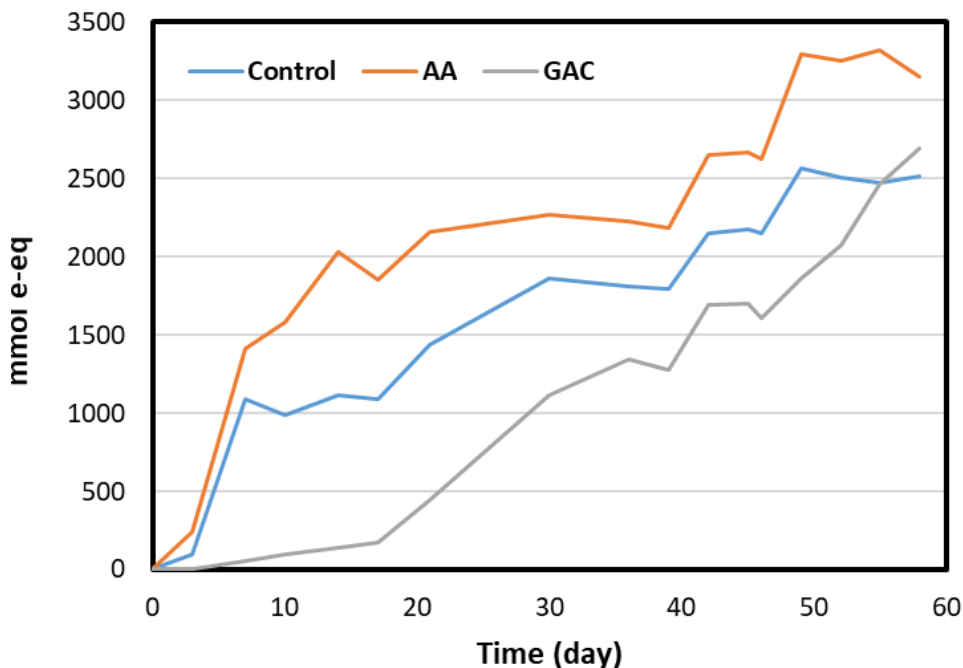


Figure 7-3. The concentration of electrons based on e- equivalent in the formed products across the whole fermentation.

* The calculation was based on the number of electrons contained in the reduced compounds (mol e⁻/mol: 32 for caproate, 20 for butyrate, 24 for butanol).

7.2.2 Microbial community and community composition convergence in chain elongation

To evaluate the microbial community response to the addition of casamino acids and GAC, as well as the changes over time, samples were taken on Days 0, 10, 14, 21, 30, 45 and 51 for 16S rRNA sequencing analysis. The high Good's coverage (>0.95) indicated that sequencing depth was adequate to reflect the whole microbial community (Table 7-1). PCoA was applied to evaluate the similarity among those microbial communities. Fig. 7-5 showed that samples from the reactors Control and AA were clustered

together indicating that a high similarity of microbial community structure over time for the Control and AA. Whereas the communities from the GAC formed distinct clusters and closed to the raw sludge in the initial stage of fermentation. Fig. 7-5 showed significant microbial structure variations in the GAC, suggesting that the addition of GAC induced adaptation and changes of microbe consortia. Moreover, after 51 days of fermentation, the communities of three reactors were clustered closely, illustrating that the microbial community structures were similar and well-formed after cultivation and enrichment. Additionally, alpha-diversity analysis showed that microbial communities of the three reactors were much less diverse and less evenly distributed than the raw sludge, implying an effective enrichment of microbial consortia (Table 7-1).

Table 7-1. The coverage and alpha-diversity indices of the 19 microbial communities at 3% cutoff.

Sample	Coverage	Shannon diversity	Chao richness	Shannon evenness
raw_sludge	0.95	3.97	742.05	0.68
D10_AA	0.98	1.51	273.59	0.32
D10_CON	0.98	1.40	307.16	0.29
D10_GAC	0.98	2.08	287.17	0.43
D14_AA	0.98	1.36	294.80	0.29
D14_CON	0.96	2.33	500.09	0.43
D14_GAC	0.99	1.23	204.28	0.28

D21_AA	0.98	1.48	236.16	0.32
D21_CON	0.98	1.35	273.05	0.28
D21_GAC	0.99	1.24	115.68	0.34
D30_AA	0.99	1.54	183.96	0.35
D30_CON	0.98	1.37	229.38	0.30
D30_GAC	1.00	1.23	80.93	0.37
D45_AA	0.99	2.01	171.58	0.46
D45_CON	0.98	1.34	269.88	0.28
D45_GAC	1.00	1.58	53.08	0.47
D51_AA	0.99	1.67	153.26	0.39
D51_CON	0.99	1.09	215.57	0.25
D51_GAC	1.00	0.99	36.15	0.33

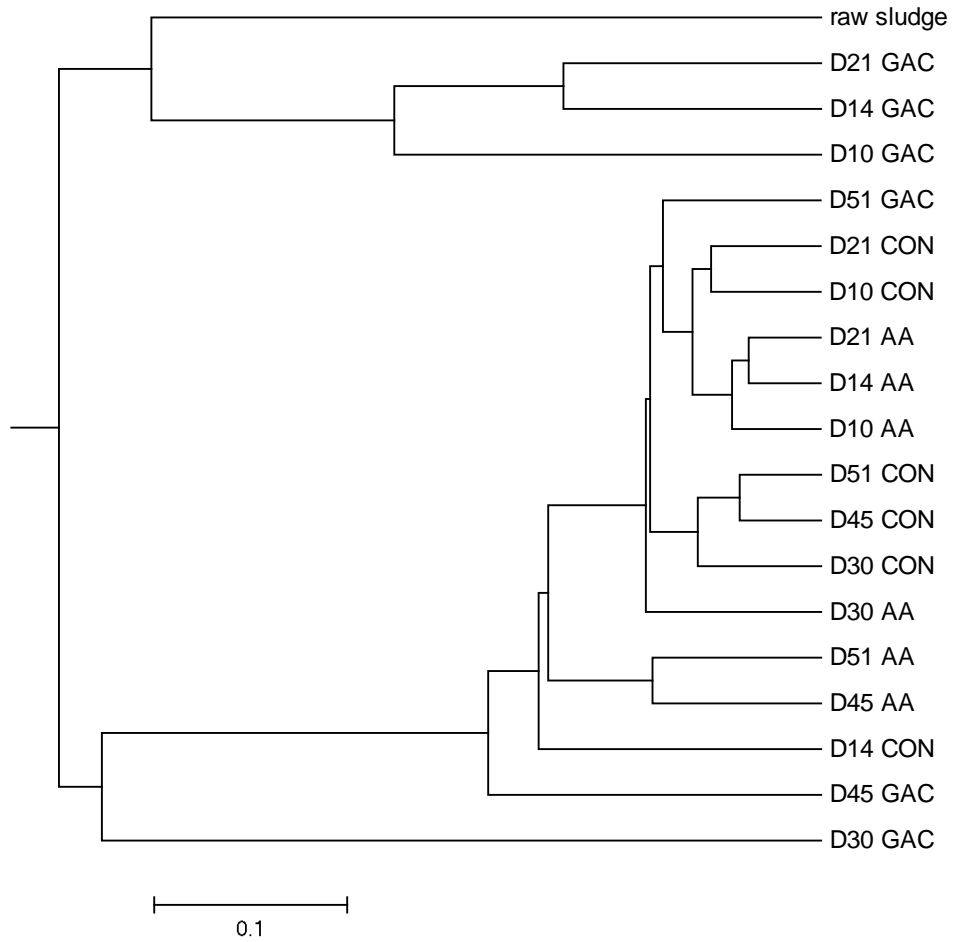


Figure 7-4. Beta-diversity analysis among groups with UNIFRAC dendrogram tree;

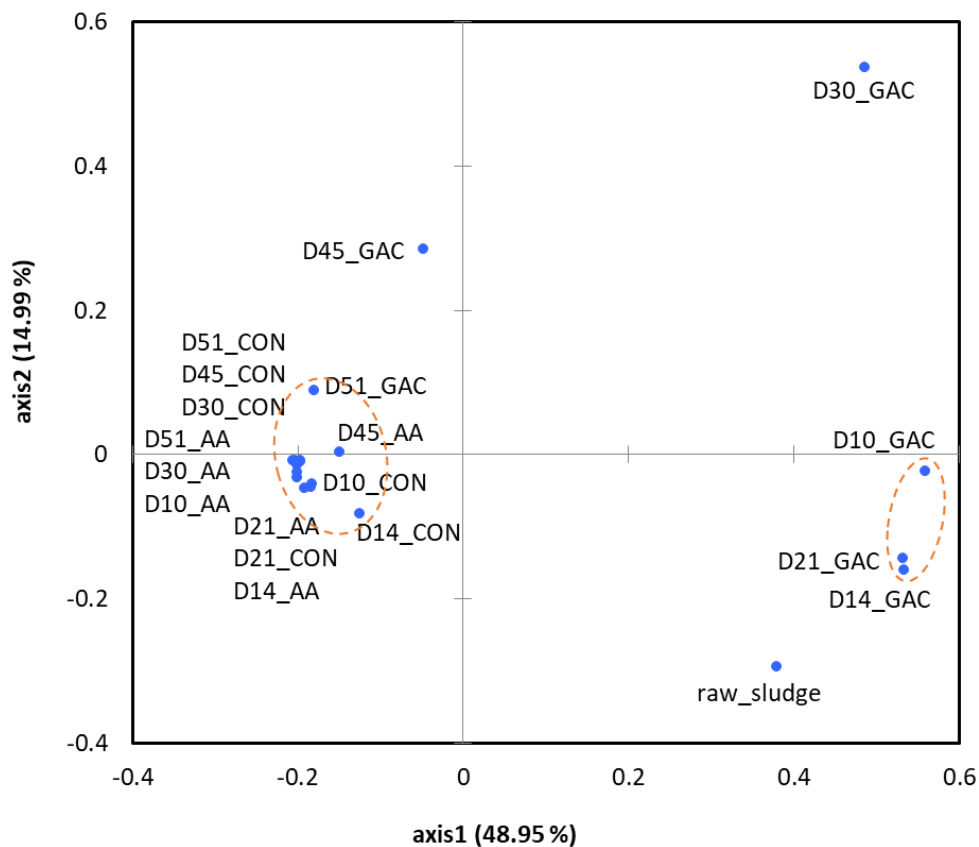


Figure 7-5. Principal coordinate analysis (PCoA) of community similarity comparing the 19 samples. Principal coordinate 1 (axis 1) vs. Principal coordinate 2 (axis 2) are represented. axes 1 and 2: 63.94 %. Each dot was named after the form of “sampling day_the reactor”.

Specifically, as shown in Fig. 7-6a, the phyla Proteobacteria, Firmicutes and Spirochaetes almost evenly predominated in the microbial community of raw sludge, accounting for 60% of the total population. Nevertheless, after 10 days cultivation, Firmicutes was remarkably enriched in the reactor AA (91.7%) and Control (88.56%), and the predominance was maintained during the whole fermentation period. In comparison, the microbial community in reactor GAC was predominated by Proteobacteria in the first 21 days, then the predominance shifted to Firmicutes after Day 30 and was

consistent with the other two reactors then. From the taxonomic distribution of microbial community at genus level, as shown in Fig. 7-6b, the proportion of “others”, generic groups with a relative abundance lower than 1%, decreased distinctly as fermentation proceeded. This indicated an effective enrichment of community from raw sludge under experimental conditions. The most dominant genera in raw sludge, *Exilispira* and *Escherichia-Shigella*, later diminished as the fermentation proceeded. Particularly, a gradual enrichment of *Clostridium* happened in the three reactors, reaching abundance of 58% (in the Control), 38% (in the AA) and 76% (in the GAC). Such predominance of *Clostridium* was also observed in previous chain elongation system (Matthew T. Agler et al., 2012; Leng et al., 2017). *Clostridium spp.* were closely associated with carboxylates chain elongation, including the well-known caproate-producer *C. kluveri* (Seedorf, Fricke, Veith, Bruggemann, Liesegang, Strittmatter, et al., 2008). Besides, *Brassicibacter* was well-enriched in the AA and the Control, which utilizes amino acids and forms acetate and ethanol (Fang et al., 2012). The amino acids-rich environment in the AA was favorable for *Brassicibacter* and supplied it more sufficient substrates for the products formation than in the Control, in which microbial debris were its main substrates sources. Moreover, another dominated genus in the AA and the Control, *Proteiniphilum*, is also proteolytic and capable to use several amino acids, such as glycine and L-arginine, or yeast extract to produce acetic acid as the main product (S. Y. Chen & Dong, 2005). The microbial communities in AA and the Control were similar and maintain relatively consistent over the whole fermentation period. Comparatively, microbial

community of the GAC shifted greatly, and a well-enriched community for effective CE was formed till Day 30. In the initial stage, other than *Clostridium*, the community was mainly dominated by *Pseudomonas* and *Kluyvera*. Specifically, *Pseudomonas* was associated with biofilm formation and only dominated in the GAC. It was highly enriched in the first stage of fermentation to facilitated biofilm formation on GAC and it diminished after 30 days probably because a biofilm was well-formed then. Similarly, the fermenting bacteria *Kluyvera* dominated in community in the first 30 days and diminished afterwards. It was able to utilize acetate and potentially competed for acetate as substrate with *Clostridium* (Farmer et al., 1981), especially at the beginning when *Clostridium* was not well-enriched. After 30 days of cultivation, the communities of the GAC shifted and turned to be similar to the other two and predominating by *Clostridium* and *Proteiniphilum*, which mainly attributed to MCFAs formation.

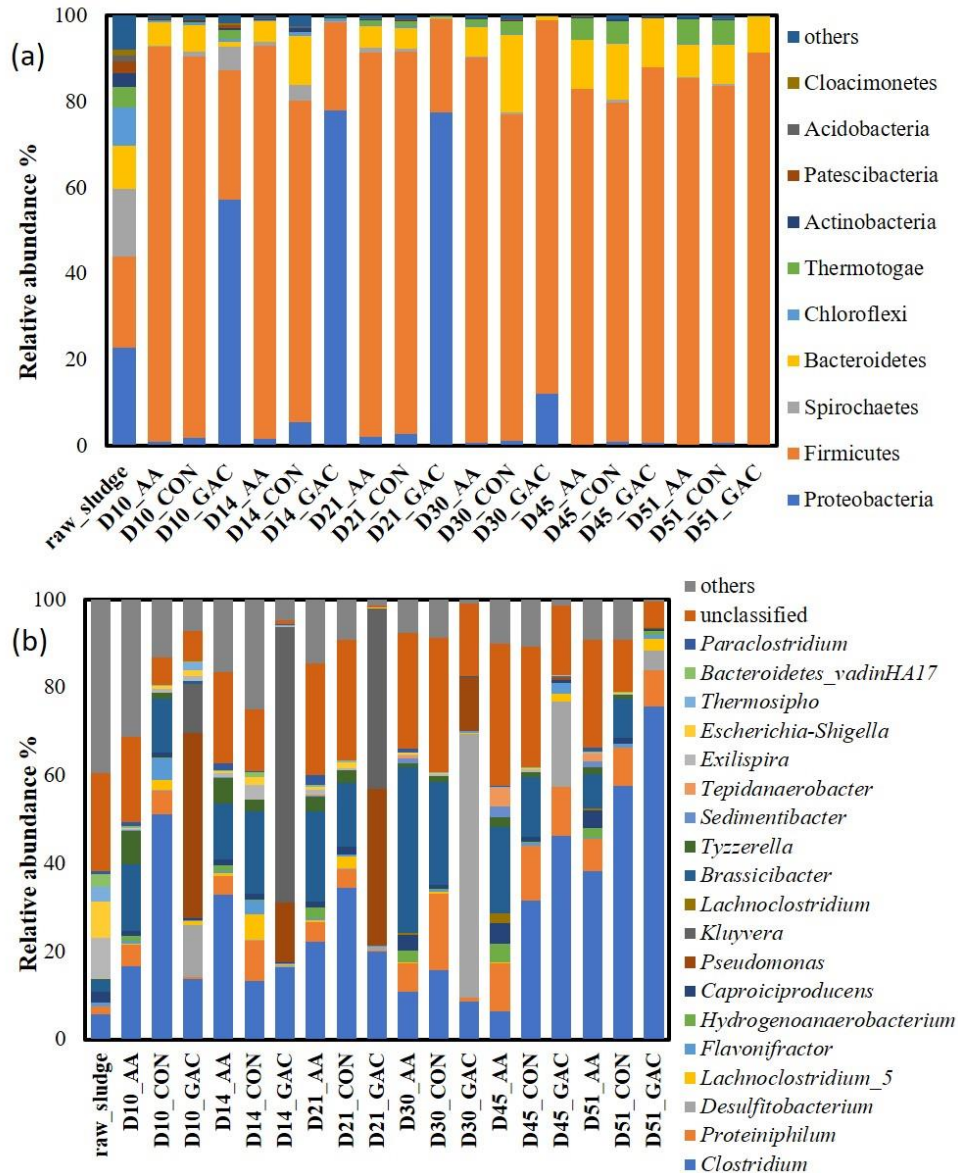


Figure 7-6. Taxonomic classification of the bacterial communities of the raw sludge and the three reactors (Control, GAC and AA) on different days (a) at phylum level; (b) at genus level. Phylum or genus occurred at abundance more than 1 % in at least one sample was annotated whereas rests were grouped as “others”.

7.2.3 Reconstruction of highly active pathways in the reactor AA

To further explore the interspecies metabolic interactions, a sample was taken from the AA on Day 14, on which the concentration of caproate was

significant, for metagenomics and transcriptomics analysis. Microbial community of the AA was predominated *Clostridium*, *Proteiniphilum*, and *Brassicibacter* based on the 16s rRNA genes analysis. The recovered high-quality genome bins (with > 90% completeness) that phylogenetically identified to be closely related to the genomes of *Clostridium kluyveri*, *Proteiniphilum acetatigenes*, and *Clostridium aminophilum*, respectively (Fig. 7-7, Appendix III) were analyzed further for metabolic pathways reconstruction. These functional microorganisms together represented the majority of the microbial community in the AA.

Table 7-2. High-quality genome bins recovered from sample in reactor AA on Day 14.

Bin name	Completeness	Genome size (bp)	GC content (%)
CE_AA_MaxBin.015.fasta	100.00%	3194683	36.3
CE_AA_MaxBin.010.fasta	97.50%	3140142	39
CE_AA_MaxBin.011.fasta	97.50%	2556319	41.7
CE_AA_MaxBin.013.fasta	97.50%	2761694	57.5
CE_AA_MaxBin.014.fasta	97.50%	2270987	63.4
CE_AA_MaxBin.016.fasta	97.50%	3152192	37
CE_AA_MaxBin.022.fasta	97.50%	4774835	49.5
CE_AA_MaxBin.031.fasta	97.50%	4143188	55.6
CE_AA_MaxBin.042.fasta	97.50%	2627794	52.5
CE_AA_MaxBin.052.fasta	97.50%	2840435	53.2
CE_AA_MaxBin.012.fasta	95.00%	2713814	60.4
CE_AA_MaxBin.029.fasta	95.00%	2241905	61
CE_AA_MaxBin.030.fasta	95.00%	2840808	57.5

CE_AA_MaxBin.080.fasta	95.00%	2056004	53.7
CE_AA_MaxBin.081.fasta	95.00%	3041418	50.3
CE_AA_MaxBin.006.fasta	92.50%	4141739	48.2
CE_AA_MaxBin.017.fasta	92.50%	2403002	53.5
CE_AA_MaxBin.067.fasta	92.50%	3216504	45.4
CE_AA_MaxBin.060.fasta	90.00%	2524328	53.4

As an exceptional anaerobe, *C. kluyveri* was reported to be capable to accomplish ethanol–acetate chain elongation for caproate production using the reversed β -oxidation pathway, which can be characterized by three coupled reactions (Seedorf, Fricke, Veith, Bruggemann, Liesegang, Strittmatter, et al., 2008). Ethanol, as the electron donor, is first oxidation to acetate (ethanol is converted to acetate producing NADH and ATP via substrate level phosphorylation). Then, acetate together with CoA is converted to acetyl CoA and elongated to butyrate using NADH and FADH₂ in a cyclic pathway. Lastly, by using a similar cyclic pattern of coupling butyryl-CoA with acetyl-CoA, caproate is elongated from butyrate and ethanol (Seedorf, Fricke, Veith, Bruggemann, Liesegang, Strittmatter, et al., 2008; Steinbusch et al., 2011). Based on the observation in the experiments, the fermentation occurs in a similar way that first ethanol was consumed, and then butyrate was produced, followed by caproate production (Fig. 7-2). The complete ethanol-acetate fermentation pathway for caproate was fully recovered from the *C. kluyveri* (CE_AA_MaxBin.002) genome bin (Fig. 7-7; Appendix III). Caprylate formation has not been reported before for *C. kluyveri*, and no caprylate production was observed across the whole fermentation in our study.

Metatranscriptomics analysis confirms that the genes involved in this reversed β -oxidation pathway for caproate production were actively-transcribed (Appendix IV).

The proteolytic bacteria, *Proteiniphilum acetatigenes*, is capable to ferment yeast extract, peptone and amino acids, such as L-serine and L-alanine, to produce short chain fatty acids (SCFAs), especially acetic acid as the main product (S. Y. Chen & Dong, 2005). Similarly, the amino acids-utilizing bacteria, *Clostridium aminophilum*, uses serine, glutamine, and histidine to produce SCFAs, specifically acetate and butyrate. In the recovered genome bins related to *P. acetatigenes* (CE_AA_MaxBin.018) and *C. aminophilum* (CE_AA_MaxBin.016), the pathway of glycine/serine degradation for butyrate production was fully recovered, as shown in Fig. 7-7, and confirmed to be transcriptionally active (Appendix III; Appendix IV). Therefore, these amino acids-utilizing activities indirectly facilitate the chain elongation pathway by supplying the key intermediate, butyrate. It also explains the higher butyrate concentration in the reactor AA than the other two. When the ethanol was supplied sufficiently and there was no products-inhibition effect, the further chain elongation step into caproate would be thermodynamically feasible and proceed.

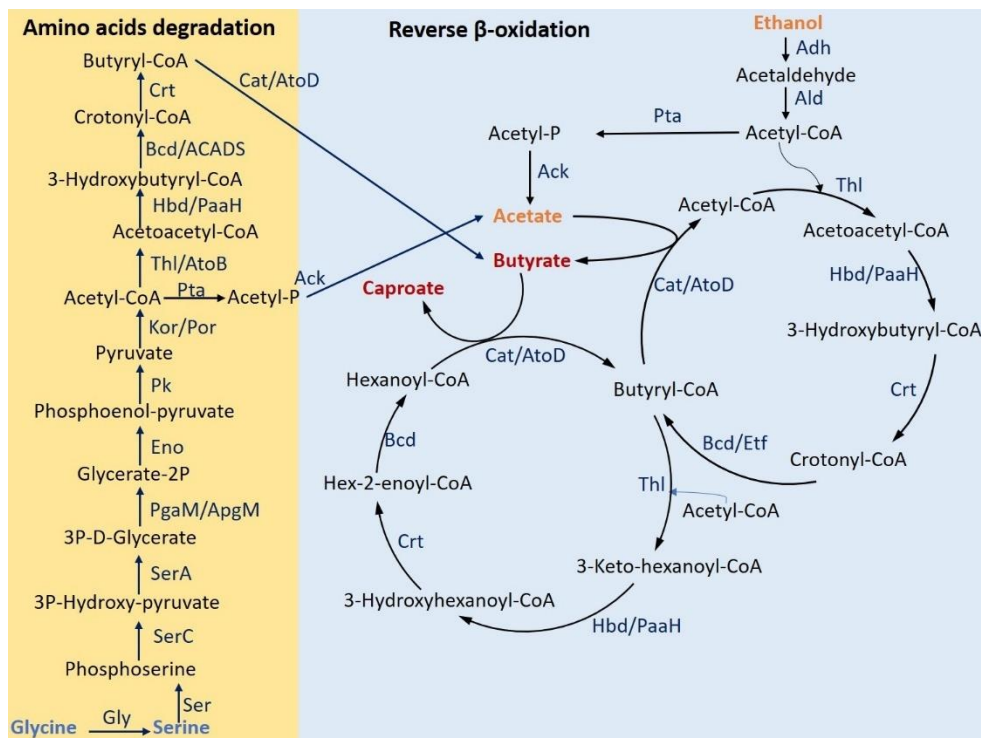


Figure 7-7. Annotated metabolic pathways of ethanol-acetate fermentation for butyrate and caproate production (in blue) and degradation of glycine and serine for butyrate production (in yellow) in the reactor AA on Day 14.

7.3 Chapter summary

In this chapter, chain elongation processes for caproate production are tested in three reactors: reactor AA with extra casamino acids supplement, reactor GAC with extra GAC particles addition and reactor Control without extra supplement. During 60 days of fermentation, it shows that the addition of casamino acids greatly shortened the lag phase for caproate production. The microbial community structures of the Control and AA show high similarity across the whole fermentation. *Clostridium* and *Proteiniphilum* significantly predominated and contributed to MCCs production. Comparatively, the reactor with GAC has a longer lag phase for butyrate production, but not for caproate formation, mostly because the disturbance

of GAC on the microbial aggregates necessitated microorganisms to adjust and reform a well-functional microbial community structure. In the reactor AA, metagenomics analysis recovers high quality genome bins closely related to the chain elongating bacteria *Clostridium kluyveri* and amino acids utilizing bacteria *Proteiniphilum acetatigenes*. Pathway reconstruction indicates that *C. kluyveri* produces butyrate and caproate via the reversed β -oxidation pathway. Meanwhile, *P. acetatigenes* utilizes amino acids, such as glycine and serine, to produce the crucial intermediate butyrate, which indirectly facilitate further chain elongation into caproate. The genes involved in these pathways are confirmed to be metabolic active. Shortening the lag phase is an applicable approach to improve the chain elongation process, since it can potentially decrease the retention time and reduce to volume of reactor in the operation of fermentation. A deeper understanding of the associated microbial activities would help to cultivate a robust and well-functional microbial community, resulting in an efficient and predictable system.

8. Chapter 8 Conclusions and Recommendations

8.1 Conclusions

In this thesis, the methanogenic anaerobic digestion systems were investigated in depth by examining the microbial communities and further analysis of interspecies interactions and metabolic pathways facilitated by GAC for the final methane production. Moreover, an environmental-friendly anaerobic chain elongation processes to recovery the value-added chemical, caproate, was set up and explored by examining its physiological performance, corresponding microbial communities, microbial kinetics and the main metabolic pathways. The results obtained in this study may help to predict and improve the anaerobic fermentation processes under certain conditions, so as to assist the development and/or optimization of the pilot-scale and full-scale anaerobic fermentation system. Unveiling the microbial interactions would help to elucidate microbial behavior and provide strategies for the further improvement of bioenergy processes.

Firstly, it reported the microbial community structures and dominance of microbial groups of two methanogenic novel staged anaerobic fluidized bed ceramic membrane bioreactor (SAF-CMBR) systems using electronically conductive GAC and non-conductive PET as fluidizing media. GAC is found to be a more selective environment for microorganisms, particularly syntrophic propionate oxidizing bacteria (SPOB) and methanogens, than the bulk liquid for methane production. SPOB (*Syntrophobacter* and *Smithella*), acetoclastic/DIET-dependent CO₂ reduction methanogens *Methanotherix* and exoelectrogenic bacteria,

Geobacter predominated on GAC particles. While the microbial community developed on PET beads differed greatly, predominating by *Pseudomonas* associated with biofilm formation and the exoelectrogenic and acetate-utilizing bacteria, *Geobacter* and *Arcobacter*. By using GAC as carrier, anaerobic treatment, especially methane production, was achieved mainly by microorganism grown on the GAC particles in which SPOC, methanogens and exoelectrogenic bacteria cooperate and gain mutual benefit.

Specifically, in the energy-efficient SFA-CMBR with GAC as fluidizing media, metagenomic and metatranscriptomic analyses verified that SPOB degraded propionate into acetate, which was further converted into methane and CO₂ by *M. concilii* via the acetoclastic methanogenesis pathway. Concurrently, *G. lovleyi* oxidized acetate into CO₂ and released electrons into the extracellular environment. Such acetate-rich system favored the synergic growth of *M. concilii* and *G. lovleyi*. Importantly, facilitated by DIET, *M. concilii* received electrons from *Geobacter* and reduced CO₂ into methane via both the classical CO₂ reduction and the reductive hexulose-phosphate (RHP) pathway. The RHP pathway, analogous to the Calvin–Benson cycle in plant photosynthesis, was found to be metabolically active and it enables *M. concilii* to gain dominance and energy through carbon anabolism and yielding carbon intermediates for catabolism, respectively. Also, it was found that these two the CO₂ reduction pathways were metabolically linked with the acetoclastic methanogenesis via a methyl-H₄MPT intermediate. Further

thermodynamics calculation verified the feasibility of the acetoclastic methanogenesis and classical and RHP CO₂ reduction pathway under such system conditions. Therefore, acetate could be completely reduced to methane (2 mole methane formation per 1 mole acetate consumption) and attributed to high methane yield from the system.

Moreover, the chain elongation (CE) process with mix-culture was set up to evaluate the feasibility of upgrading lignocellulosic ethanol (LE) for caproate production, as well as the effects of yeast extract and cellulose on CE. LE showed a great potential as a promising feedstock for caproate production. The results showed that the lag phase of caproate production were shortened in experimental group LE (4 days), yeast extract (6 days), and cellulose (9 days) compared with the control group (17 days) without extra supplement. Caproate yields and carbon conversion ratios were limited by the deficiency of ethanol. By microbial community and microbial kinetics analysis, it was revealed that both yeast extract and cellulose could be metabolized by protein-utilizing and cellulolytic bacteria, respectively, into short chain carboxylates (SCCs), which facilitated biological chain elongation. Meanwhile, yeast extract boosted microbial growth by serving as nitrogen and other nutrient sources. Together, the CE process for caproate production was improved with enhanced microbial activities and intermediates formation using LE. Via such energy-efficient process, LE was upgraded from diluted feedstock to a higher energy density product, caproate.

Furthermore, in the semi-continuous CE process, the physiological performance of ethanol-acetate fermentation for caproate production with extra addition of casamino acids and GAC, respectively, showed that addition of casamino acids greatly shortened the lag phase for caproate production. The experimental results show that the addition of casamino acids greatly shortened the lag phase (time required for caproate production). While the reactor with GAC resulted in a longer lag phase for butyrate production, but not for caproate formation compared to the control, because microorganisms need to adapt and reform well-functional microbial consortia after the disturbance of GAC on the original microbial aggregates. Via the microbial analysis, it was shown that the reactors Control and AA shared high similarity in the microbial community structure and remarkably predominated by *Clostridium* and *Proteiniphilum*, which cooperated and contributed to MCCs production. Although the reactor GAC displayed great variations in microbial community, it was gradually enriched and became similar with the other two after 51 days of cultivation. In the reactor with casamino acids supplement, metagenomics analysis recovers high quality genome bins closely related to the chain elongating bacteria *Clostridium kluyveri* and amino acids utilizing bacteria *Proteiniphilum acetatigenes*. Pathway reconstruction indicates that *C. kluyveri* produces butyrate and caproate via the reversed β -oxidation pathway. Meanwhile, *P. acetatigenes* utilizes amino acids, such as glycine and serine, to produce the crucial intermediate butyrate, which indirectly facilitate further chain elongation into caproate. The genes involved in these pathways are confirmed to be metabolic active. It indicated that

amino acids could not only support microbial growth, but also be directly involved in the CE metabolism and attributed to increased efficiency of the process.

8.2 Recommendations for Future Work

For the methanogenic anaerobic digestion systems, adjustment and optimization of operation conditions is applicable to fully utilize the interspecies interactions and capability of CO₂ assimilation of *Methanotherix* to improve methane production and energy recovery efficiency in AD systems. In the chain elongation process study, experiments were conducted in lab-scale or batch reactors, which was impractical for real application. In future work, experiments in continuous operation and pilot-scale are needed to amend the results obtained under idealized conditions. Also, optimization of feedstock supplement is beneficial to further improve the fermentation performance.

Appendix I Coding DNA sequences (CDS) predicted to be involved in the metabolism of main pathways.

CDS	Predicted function	Gene name	Gene name	Enzyme commission
AFBR_GAC_MaxBin.001- <i>Geobacter lovleyi</i> - acetate oxidation to CO₂ (TCA cycle)				
AFBR_GAC_MaxBin.001_02087	phosphate acetyltransferase	pta	phosphate acetyltransferase	EC:2.3.1.8
AFBR_GAC_MaxBin.001_00587	acetate kinase	AckA	acetate kinase	EC:2.7.2.1
AFBR_GAC_MaxBin.001_00963	acetyl-CoA C-acetyltransferase	ato	acetyl-CoA C-acetyltransferase	EC:2.3.1.9
AFBR_GAC_MaxBin.001_00357	citrate synthase	CS	citrate (Si)-synthase	EC:2.3.3.1
AFBR_GAC_MaxBin.001_01231	aconitate hydratase 2 / 2-methylisocitrate dehydratase	acnB	aconitate hydratase	EC:4.2.1.3 4.2.1.99
AFBR_GAC_MaxBin.001_02542	aconitate hydratase	ACO	aconitate hydratase	EC:4.2.1.3
AFBR_GAC_MaxBin.001_01771	isocitrate dehydrogenase	IDH1	isocitrate dehydrogenase (NADP+)	EC:1.1.1.42

	2-oxoglutarate ferredoxin			
AFBR_GAC_MaxBin.001_01766	oxidoreductase subunit gamma	korC	2-oxoglutarate synthase	EC 1.2.7.3
	2-oxoglutarate/2-oxoacid			EC:1.2.7.3
AFBR_GAC_MaxBin.001_01767	ferredoxin oxidoreductase subunit beta	korB	2-oxoglutarate synthase	1.2.7.11
	2-oxoglutarate/2-oxoacid			EC:1.2.7.3
AFBR_GAC_MaxBin.001_01768	ferredoxin oxidoreductase subunit alpha	korA	2-oxoglutarate synthase	1.2.7.11
AFBR_GAC_MaxBin.001_01769	2-oxoglutarate ferredoxin oxidoreductase subunit delta	korD	2-oxoglutarate synthase	EC 1.2.7.3
AFBR_GAC_MaxBin.001_01643	succinyl-CoA synthetase alpha subunit	SucD	succinate---CoA ligase (ADP- forming)	EC 6.2.1.5
AFBR_GAC_MaxBin.001_01644	succinyl-CoA synthetase	SucC	succinate---CoA ligase (ADP-	EC 6.2.1.5

	beta subunit		forming)	
	succinate dehydrogenase /			
	fumarate reductase, iron-			
	sulfur subunit			
AFBR_GAC_MaxBin.001_01720		sdhB	succinate dehydrogenase	EC 1.3.5.1
	succinate dehydrogenase /			
AFBR_GAC_MaxBin.001_01721	fumarate reductase,	sdhA	fumarate reductase (quinol)	EC 1.3.5.4
	flavoprotein subunit			
AFBR_GAC_MaxBin.001_01936	fumarate hydratase	Fum	fumarate hydratase	EC:4.2.1.2
AFBR_GAC_MaxBin.001_01770	malate dehydrogenase	mdh	malate dehydrogenase	EC 1.1.1.37

AFBR_GAC_Bin72 - *Syntrophobacter fumaroxidans* - methylmalonyl-CoA (MMC) pathway

AFBR_GAC_MaxBin.072_00988	propionate CoA transferase	PCT	propionate CoA-transferase	EC:2.8.3.1
AFBR_GAC_MaxBin.072_03848	propionyl-CoA:oxaloacetate transcarboxylase	POT, pccA	methylmalonyl-CoA carboxytransferase	EC:2.1.3.1
AFBR_GAC_MaxBin.072_00452	methylmalonyl- CoA/ethylmalonyl-CoA epimerase	MCEE, epi	methylmalonyl-CoA/ethylmalonyl- CoA epimerase	EC:5.1.99.1
AFBR_GAC_MaxBin.072_00277	methylmalonyl-CoA mutase	MCM	methylmalonyl-CoA mutase	EC:5.4.99.2
AFBR_GAC_MaxBin.072_01546	succinyl-CoA synthetase	SCS	succinyl-CoA synthetase alpha subunit	EC:6.2.1.5
AFBR_GAC_MaxBin.072_03945	succinyl-CoA synthetase	SCS	succinyl-CoA synthetase alpha subunit	EC:6.2.1.5

AFBR_GAC_MaxBin.072_01935	succinate dehydrogenase	SDH/FR	succinate dehydrogenase	EC:1.3.5.1 1.3.5.4
AFBR_GAC_MaxBin.072_02545	fumarate hydratase (fumarase)	FHT	fumarate hydratase	EC:4.2.1.2
AFBR_GAC_MaxBin.072_03984	malate dehydrogenase	MDH	malate dehydrogenase (oxaloacetate- decarboxylating)(NADP+)	EC:1.1.1.40
AFBR_GAC_MaxBin.072_02538	malate dehydrogenase	MDH	malate dehydrogenase (oxaloacetate- decarboxylating)(NADP+)	EC:1.1.1.40
AFBR_GAC_MaxBin.072_02198	pyruvate dehydrogenase	PDHA	pyruvate dehydrogenase E1 component	EC:1.2.4.1
AFBR_GAC_MaxBin.072_02199	pyruvate dehydrogenase	PDHB	pyruvate dehydrogenase E1 component	EC:1.2.4.1

			pyruvate dehydrogenase E2	
AFBR_GAC_MaxBin.072_02200	pyruvate dehydrogenase	DLAT	component (dihydrolipoamide acetyltransferase)	EC:2.3.1.12
			2-oxoglutarate/2-oxoacid	EC:1.2.7.3
AFBR_GAC_MaxBin.072_01790	2-oxoglutarate/2-oxoacid ferredoxin oxidoreductase	korA	ferredoxin oxidoreductase subunit alpha	1.2.7.11
			acetyl-CoA synthetase (ADP-forming)	EC:6.2.1.13
AFBR_GAC_MaxBin.072_00502	acetyl-CoA synthetas	ACS		
			carbon-monoxide dehydrogenase	EC:1.2.7.4
AFBR_GAC_MaxBin.072_00503	carbon-monoxide dehydrogenase	cooS	carbon-monoxide dehydrogenase	EC:1.2.7.4

AFCMBR_GAC_MaxBin.090 - *Methanotherx concilii* - acetoclastic methanogenesis

AFCMBR_GAC_MaxBin.090_00490	acetyl-CoA synthetase	ACS	acetyl-CoA synthetase	EC:6.2.1.1
-----------------------------	-----------------------	-----	-----------------------	------------

AFCMBR_GAC_MaxBin.090_00611	acetyl-CoA synthetase	ACS	acetyl-CoA synthetase	EC:6.2.1.1
AFCMBR_GAC_MaxBin.090_00613	acetyl-CoA synthetase	ACS	acetyl-CoA synthetase	EC:6.2.1.1
AFCMBR_GAC_MaxBin.090_01997	acetyl-CoA synthetase	ACS	acetyl-CoA synthetase	EC:6.2.1.1
AFCMBR_GAC_MaxBin.090_01578	acetyl-CoA decarbonylase/synthase	cdhA	acetyl-CoA decarbonylase/synthase	EC:1.2.7.4
AFCMBR_GAC_MaxBin.090_01577	acetyl-CoA decarbonylase/synthase	cdhB	acetyl-CoA decarbonylase/synthase	EC:1.2.7.4
AFCMBR_GAC_MaxBin.090_01576	acetyl-CoA decarbonylase/synthase	cdhC	acetyl-CoA decarbonylase/synthase	EC:2.3.1.-
AFCMBR_GAC_MaxBin.090_01573	acetyl-CoA decarbonylase/synthase	cdhD	acetyl-CoA decarbonylase/synthase	EC:2.1.1.245
AFCMBR_GAC_MaxBin.090_01572	acetyl-CoA decarbonylase/synthase	cdhE	acetyl-CoA decarbonylase/synthase	EC:2.1.1.24

	methyl-H4MPT			
AFCMBR_GAC_MaxBin.090_00058	coenzyme M methyltransferase	mtrA	tetrahydromethanopterin S- methyltransferase	EC:2.1.1.86
	methyl-H4MPT			
AFCMBR_GAC_MaxBin.090_00057	coenzyme M methyltransferase	mtrB	tetrahydromethanopterin S- methyltransferase	EC:2.1.1.86
	methyl-H4MPT			
AFCMBR_GAC_MaxBin.090_00056	coenzyme M methyltransferase	mtrC	tetrahydromethanopterin S- methyltransferase	EC:2.1.1.86
	methyl-H4MPT			
AFCMBR_GAC_MaxBin.090_00055	coenzyme M methyltransferase	mtrD	tetrahydromethanopterin S- methyltransferase	EC:2.1.1.86
	methyl-H4MPT			
AFCMBR_GAC_MaxBin.090_00054	coenzyme M methyltransferase	mtrE	tetrahydromethanopterin S- methyltransferase	EC:2.1.1.86

	methyltransferase			
	methyl-H4MPT			
AFCMBR_GAC_MaxBin.090_00059	coenzyme M	mtrF	tetrahydromethanopterin S- methyltransferase	EC:2.1.1.86
	methyltransferase			
	methyl-H4MPT			
AFCMBR_GAC_MaxBin.090_00060	coenzyme M	mtrG	tetrahydromethanopterin S- methyltransferase	EC:2.1.1.86
	methyltransferase			
	methyl-H4MPT			
AFCMBR_GAC_MaxBin.090_00061	coenzyme M	mtrH	tetrahydromethanopterin S- methyltransferase	EC:2.1.1.86
	methyltransferase			
	methyl-CoM			
AFCMBR_GAC_MaxBin.090_00918	methylreductase	mcr	methyl-CoM reductase	EC:2.8.4.1
	heterodisulfide reductase			
AFCMBR_GAC_MaxBin.090_02073	subunit A	hdrA	dihydromethanophenazine:CoB- CoM heterodisulfide reductase	EC:1.8.98.1

AFCMBR_GAC_MaxBin.090_02077	heterodisulfide reductase subunit B	hdrB	dihydromethanophenazine:CoB- CoM heterodisulfide reductase	EC:1.8.98.1
AFCMBR_GAC_MaxBin.090_02076	heterodisulfide reductase subunit C	hdrC	dihydromethanophenazine:CoB- CoM heterodisulfide reductase	EC:1.8.98.1
AFCMBR_GAC_MaxBin.090_01697	heterodisulfide reductase subunit D	hdrD	dihydromethanophenazine:CoB- CoM heterodisulfide reductase	EC:1.8.98.1
AFCMBR_GAC_MaxBin.090_01698	heterodisulfide reductase subunit E	hdrE	dihydromethanophenazine:CoB- CoM heterodisulfide reductase	EC:1.8.98.1
AFCMBR_GAC_MaxBin.090_00779	inorganic pyrophosphatase	Ppase	inorganic diphosphatase	EC 3.6.1.1
AFCMBR_GAC_MaxBin.090_03846	inorganic pyrophosphatase	Ppase	inorganic diphosphatase	EC 3.6.1.1
AFCMBR_GAC_MaxBin.090_00723	carbonic anhydrase	CA	carbonic anhydrase	EC 4.2.1.1
AFCMBR_GAC_MaxBin.090_03493	carbonic anhydrase	CA	carbonic anhydrase	EC 4.2.1.1
AFCMBR_GAC_MaxBin.090_03897	carbonic anhydrase	CA	carbonic anhydrase	EC 4.2.1.1

substrate transporter & energy related

AFCMBR_GAC_MaxBin.090_00065	TC.SSS/putative acetate transporter	ADY2	putative acetate transporter	/
AFCMBR_GAC_MaxBin.090_02156	TC.SSS/putative acetate transporter	ADY2	putative acetate transporter	/
AFCMBR_GAC_MaxBin.090_02179	TC.SSS/putative acetate transporter	ADY2	putative acetate transporter	/
AFCMBR_GAC_MaxBin.090_01416	energy-conserving hydrogenases	ehb	energy-conserving hydrogenases	/
AFCMBR_GAC_MaxBin.090_04135	energy-conserving hydrogenases	ehb	energy-conserving hydrogenases	/
AFCMBR_GAC_MaxBin.090_00638	F-type H ⁺ -transporting ATPase subunit a	ATPS	H ⁺ -transporting ATPase	EC:3.6.3.14
AFCMBR_GAC_MaxBin.090_02459	F-type H ⁺ -transporting	ATPS	H ⁺ -transporting ATPase	EC:3.6.3.14

	ATPase subunit a			
AFCMBR_GAC_MaxBin.090_02456	F-type H ⁺ -transporting ATPase subunit alpha	ATPS	H ⁺ -transporting ATPase	EC:3.6.3.14
AFCMBR_GAC_MaxBin.090_00641	F-type H ⁺ -transporting ATPase subunit alpha	ATPS	H ⁺ -transporting ATPase	EC:3.6.3.14
AFCMBR_GAC_MaxBin.090_02457	F-type H ⁺ -transporting ATPase subunit b	ATPS	H ⁺ -transporting ATPase	EC:3.6.3.14
AFCMBR_GAC_MaxBin.090_00640	F-type H ⁺ -transporting ATPase subunit b	ATPS	H ⁺ -transporting ATPase	EC:3.6.3.14
AFCMBR_GAC_MaxBin.090_00634	F-type H ⁺ -transporting ATPase subunit beta	ATPS	H ⁺ -transporting ATPase	EC:3.6.3.14
AFCMBR_GAC_MaxBin.090_02463	F-type H ⁺ -transporting ATPase subunit beta	ATPS	H ⁺ -transporting ATPase	EC:3.6.3.14
AFCMBR_GAC_MaxBin.090_00639	F-type H ⁺ -transporting	ATPS	H ⁺ -transporting ATPase	EC:3.6.3.14

	ATPase subunit c			
AFCMBR_GAC_MaxBin.090_02458	F-type H ⁺ -transporting ATPase subunit c	ATPS	H ⁺ -transporting ATPase	EC:3.6.3.14
AFCMBR_GAC_MaxBin.090_02462	F-type H ⁺ -transporting ATPase subunit epsilon	ATPS	H ⁺ -transporting ATPase	EC:3.6.3.14
AFCMBR_GAC_MaxBin.090_00635	F-type H ⁺ -transporting ATPase subunit epsilon	ATPS	H ⁺ -transporting ATPase	EC:3.6.3.14
AFCMBR_GAC_MaxBin.090_00642	F-type H ⁺ -transporting ATPase subunit gamma	ATPS	H ⁺ -transporting ATPase	EC:3.6.3.14
AFCMBR_GAC_MaxBin.090_02455	F-type H ⁺ -transporting ATPase subunit gamma	ATPS	H ⁺ -transporting ATPase	EC:3.6.3.14

AFCMBR_GAC_MaxBin.090 - *Methanotherx concilii* - RHP pathway

AFCMBR_GAC_MaxBin.090_00783	phosphoribulokinase	PRK	phosphoribulokinase	EC:2.7.1.19
AFCMBR_GAC_MaxBin.090_02729	ribulose-bisphosphate carboxylase large chain	RuBisCO	ribulose-bisphosphate carboxylase	EC 4.1.1.39
AFCMBR_GAC_MaxBin.090_00965	3-phosphoglycerate kinase	PGK	phosphoglycerate kinase	EC:2.7.2.3
	glyceraldehyde-3-phosphate		glyceraldehyde-3-phosphate	
AFCMBR_GAC_MaxBin.090_02093	dehydrogenase (NAD(P)+) (phosphorylating)	gap2	dehydrogenase (NAD(P)+) (phosphorylating);	EC:1.2.1.59
	glyceraldehyde-3-phosphate		glyceraldehyde-3-phosphate	
AFCMBR_GAC_MaxBin.090_02711	dehydrogenase (NAD(P)+) (phosphorylating)	gap2	dehydrogenase (NAD(P)+) (phosphorylating);	EC:1.2.1.59
AFCMBR_GAC_MaxBin.090_00498	fructose-bisphosphate aldolase	Aldolase	fructose-bisphosphate aldolase	EC 4.1.2.13
AFCMBR_GAC_MaxBin.090_00256	fructose-1,6- bisphosphatase	FBPase	fructose-bisphosphatase	EC 3.1.3.11

AFCMBR_GAC_MaxBin.090_04006	fructose-1,6- bisphosphatase	FBPase	fructose-bisphosphatase	EC 3.1.3.11
AFCMBR_GAC_MaxBin.090_01312	6-phospho-3- hexuloisomerase	PHI	6-phospho-3-hexuloisomerase	EC 5.3.1.27
AFCMBR_GAC_MaxBin.090_01348	3-hexulose-6-phosphate synthase	HPS	3-hexulose-6-phosphate synthase	EC:4.2.1.147 4.1.2.43
AFCMBR_GAC_MaxBin.090_02991	3-hexulose-6-phosphate synthase	HPS	3-hexulose-6-phosphate synthase	EC:4.2.1.147 4.1.2.43
AFCMBR_GAC_MaxBin.090_04145	3-hexulose-6-phosphate synthase	HPS	3-hexulose-6-phosphate synthase	EC:4.2.1.147 4.1.2.43
AFCMBR_GAC_MaxBin.090_00600	AMP phosphorylase	AMPpase	AMP phosphorylase	EC:2.4.2.57
AFCMBR_GAC_MaxBin.090_01365	ribose-5-phosphate isomerase	RiBP isomerase	ribose-5-phosphate isomerase	EC 5.3.1.6
AFCMBR_GAC_MaxBin.090_01068	5,6,7,8- tetrahydromethanopterin	fae	5,6,7,8-tetrahydromethanopterin hydro-lyase	EC:4.2.1.147

	hydro-lyase			
	5,6,7,8-			
AFCMBR_GAC_MaxBin.090_01348	tetrahydromethanopterin	fae	5,6,7,8-tetrahydromethanopterin hydro-lyase	EC:4.2.1.147
	hydro-lyase			
	5,6,7,8-			
AFCMBR_GAC_MaxBin.090_02991	tetrahydromethanopterin	fae	5,6,7,8-tetrahydromethanopterin hydro-lyase	EC:4.2.1.147
	hydro-lyase			
	5,6,7,8-			
AFCMBR_GAC_MaxBin.090_04145	tetrahydromethanopterin	fae	5,6,7,8-tetrahydromethanopterin hydro-lyase	EC:4.2.1.147
	hydro-lyase			

AFCMBR_GAC_MaxBin.090-Methanothrix concilii-CO2 reduction

AFCMBR_GAC_MaxBin.090_01093	formylmethanofuran dehydrogenase	fwd	formylmethanofuran dehydrogenase	EC:1.2.7.12
-----------------------------	-------------------------------------	-----	-------------------------------------	-------------

AFCMBR_GAC_MaxBin.090_01090	formylmethanofuran dehydrogenase	fwd	formylmethanofuran dehydrogenase	EC:1.2.7.12
AFCMBR_GAC_MaxBin.090_00501	formylmethanofuran dehydrogenase	fwd	formylmethanofuran dehydrogenase	EC:1.2.7.12
AFCMBR_GAC_MaxBin.090_01091	formylmethanofuran dehydrogenase	fwd	formylmethanofuran dehydrogenase	EC:1.2.7.12
AFCMBR_GAC_MaxBin.090_01258	formylmethanofuran dehydrogenase	fwd	formylmethanofuran dehydrogenase	EC:1.2.7.12
AFCMBR_GAC_MaxBin.090_01278	formyl methanofuran- H4MPT formyltransferase	ftt	formylmethanofuran--- tetrahydromethanopterin N- formyltransferase;	EC:2.3.1.101
AFCMBR_GAC_MaxBin.090_00012	methenyl-H4MPT cyclohydrolase	mch	methenyltetrahydromethanopterin cyclohydrolase	EC:3.5.4.27
AFCMBR_GAC_MaxBin.090_00079	F420-dependent methylene-	mtd	methylenetetrahydromethanopterin	EC:1.5.98.1

	H4MPT dehydrogenase		dehydrogenase	
AFCMBR_GAC_024_02542	F420-dependent methylene H4MPT reductase	mer	5,10- methylenetetrahydromethanopterin reductase	EC:1.5.98.2
AFCMBR_GAC_MaxBin.090_03089	coenzyme F420 hydrogenase	frh	coenzyme F420 hydrogenase	EC:1.12.98.1
AFCMBR_GAC_MaxBin.090_03298	coenzyme F420 hydrogenase	frh	coenzyme F420 hydrogenase	EC:1.12.98.1
AFCMBR_GAC_MaxBin.090_00058	tetrahydromethanopterin S- methyltransferase subunit A	mtrA	tetrahydromethanopterin S- methyltransferase	EC:2.1.1.86
AFCMBR_GAC_MaxBin.090_00057	tetrahydromethanopterin S- methyltransferase subunit B	mtrB	tetrahydromethanopterin S- methyltransferase	EC:2.1.1.86
AFCMBR_GAC_MaxBin.090_00056	tetrahydromethanopterin S- methyltransferase subunit C	mtrC	tetrahydromethanopterin S- methyltransferase	EC:2.1.1.86

AFCMBR_GAC_MaxBin.090_00055	tetrahydromethanopterin S- methyltransferase subunit D	mtrD	tetrahydromethanopterin S- methyltransferase	EC:2.1.1.86
AFCMBR_GAC_MaxBin.090_00054	tetrahydromethanopterin S- methyltransferase subunit E	mtrE	tetrahydromethanopterin S- methyltransferase	EC:2.1.1.86
AFCMBR_GAC_MaxBin.090_00059	tetrahydromethanopterin S- methyltransferase subunit F	mtrF	tetrahydromethanopterin S- methyltransferase	EC:2.1.1.86
AFCMBR_GAC_MaxBin.090_00060	tetrahydromethanopterin S- methyltransferase subunit G	mtrG	tetrahydromethanopterin S- methyltransferase	EC:2.1.1.86
AFCMBR_GAC_MaxBin.090_00061	tetrahydromethanopterin S- methyltransferase subunit H	mtrH	tetrahydromethanopterin S- methyltransferase	EC:2.1.1.86
AFCMBR_GAC_MaxBin.090_00987	methyl-coenzyme M reductase alpha subunit	mcrA	coenzyme-B sulfoethylthiotransferase	EC:2.8.4.1
AFCMBR_GAC_MaxBin.090_00984	methyl-coenzyme M reductase beta subunit	mcrB	coenzyme-B sulfoethylthiotransferase	EC:2.8.4.1

AFCMBR_GAC_MaxBin.090_00918	methyl-coenzyme M reductase subunit C	mcrC	coenzyme-B sulfoethylthiotransferase	EC:2.8.4.1
AFCMBR_GAC_MaxBin.090_00985	methyl-coenzyme M reductase subunit D	mcrD	coenzyme-B sulfoethylthiotransferase	EC:2.8.4.1
AFCMBR_GAC_MaxBin.090_00986	methyl-coenzyme M reductase gamma subunit	mcrG	coenzyme-B sulfoethylthiotransferase	EC:2.8.4.1
AFCMBR_GAC_MaxBin.090_03695	methyl-coenzyme M reductase gamma subunit	mcrG	coenzyme-B sulfoethylthiotransferase	EC:2.8.4.1
AFCMBR_GAC_MaxBin.090_02073	heterodisulfide reductase subunit A	hdrA	dihydromethanophenazine:CoB- CoM heterodisulfide reductase	EC:1.8.98.1
AFCMBR_GAC_MaxBin.090_02077	heterodisulfide reductase subunit B	hdrB	dihydromethanophenazine:CoB- CoM heterodisulfide reductase	EC:1.8.98.1
AFCMBR_GAC_MaxBin.090_02076	heterodisulfide reductase subunit C	hdrC	dihydromethanophenazine:CoB- CoM heterodisulfide reductase	EC:1.8.98.1

AFCMBR_GAC_MaxBin.090_01697	heterodisulfide reductase subunit D	hdrD	dihydromethanophenazine:CoB- CoM heterodisulfide reductase	EC:1.8.98.1
AFCMBR_GAC_MaxBin.090_01698	heterodisulfide reductase subunit E	hdrE	dihydromethanophenazine:CoB- CoM heterodisulfide reductase	EC:1.8.98.1

Appendix II Genes expression of the of main pathways (propionate degradation, methane generation) in *S. fumaroxidans*, *M. concilii* and *G. lovleyi*.

Function	Gene Abbrev.	CDS	log2RPKM
Acetate oxidation to CO₂ (TCA cycle)			
phosphate acetyltransferase	pta	AFBR_GAC_MaxBin.001_02087	5.47
acetate kinase	AckA	AFBR_GAC_MaxBin.001_00587	7.45
acetyl-CoA C-acetyltransferase	ato	AFBR_GAC_MaxBin.001_00963	4.79
citrate synthase	CS	AFBR_GAC_MaxBin.001_00357	5.06
aconitate hydratase	ACO	AFBR_GAC_MaxBin.001_01231	5.13
aconitate hydratase	ACO	AFBR_GAC_MaxBin.001_02542	4.51
isocitrate dehydrogenase	IDH1	AFBR_GAC_MaxBin.001_01771	5.31
2-oxoglutarate/2-oxoacid ferredoxin oxidoreductase	kor	AFBR_GAC_MaxBin.001_02544	4.61
succinyl-CoA synthetase alpha subunit	Suc	AFBR_GAC_MaxBin.001_01643	5.66

succinyl-CoA synthetase beta subunit	Suc	AFBR_GAC_MaxBin.001_01644	5.25
succinate dehydrogenase / fumarate reductase	Frd	AFBR_GAC_MaxBin.001_01721	4.53
fumarate hydratase	Fum	AFBR_GAC_MaxBin.001_01936	4.77
malate dehydrogenase	mdh	AFBR_GAC_MaxBin.001_01770	8.30

Methylmalonyl-CoA (MMC) pathway

propionate CoA transferase	PCT	AFBR_GAC_MaxBin.072_00988	7.11
propionyl-CoA:oxaloacetate transcarboxylase	POT, pccA	AFBR_GAC_MaxBin.072_03848	6.50
methylmalonyl-CoA/ethylmalonyl-CoA epimerase	MCEE, epi	AFBR_GAC_MaxBin.072_00452	8.40
methylmalonyl-CoA mutase	MCM	AFBR_GAC_MaxBin.072_00277	8.24
succinyl-CoA synthetase	SCS	AFBR_GAC_MaxBin.072_01546	10.13
succinyl-CoA synthetase	SCS	AFBR_GAC_MaxBin.072_03945	7.32
succinate dehydrogenase	SDH/FR	AFBR_GAC_MaxBin.072_01935	6.39

	(2)		
fumarate hydratase (fumarase)	FHT	AFBR_GAC_MaxBin.072_02545	8.76
malate dehydrogenase	MDH	AFBR_GAC_MaxBin.072_03984	8.37
malate dehydrogenase	MDH	AFBR_GAC_MaxBin.072_02538	5.95
pyruvate dehydrogenase	PDH	AFBR_GAC_MaxBin.072_02198	5.41
pyruvate dehydrogenase	PDH	AFBR_GAC_MaxBin.072_02200	5.17
2-oxoglutarate/2-oxoacid ferredoxin oxidoreductase	korA	AFBR_GAC_MaxBin.072_01790	5.37
acetyl-CoA synthetas	ACS	AFBR_GAC_MaxBin.072_00502	8.72
carbon-monoxide dehydrogenase	cooS	AFBR_GAC_MaxBin.072_00503	6.89

Acetoclastic methanogenesis

acetyl-CoA synthetase	ACS	AFCMBR_GAC_MaxBin.090_00490	7.57
acetyl-CoA synthetase	ACS	AFCMBR_GAC_MaxBin.090_00611	11.96
acetyl-CoA synthetase	ACS	AFCMBR_GAC_MaxBin.090_00613	11.26

acetyl-CoA synthetase	ACS	AFCMBR_GAC_MaxBin.090_01997	6.51
acetyl-CoA synthetase	ACS	AFCMBR_GAC_MaxBin.090_03370	10.16
acetyl-CoA decarboxylase/synthase	cdh	AFCMBR_GAC_MaxBin.090_01578	11.13
acetyl-CoA decarboxylase/synthase	cdh	AFCMBR_GAC_MaxBin.090_01577	11.13
acetyl-CoA decarboxylase/synthase	cdh	AFCMBR_GAC_MaxBin.090_01576	11.48
acetyl-CoA decarboxylase/synthase	cdh	AFCMBR_GAC_MaxBin.090_01573	11.06
acetyl-CoA decarboxylase/synthase	cdh	AFCMBR_GAC_MaxBin.090_01572	11.41
Carbon monoxide dehydrogenase	cdh	AFCMBR_GAC_MaxBin.090_00633	8.61
Carbon monoxide dehydrogenase	cdh	AFCMBR_GAC_MaxBin.090_03405	8.82
methyl-H4MPT coenzyme M methyltransferase	mtr	AFCMBR_GAC_MaxBin.090_00058	10.27
methyl-H4MPT coenzyme M methyltransferase	mtr	AFCMBR_GAC_MaxBin.090_00057	10.22
methyl-H4MPT coenzyme M methyltransferase	mtr	AFCMBR_GAC_MaxBin.090_00056	10.22
methyl-H4MPT coenzyme M methyltransferase	mtr	AFCMBR_GAC_MaxBin.090_00055	10.15
methyl-H4MPT coenzyme M methyltransferase	mtr	AFCMBR_GAC_MaxBin.090_00054	10.96

methyl-H4MPT coenzyme M methyltransferase	mtr	AFCMBR_GAC_MaxBin.090_00059	9.04
methyl-H4MPT coenzyme M methyltransferase	mtr	AFCMBR_GAC_MaxBin.090_00060	10.74
methyl-H4MPT coenzyme M methyltransferase	mtr	AFCMBR_GAC_MaxBin.090_00061	9.91
methyl-CoM methylreductase	mcr	AFCMBR_GAC_MaxBin.090_00918	9.70
heterodisulfide reductase subunit A	hdr	AFCMBR_GAC_MaxBin.090_02073	9.14
heterodisulfide reductase subunit B	hdr	AFCMBR_GAC_MaxBin.090_02077	6.16
heterodisulfide reductase subunit C	hdr	AFCMBR_GAC_MaxBin.090_02076	7.83
heterodisulfide reductase subunit D	hdr	AFCMBR_GAC_MaxBin.090_01697	7.04
heterodisulfide reductase subunit E	hdr	AFCMBR_GAC_MaxBin.090_01698	9.90
inorganic pyrophosphatase	Ppase	AFCMBR_GAC_MaxBin.090_00779	9.41
inorganic pyrophosphatase	Ppase	AFCMBR_GAC_MaxBin.090_03846	11.29
carbonic anhydrase	CA	AFCMBR_GAC_MaxBin.090_03897	6.54
substrate transporter & energy related			
TC.SSS/putative acetate transporter		AFCMBR_GAC_MaxBin.090_02156	6.24

TC.SSS/putative acetate transporter		AFCMBR_GAC_MaxBin.090_02179	7.80
F-type H ⁺ -transporting ATPase subunit alpha		AFCMBR_GAC_MaxBin.090_02456	7.31
F-type H ⁺ -transporting ATPase subunit b		AFCMBR_GAC_MaxBin.090_02457	6.26
F-type H ⁺ -transporting ATPase subunit beta		AFCMBR_GAC_MaxBin.090_00634	5.45
F-type H ⁺ -transporting ATPase subunit beta		AFCMBR_GAC_MaxBin.090_02463	5.45
F-type H ⁺ -transporting ATPase subunit gamma		AFCMBR_GAC_MaxBin.090_02455	7.09
F-type H ⁺ -transporting ATPase subunit c		AFCMBR_GAC_MaxBin.090_02458	7.81
energy-conserving hydrogenases		AFCMBR_GAC_MaxBin.090_01416	6.50
energy-conserving hydrogenases		AFCMBR_GAC_MaxBin.090_04135	8.97

The RHP pathway

phosphoribulokinase	PRK	AFCMBR_GAC_MaxBin.090_00783	6.95
ribulose-bisphosphate carboxylase large chain	RuBisCO	AFCMBR_GAC_MaxBin.090_02729	6.05
ribulose-bisphosphate carboxylase large chain	RuBisCO	AFCMBR_GAC_MaxBin.090_02062	7.72

3-phosphoglycerate kinase		PGK	AFCMBR_GAC_MaxBin.090_00965	6.62
glyceraldehyde-3-phosphate (phosphorylating)	dehydrogenase (NAD(P)+)	GAPDH	AFCMBR_GAC_MaxBin.090_02093	6.70
glyceraldehyde-3-phosphate (phosphorylating)	dehydrogenase (NAD(P)+)	GAPDH	AFCMBR_GAC_MaxBin.090_02711	9.79
fructose-bisphosphate aldolase		Aldo	AFCMBR_GAC_MaxBin.090_00498	6.99
fructose-bisphosphate aldolase		Aldo	AFCMBR_GAC_MaxBin.090_00257	7.75
fructose-1,6- bisphosphatase		FBP	AFCMBR_GAC_MaxBin.090_00256	8.41
fructose-1,6- bisphosphatase		FBP	AFCMBR_GAC_MaxBin.090_04006	9.52
fructose-bisphosphate aldolase		FBP	AFCMBR_GAC_MaxBin.090_01228	7.19
6-phospho-3-hexuloisomerase		PHI	AFCMBR_GAC_MaxBin.090_01312	7.89
3-hexulose-6-phosphate synthase		HPS	AFCMBR_GAC_MaxBin.090_01348	8.66
3-hexulose-6-phosphate synthase		HPS	AFCMBR_GAC_MaxBin.090_02991	7.54
3-hexulose-6-phosphate synthase		HPS	AFCMBR_GAC_MaxBin.090_04145	7.75

3-hexulose-6-phosphate synthase	HPS	AFCMBR_GAC_MaxBin.090_00019	7.24
AMP phosphorylase	AMP	AFCMBR_GAC_MaxBin.090_00600	9.40
ribose-5-phosphate isomerase	RiBP	AFCMBR_GAC_MaxBin.090_01365	6.44
5,6,7,8-tetrahydromethanopterin hydro-lyase	fae	AFCMBR_GAC_MaxBin.090_01348	8.66
5,6,7,8-tetrahydromethanopterin hydro-lyase	fae	AFCMBR_GAC_MaxBin.090_02991	7.54
5,6,7,8-tetrahydromethanopterin hydro-lyase	fae	AFCMBR_GAC_MaxBin.090_04145	7.75

Classical CO₂ reduction

formylmethanofuran dehydrogenase	fwd	AFCMBR_GAC_MaxBin.090_01093	8.97
formylmethanofuran dehydrogenase	fwd	AFCMBR_GAC_MaxBin.090_01090	8.52
formylmethanofuran dehydrogenase	fwd	AFCMBR_GAC_MaxBin.090_01091	9.68
formylmethanofuran dehydrogenase	fwd	AFCMBR_GAC_MaxBin.090_00242	5.89
formylmethanofuran dehydrogenase	fwd	AFCMBR_GAC_MaxBin.090_00315	6.47
formylmethanofuran dehydrogenase	fwd	AFCMBR_GAC_MaxBin.090_01781	5.84

formylmethanofuran dehydrogenase	fwd	AFCMBR_GAC_MaxBin.090_01923	6.52
formylmethanofuran dehydrogenase	fwd	AFCMBR_GAC_MaxBin.090_02023	7.61
formylmethanofuran dehydrogenase	fwd	AFCMBR_GAC_MaxBin.090_00007	9.03
formyl methanofuran–H4MPT formyltransferase	frt	AFCMBR_GAC_MaxBin.090_01278	6.08
formyl methanofuran–H4MPT formyltransferase	frt	AFCMBR_GAC_MaxBin.090_01924	7.14
formyl methanofuran–H4MPT formyltransferase	frt	AFCMBR_GAC_MaxBin.090_01925	6.28
formyl methanofuran–H4MPT formyltransferase	frt	AFCMBR_GAC_MaxBin.090_01092	6.24
formyl methanofuran–H4MPT formyltransferase	frt	AFCMBR_GAC_MaxBin.090_01093	8.97
formyl methanofuran–H4MPT formyltransferase	frt	AFCMBR_GAC_MaxBin.090_01278	6.08
methenyl-H4MPT cyclohydrolase	mch	AFCMBR_GAC_MaxBin.090_00012	9.17
F420-dependent methylene-H4MPT dehydrogenase	mtd	AFCMBR_GAC_MaxBin.090_00079	7.77
5,10-methylenetetrahydromethanopterin reductase, mer	mer	AFCMBR_GAC_024_02542	7.96
coenzyme F420 hydrogenase	frh	AFCMBR_GAC_MaxBin.090_03089	9.78
tetrahydromethanopterin S-methyltransferase subunit A	mtr	AFCMBR_GAC_MaxBin.090_00058	10.27

tetrahydromethanopterin S-methyltransferase subunit B	mtr	AFCMBR_GAC_MaxBin.090_00057	10.22
tetrahydromethanopterin S-methyltransferase subunit C	mtr	AFCMBR_GAC_MaxBin.090_00056	10.22
tetrahydromethanopterin S-methyltransferase subunit D	mtr	AFCMBR_GAC_MaxBin.090_00055	10.15
tetrahydromethanopterin S-methyltransferase subunit E	mtr	AFCMBR_GAC_MaxBin.090_00054	10.96
tetrahydromethanopterin S-methyltransferase subunit F	mtr	AFCMBR_GAC_MaxBin.090_00059	9.04
tetrahydromethanopterin S-methyltransferase subunit G	mtr	AFCMBR_GAC_MaxBin.090_00060	10.74
tetrahydromethanopterin S-methyltransferase subunit H	mtr	AFCMBR_GAC_MaxBin.090_00061	9.91
methyl-coenzyme M reductase alpha subunit	mcr	AFCMBR_GAC_MaxBin.090_00987	12.08
methyl-coenzyme M reductase beta subunit	mcr	AFCMBR_GAC_MaxBin.090_00984	12.03
methyl-coenzyme M reductase subunit C	mcr	AFCMBR_GAC_MaxBin.090_00918	9.70
methyl-coenzyme M reductase subunit D	mcr	AFCMBR_GAC_MaxBin.090_00985	8.90
methyl-coenzyme M reductase gamma subunit	mcr	AFCMBR_GAC_MaxBin.090_00986	10.75
methyl-coenzyme M reductase gamma subunit	mcr	AFCMBR_GAC_MaxBin.090_03695	11.68
heterodisulfide reductase subunit A	Hdr	AFCMBR_GAC_MaxBin.090_02073	9.14

heterodisulfide reductase subunit B	Hdr	AFCMBR_GAC_MaxBin.090_02077	6.16
heterodisulfide reductase subunit C	Hdr	AFCMBR_GAC_MaxBin.090_02076	7.83
heterodisulfide reductase subunit D	Hdr	AFCMBR_GAC_MaxBin.090_01697	7.04
heterodisulfide reductase subunit E	Hdr	AFCMBR_GAC_MaxBin.090_01698	9.90

Appendix III Coding DNA sequences (CDS) predicted to be involved in the metabolism of main pathways associated with caproate production.

CDS	Predicted function	Gene name	Gene name	Enzyme commission
CE_AA_MaxBin.002 - <i>Clostridium kluyveri</i> - Ethanol oxidation				
CE_AA_MaxBin.002_01458	alcohol dehydrogenase	ald	alcohol dehydrogenase	EC:1.1.1.1
CE_AA_MaxBin.002_02477	alcohol dehydrogenase	ald	alcohol dehydrogenase	EC:1.1.1.1
CE_AA_MaxBin.002_01849	alcohol dehydrogenase	ald	alcohol dehydrogenase	EC:1.1.1.1
CE_AA_MaxBin.002_02426	alcohol dehydrogenase	ald	alcohol dehydrogenase	EC:1.1.1.1
CE_AA_MaxBin.002_01234	acetaldehyde dehydrogenase	adh	acetaldehyde dehydrogenase	EC:1.2.1.10
CE_AA_MaxBin.002_00337	phosphate acetyltransferase	pta	phosphate acetyltransferase	EC 2.3.1.8

CE_AA_MaxBin.002_00921	phosphate acetyltransferase	pta	phosphate acetyltransferase	EC 2.3.1.8
CE_AA_MaxBin.002_01832	phosphate acetyltransferase	pta	phosphate acetyltransferase	EC 2.3.1.8
CE_AA_MaxBin.002_00077	butyrate kinase	buk	butyrate kinase	EC 2.7.2.7
CE_AA_MaxBin.002_00079	butyrate kinase	buk	butyrate kinase	EC 2.7.2.7

CE_AA_MaxBin.002 - *Clostridium kluyveri* - Reverse β -oxidation

CE_AA_MaxBin.002_01439	acetyl-CoA C-acetyltransferase	thl	acetoacetyl-CoA thiolase	EC:2.3.1.9
CE_AA_MaxBin.002_01640	acetyl-CoA C-acetyltransferase	thl	acetoacetyl-CoA thiolase	EC:2.3.1.9
CE_AA_MaxBin.002_01930	acetyl-CoA C-acetyltransferase	thl	acetoacetyl-CoA thiolase	EC:2.3.1.9
CE_AA_MaxBin.002_00738	3-hydroxybutyryl-CoA dehydrogenase	hbd/paaH	3-hydroxybutyryl-CoA dehydrogenase	EC:1.1.1.157
CE_AA_MaxBin.002_00758	3-hydroxybutyryl-CoA	hbd/paaH	3-hydroxybutyryl-CoA	EC:1.1.1.157

	dehydrogenase		dehydrogenase	
CE_AA_MaxBin.002_01241	3-hydroxybutyryl-CoA dehydrogenase	hbd/paaH	3-hydroxybutyryl-CoA dehydrogenase	EC:1.1.1.157
CE_AA_MaxBin.002_00734	enoyl-CoA hydratase	crt	3-hydroxybutyryl-CoA dehydratase	EC:4.2.1.17
CE_AA_MaxBin.002_00759	enoyl-CoA hydratase	crt	3-hydroxybutyryl-CoA dehydratase	EC:4.2.1.17
CE_AA_MaxBin.002_01237	enoyl-CoA hydratase	crt	3-hydroxybutyryl-CoA dehydratase	EC:4.2.1.17
CE_AA_MaxBin.002_00735	butyryl-CoA dehydrogenase	bcd	butyryl-CoA dehydrogenase	EC:1.3.8.1
CE_AA_MaxBin.002_01238	butyryl-CoA dehydrogenase	bcd	butyryl-CoA dehydrogenase	EC:1.3.8.1
CE_AA_MaxBin.002_00986	butyryl-CoA dehydrogenase	bcd	butyryl-CoA dehydrogenase	EC:1.3.8.1

CE_AA_MaxBin.002_01639	acetate CoA/acetoacetate CoA-transferase	atoA	butyryl-CoA: acetate CoA transferase	EC:2.8.3.8
CE_AA_MaxBin.002_02136	acetate CoA/acetoacetate CoA-transferase	atoA	butyryl-CoA: acetate CoA transferase	EC:2.8.3.8
CE_AA_MaxBin.002 - <i>Clostridium kluyveri</i> - Membrane proteins involved in energy conservation-Fix system				
CE_AA_MaxBin.002_00739	ferredoxin/ flavodoxin---NADP+ reductase	fpr	ferredoxin--NADP+ reductase	EC:1.18.1.2
CE_AA_MaxBin.002_00736	electron transfer flavoprotein beta subunit	etfA/fixA	electron transfer flavoprotein	/
CE_AA_MaxBin.002_01239	electron transfer flavoprotein beta subunit	etfA/fixA	electron transfer flavoprotein	/

CE_AA_MaxBin.002_01317	electron transfer flavoprotein beta subunit	etfA/fixA	electron transfer flavoprotein	/
CE_AA_MaxBin.002_02465	electron transfer flavoprotein beta subunit	etfA/fixA	electron transfer flavoprotein	/
CE_AA_MaxBin.002_01240	electron transfer flavoprotein alpha subunit	etfB/fixB		/
CE_AA_MaxBin.002_01318	electron transfer flavoprotein alpha subunit	etfB/fixB		/
CE_AA_MaxBin.002_00737	electron transfer flavoprotein alpha subunit	etfB/fixB		/

CE_AA_MaxBin.018 - *Proteiniphilum acetatigenes* – glycine to pyruvate

CE_AA_MaxBin.018_01722	glycine hydroxymethyltransferase	glyA	glycine hydroxymethyltransferase	EC:2.1.2.1
CE_AA_MaxBin.018_01262	phosphoserine phosphatase	psp	phosphohydrolase	EC 3.1.3.-
CE_AA_MaxBin.018_00672	phosphoserine transaminase	serC	phosphoserine transaminase	EC:2.6.1.52
CE_AA_MaxBin.018_01038	phosphoserine transaminase	serC	phosphoserine transaminase	EC:2.6.1.52
CE_AA_MaxBin.018_00671	phosphoglycerate dehydrogenase	serA	phosphoglycerate dehydrogenase	EC:1.1.1.95 1.1.1.399
CE_AA_MaxBin.018_01037	phosphoglycerate dehydrogenase	serA	phosphoglycerate dehydrogenase	EC:1.1.1.95 1.1.1.399
CE_AA_MaxBin.018_01444	glyceraldehyde 3-phosphate dehydrogenase	GAPDH	glyceraldehyde 3-phosphate dehydrogenase	EC:1.2.1.12

	2,3-bisphosphoglycerate-			
CE_AA_MaxBin.018_01707	dependent phosphoglycerate mutase	PGAM	phosphoglycerate mutase	5.4.2.11
	2,3-bisphosphoglycerate-			
CE_AA_MaxBin.018_00129	independent phosphoglycerate mutase	apgM	phosphoglycerate mutase	5.4.2.12
CE_AA_MaxBin.018_01779	phosphopyruvate hydratase	ENO	phosphopyruvate hydratase	4.2.1.11
	pyruvate kinase			2.7.1.40

CE_AA_MaxBin.018 - *Proteiniphilum acetatigenes* – pyruvate to acetate

CE_AA_MaxBin.018_00168	2-oxoglutarate/2-oxoacid ferredoxin oxidoreductase	korB	2-oxoacid oxidoreductase (ferredoxin)	EC:1.2.7.3 1.2.7.11
------------------------	---	------	--	------------------------

	subunit beta			
	2-oxoglutarate/2-oxoacid			
CE_AA_MaxBin.018_00169	ferredoxin oxidoreductase	korA	2-oxoacid oxidoreductase (ferredoxin)	EC:1.2.7.3 1.2.7.11
	subunit alpha			
	2-oxoglutarate/2-oxoacid			
CE_AA_MaxBin.018_01050	ferredoxin oxidoreductase	korA	2-oxoacid oxidoreductase (ferredoxin)	EC:1.2.7.3 1.2.7.11
	subunit alpha			
	2-oxoglutarate/2-oxoacid			
CE_AA_MaxBin.018_01048	ferredoxin oxidoreductase	korB	2-oxoacid oxidoreductase (ferredoxin)	EC:1.2.7.3 1.2.7.11
	subunit beta			
	pyruvate-ferredoxin/ flavodoxin oxidoreductase	por	pyruvate synthase	EC:1.2.7.1 1.2.7.-

CE_AA_MaxBin.018_00001	phosphotransacetylase	pta	phosphate acetyltransferase	EC 2.3.1.8
CE_AA_MaxBin.018_00003	acetate kinase	ackA	acetate kinase	EC 2.7.2.1

Appendix IV Genes expression of the of main pathways associated with caproate production.

Function	Gene Abbrev.	CDS	log2RPKM
Ethanol oxidation			
alcohol dehydrogenase	ald	CE_AA_MaxBin.002_01458	10.24
alcohol dehydrogenase	ald	CE_AA_MaxBin.002_02477	12.72
alcohol dehydrogenase	ald	CE_AA_MaxBin.002_02426	10.68
acetaldehyde dehydrogenase	adh	CE_AA_MaxBin.002_01234	9.70
Aldehyde-alcohol dehydrogenase	adh	CE_AA_MaxBin.002_00994	7.66
phosphate acetyltransferase	pta	CE_AA_MaxBin.002_00337	7.88
phosphate acetyltransferase	pta	CE_AA_MaxBin.002_01832	9.69
Phosphate acetyltransferase	pta	CE_AA_MaxBin.002_00078	9.03
Phosphate acetyltransferase	pta	CE_AA_MaxBin.002_01258	9.02

butyrate kinase	buk	CE_AA_MaxBin.002_00077	7.78
-----------------	-----	------------------------	------

Reverse β -oxidation

acetyl-CoA C-acetyltransferase	thl	CE_AA_MaxBin.002_01439	10.65
acetyl-CoA C-acetyltransferase	thl	CE_AA_MaxBin.002_01640	10.97
acetyl-CoA C-acetyltransferase	thl	CE_AA_MaxBin.002_01930	11.82
3-hydroxybutyryl-CoA dehydrogenase	hbd/paaH	CE_AA_MaxBin.002_00758	10.70
3-hydroxybutyryl-CoA dehydrogenase	hbd/paaH	CE_AA_MaxBin.002_01241	8.03
enoyl-CoA hydratase	crt	CE_AA_MaxBin.002_00734	10.25
enoyl-CoA hydratase	crt	CE_AA_MaxBin.002_00759	10.83
butyryl-CoA dehydrogenase	bcd	CE_AA_MaxBin.002_00735	9.28
butyryl-CoA dehydrogenase	bcd	CE_AA_MaxBin.002_01238	10.70
butyryl-CoA dehydrogenase	bcd	CE_AA_MaxBin.002_00986	8.72

acetate CoA/acetoacetate CoA-transferase	atoA	CE_AA_MaxBin.002_01639	9.50
acetate CoA/acetoacetate CoA-transferase	atoA	CE_AA_MaxBin.002_02136	10.60

***Proteiniphilum acetatigenes* – glycine to acetate**

glycine hydroxymethyltransferase	glyA	CE_AA_MaxBin.018_01722	10.48
phosphoserine phosphatase	psp	CE_AA_MaxBin.018_01262	
phosphoserine transaminase	serC	CE_AA_MaxBin.018_00672	9.60
phosphoserine transaminase	serC	CE_AA_MaxBin.018_01038	10.72
phosphoglycerate dehydrogenase	serA	CE_AA_MaxBin.018_00671	8.80
glyceraldehyde 3-phosphate dehydrogenase	GAPDH	CE_AA_MaxBin.018_01444	11.01
2,3-bisphosphoglycerate-dependent phosphoglycerate mutase	PGAM	CE_AA_MaxBin.018_01707	10.12
phosphopyruvate hydratase	ENO	CE_AA_MaxBin.018_01779	11.57

pyruvate kinase			
2-oxoglutarate/2-oxoacid ferredoxin oxidoreductase subunit alpha	korA	CE_AA_MaxBin.018_01050	9.58
2-oxoglutarate/2-oxoacid ferredoxin oxidoreductase subunit beta	korB	CE_AA_MaxBin.018_01048	9.09
pyruvate-ferredoxin/flavodoxin oxidoreductase	por	CE_AA_MaxBin.018_00762	10.56
phosphotransacetylase	pta	CE_AA_MaxBin.018_00001	11.26
acetate kinase	ackA	CE_AA_MaxBin.018_00003	

substrate transporter & energy related

TC.SSS/putative acetate transporter		AFCMBR_GAC_MaxBin.090_02156	6.24
TC.SSS/putative acetate transporter		AFCMBR_GAC_MaxBin.090_02179	7.80
F-type H ⁺ -transporting ATPase subunit alpha		AFCMBR_GAC_MaxBin.090_02456	7.31

F-type H ⁺ -transporting ATPase subunit b	AFCMBR_GAC_MaxBin.090_02457	6.26
F-type H ⁺ -transporting ATPase subunit beta	AFCMBR_GAC_MaxBin.090_00634	5.45
F-type H ⁺ -transporting ATPase subunit beta	AFCMBR_GAC_MaxBin.090_02463	5.45
F-type H ⁺ -transporting ATPase subunit gamma	AFCMBR_GAC_MaxBin.090_02455	7.09
F-type H ⁺ -transporting ATPase subunit c	AFCMBR_GAC_MaxBin.090_02458	7.81
energy-conserving hydrogenases	AFCMBR_GAC_MaxBin.090_01416	6.50
energy-conserving hydrogenases	AFCMBR_GAC_MaxBin.090_04135	8.97

References

- Agler, M. T., Spirito, C. M., Usack, J. G., Werner, J. J., & Angenent, L. T. (2012). Chain elongation with reactor microbiomes: upgrading dilute ethanol to medium-chain carboxylates. *Energy & Environmental Science*, *5*(8), 8189. doi:10.1039/c2ee22101b
- Agler, M. T., Wrenn, B. A., Zinder, S. H., & Angenent, L. T. (2011). Waste to bioproduct conversion with undefined mixed cultures: the carboxylate platform. *Trends Biotechnol*, *29*(2), 70-78. doi:10.1016/j.tibtech.2010.11.006
- Albertsen, M., Karst, S. M., Ziegler, A. S., Kirkegaard, R. H., & Nielsen, P. H. (2015). Back to basics—the influence of DNA extraction and primer choice on phylogenetic analysis of activated sludge communities. *PLoS One*, *10*(7), e0132783.
- Amend, J. P., & Shock, E. L. (2001). Energetics of overall metabolic reactions of thermophilic and hyperthermophilic Archaea and Bacteria. *Fems Microbiology Reviews*, *25*(2), 175-243.
- Angenent, L. T., Karim, K., Al-Dahhan, M. H., & Domiguez-Espinosa, R. (2004). Production of bioenergy and biochemicals from industrial and agricultural wastewater. *Trends in Biotechnology*, *22*(9), 477-485. doi:10.1016/j.tibtech.2004.07.001
- Angenent, L. T., Richter, H., Buckel, W., Spirito, C. M., Steinbusch, K. J., Plugge, C. M., . . . Hamelers, H. V. (2016). Chain Elongation with Reactor Microbiomes: Open-Culture Biotechnology To Produce Biochemicals. *Environ Sci Technol*, *50*(6), 2796-2810. doi:10.1021/acs.est.5b04847
- Appels, L., Lauwers, J., Degreve, J., Helsen, L., Lievens, B., Willems, K., . . . Dewil, R. (2011). Anaerobic digestion in global bio-energy production: Potential and research challenges. *Renewable & Sustainable Energy Reviews*, *15*(9), 4295-4301.
- Aslam, M., McCarty, P. L., Bae, J., & Kim, J. (2014). The effect of fluidized media characteristics on membrane fouling and energy consumption in anaerobic fluidized membrane bioreactors. *Separation and Purification Technology*, *132*, 10-15.

- Aslam, M., Yang, P., Lee, P. H., & Kim, J. (2018). Novel staged anaerobic fluidized bed ceramic membrane bioreactor: Energy reduction, fouling control and microbial characterization. *Journal of Membrane Science*, *553*, 200-208.
- Bankevich, A., Nurk, S., Antipov, D., Gurevich, A. A., Dvorkin, M., Kulikov, A. S., . . . Pevzner, P. A. (2012). SPAdes: A New Genome Assembly Algorithm and Its Applications to Single-Cell Sequencing. *Journal of Computational Biology*, *19*(5), 455-477. doi:10.1089/cmb.2012.0021
- Barker, H. A., Kamen, M. D., & Bornstein, B. T. (1945). The Synthesis of Butyric and Caproic Acids from Ethanol and Acetic Acid by *Clostridium kluyveri*. *Proceedings of the National Academy of Sciences of the United States of America*, *31*(12), 373.
- Berg, I. A., Kockelkorn, D., Ramos-Vera, W. H., Say, R. F., Zarzycki, J., Hugler, M., . . . Fuchs, G. (2010). Autotrophic carbon fixation in archaea. *Nature Reviews Microbiology*, *8*(6), 447-460. doi:10.1038/nrmicro2365
- Bolger, A. M., Lohse, M., & Usadel, B. (2014). Trimmomatic: a flexible trimmer for Illumina sequence data. *Bioinformatics*, *30*(15), 2114-2120. doi:10.1093/bioinformatics/btu170
- Bornstein, B. T., & Barker, H. A. (1948). The Nutrition of *Clostridium kluyveri*. *The Journal of Bacteriology*, *55*(2), 223.
- Bushnell, B. *BBTools software package*. Retrieved from <http://sourceforge.net/projects/bbmap>
- Cai, M., Wilkins, D., Chen, J., Ng, S. K., Lu, H., Jia, Y., & Lee, P. K. (2016). Metagenomic reconstruction of key anaerobic digestion pathways in municipal sludge and industrial wastewater biogas-producing systems. *Front Microbiol*, *7*, 778. doi:10.3389/fmicb.2016.00778
- Chen, P., Xie, Q. L., Addy, M., Zhou, W. G., Liu, Y. H., Wang, Y. P., . . . Ruan, R. (2016). Utilization of municipal solid and liquid wastes for bioenergy and bioproducts production. *Bioresour Technol*, *215*, 163-172. doi:10.1016/j.biortech.2016.02.094
- Chen, S., Liu, X., & Dong, X. (2005). *Syntrophobacter sulfatireducens* sp. nov., a novel syntrophic, propionate-oxidizing bacterium isolated from UASB

- reactors. *Int J Syst Evol Microbiol*, 55(Pt 3), 1319-1324. doi:10.1099/ijs.0.63565-0
- Chen, S. Y., & Dong, X. Z. (2005). Proteiniphilum acetatigenes gen. nov., sp nov., from a UASB reactor treating brewery wastewater. *International Journal of Systematic and Evolutionary Microbiology*, 55, 2257-2261. doi:10.1099/ijs.0.63807-0
- Chen, W. S., Strik, D., Buisman, C. J. N., & Kroeze, C. (2017). Production of Caproic Acid from Mixed Organic Waste: An Environmental Life Cycle Perspective. *Environ Sci Technol*, 51(12), 7159-7168. doi:10.1021/acs.est.6b06220
- Chen, W. S., Ye, Y., Steinbusch, K. J. J., Strik, D. P. B. T. B., & Buisman, C. J. N. (2016). Methanol as an alternative electron donor in chain elongation for butyrate and caproate formation. *Biomass & Bioenergy*, 93, 201-208.
- Chen, Y., Jiang, S., Yuan, H., Zhou, Q., & Gu, G. (2007). Hydrolysis and acidification of waste activated sludge at different pHs. *Water Res*, 41(3), 683-689. doi:10.1016/j.watres.2006.07.030
- Chiu, P. C., & Lee, M. (2001). 2-Bromoethanesulfonate affects bacteria in a trichloroethene-dechlorinating culture. *Appl Environ Microbiol*, 67(5), 2371-2374. doi:10.1128/AEM.67.5.2371-2374.2001
- Cruz Viggli, C., Rossetti, S., Fazi, S., Paiano, P., Majone, M., & Aulenta, F. (2014). Magnetite particles triggering a faster and more robust syntrophic pathway of methanogenic propionate degradation. *Environ Sci Technol*, 48(13), 7536-7543. doi:10.1021/es5016789
- de Bok, F. A., Harmsen, H. J., Plugge, C. M., de Vries, M. C., Akkermans, A. D., de Vos, W. M., & Stams, A. J. (2005). The first true obligately syntrophic propionate-oxidizing bacterium, Pelotomaculum schinkii sp. nov., co-cultured with Methanospirillum hungatei, and emended description of the genus Pelotomaculum. *Int J Syst Evol Microbiol*, 55(Pt 4), 1697-1703. doi:10.1099/ijs.0.02880-0
- de Bok, F. A., Plugge, C. M., & Stams, A. J. (2004). Interspecies electron transfer in methanogenic propionate degrading consortia. *Water Res*, 38(6), 1368-1375. doi:10.1016/j.watres.2003.11.028

- de Bok, F. A., Stams, A. J., Dijkema, C., & Boone, D. R. (2001). Pathway of propionate oxidation by a syntrophic culture of *Smithella propionica* and *Methanospirillum hungatei*. *Appl Environ Microbiol*, *67*(4), 1800-1804. doi:10.1128/AEM.67.4.1800-1804.2001
- de Bok, F. A., Stams, A. J., Dijkema, C., & Boone, D. R. (2001). Pathway of Propionate Oxidation by a Syntrophic Culture of *Smithella propionica* and *Methanospirillum hungatei*. *Applied and environmental microbiology*, *67*(4), 1800-1804.
- de Bok, F. A. M., Harmsen, H. J. M., Plugge, C. M., de Vries, M. C., Akkermans, A. D. L., de Vos, W. M., & Stams, A. J. M. (2005). The first true obligately syntrophic propionate-oxidizing bacterium, *Pelotomaculum schinkii* sp nov., co-cultured with *Methanospirillum hungatei*, and emended description of the genus *Pelotomaculum*. *International Journal of Systematic and Evolutionary Microbiology*, *55*, 1697-1703.
- de Bok, F. A. M., Plugge, C. M., & Stams, A. J. M. (2004). Interspecies electron transfer in methanogenic propionate degrading consortia. *Water Research*, *38*(6), 1368-1375. doi:10.1016/j.watres.2003.11.028
- Demirel, B., & Scherer, P. (2008). The roles of acetotrophic and hydrogenotrophic methanogens during anaerobic conversion of biomass to methane: a review. *Reviews in Environmental Science and Biotechnology*, *7*(2), 173-190.
- Ding, H. B., Tan, G. Y., & Wang, J. Y. (2010). Caproate formation in mixed-culture fermentative hydrogen production. *Bioresour Technol*, *101*(24), 9550-9559. doi:10.1016/j.biortech.2010.07.056
- Dolfing, J. (2013). Syntrophic propionate oxidation via butyrate: a novel window of opportunity under methanogenic conditions. *Appl Environ Microbiol*, *79*(14), 4515-4516. doi:10.1128/AEM.00111-13
- Dolfing, J. (2017). Comment on “Thermodynamically enhancing propionic acid degradation by using sulfate as an external electron acceptor in a thermophilic anaerobic membrane reactor” by Qiao, W., Takayanagi, K., Li, Q., Shofie, M., Gao, F., Dong, R., Li, YY. *Water Res.*(2016). *Water Res*, *116*, 266-267.

- Dong, C., Wang, Y., Zhang, H., & Leu, S. Y. (2017). Feasibility of high-concentration cellulosic bioethanol production from undetoxified whole Monterey pine slurry. *Bioresour Technol*, *250*, 102-109. doi:10.1016/j.biortech.2017.11.029
- Edgar, R. C., Haas, B. J., Clemente, J. C., Quince, C., & Knight, R. (2011). UCHIME improves sensitivity and speed of chimera detection. *Bioinformatics*, *27*(16), 2194-2200. doi:10.1093/bioinformatics/btr381
- Estevez-Canales, M., Kuzume, A., Borjas, Z., Füeg, M., Lovley, D., Wandlowski, T., & Esteve-Núñez, A. (2015). A severe reduction in the cytochrome C content of *Geobacter sulfurreducens* eliminates its capacity for extracellular electron transfer. *Environmental microbiology reports*, *7*(2), 219-226.
- Fang, M. X., Zhang, W. W., Zhang, Y. Z., Tan, H. Q., Zhang, X. Q., Wu, M., & Zhu, X. F. (2012). *Brassicibacter mesophilus* gen. nov., sp nov., a strictly anaerobic bacterium isolated from food industry wastewater. *International Journal of Systematic and Evolutionary Microbiology*, *62*, 3018-3023.
- Farmer, J. J., Fanning, G. R., Huntley Carter, G. P., Holmes, B., Hickman, F. W., Richard, C., & Brenner, D. J. (1981). *Kluyvera*, a New (Redefined) Genus in the Family Enterobacteriaceae - Identification of *Kluyvera-Ascorbata* Sp-Nov and *Kluyvera-Cryocrescens* Sp-Nov in Clinical Specimens. *Journal of Clinical Microbiology*, *13*(5), 919-933.
- Fedorovich, V., Knighton, M. C., Pagaling, E., Ward, F. B., Free, A., & Goryanin, I. (2009). Novel electrochemically active bacterium phylogenetically related to *Arcobacter butzleri*, isolated from a microbial fuel cell. *Appl Environ Microbiol*, *75*(23), 7326-7334. doi:10.1128/AEM.01345-09
- Feng, L., Chen, Y., & Zheng, X. (2009). Enhancement of waste activated sludge protein conversion and volatile fatty acids accumulation during waste activated sludge anaerobic fermentation by carbohydrate substrate addition: the effect of pH. *Environ Sci Technol*, *43*(12), 4373-4380.
- Gallert, C., & Winter, J. (2008). Propionic acid accumulation and degradation during restart of a full-scale anaerobic biowaste digester. *Bioresour Technol*, *99*(1), 170-178. doi:10.1016/j.biortech.2006.11.014

- Galperin, M. Y., Brover, V., Tolstoy, I., & Yutin, N. (2016). Phylogenomic analysis of the family Peptostreptococcaceae (Clostridium cluster XI) and proposal for reclassification of *Clostridium litorale* (Fendrich et al. 1991) and *Eubacterium acidaminophilum* (Zindel et al. 1989) as *Peptoclostridium litorale* gen. nov. comb. nov. and *Peptoclostridium acidaminophilum* comb. nov. *International Journal of Systematic and Evolutionary Microbiology*, *66*, 5506-5513.
- Gao, D.-W., Zhang, T., Tang, C.-Y. Y., Wu, W.-M., Wong, C.-Y., Lee, Y. H., . . . Criddle, C. S. (2010). Membrane fouling in an anaerobic membrane bioreactor: differences in relative abundance of bacterial species in the membrane foulant layer and in suspension. *Journal of Membrane Science*, *364*(1), 331-338.
- Ge, S., Usack, J. G., Spirito, C. M., & Angenent, L. T. (2015). Long-Term n-Caproic Acid Production from Yeast-Fermentation Beer in an Anaerobic Bioreactor with Continuous Product Extraction. *Environ Sci Technol*, *49*(13), 8012-8021. doi:10.1021/acs.est.5b00238
- Gildemyn, S., Molitor, B., Usack, J. G., Nguyen, M., Rabaey, K., & Angenent, L. T. (2017). Upgrading syngas fermentation effluent using *Clostridium kluyveri* in a continuous fermentation. *Biotechnology for Biofuels*, *10*.
- Grabherr, M. G., Haas, B. J., Yassour, M., Levin, J. Z., Thompson, D. A., Amit, I., . . . Regev, A. (2011). Full-length transcriptome assembly from RNA-Seq data without a reference genome. *Nature Biotechnology*, *29*(7), 644-U130.
- Grootscholten, T. I., Steinbusch, K. J., Hamelers, H. V., & Buisman, C. J. (2013). Chain elongation of acetate and ethanol in an upflow anaerobic filter for high rate MCFA production. *Bioresour Technol*, *135*, 440-445. doi:10.1016/j.biortech.2012.10.165
- Grootscholten, T. I. M., Steinbusch, K. J. J., Hamelers, H. V. M., & Buisman, C. J. N. (2012). Chain elongation of acetate and ethanol in an upflow anaerobic filter for high rate MCFA production. *Bioresource Technology*. doi:10.1016/j.biortech.2012.10.165

- Grootscholten, T. I. M., Steinbusch, K. J. J., Hamelers, H. V. M., & Buisman, C. J. N. (2013a). High rate heptanoate production from propionate and ethanol using chain elongation. *Bioresource Technology*, *136*, 715-718. doi:10.1016/j.biortech.2013.02.085
- Grootscholten, T. I. M., Steinbusch, K. J. J., Hamelers, H. V. M., & Buisman, C. J. N. (2013b). Improving medium chain fatty acid productivity using chain elongation by reducing the hydraulic retention time in an upflow anaerobic filter. *Bioresource Technology*, *136*, 735-738. doi:10.1016/j.biortech.2013.02.114
- Grootscholten, T. I. M., Strik, D. P. B. T. B., Steinbusch, K. J. J., Buisman, C. J. N., & Hamelers, H. V. M. (2014). Two-stage medium chain fatty acid (MCFA) production from municipal solid waste and ethanol. *Applied Energy*, *116*, 223-229. doi:10.1016/j.apenergy.2013.11.061
- Holmes, D. E., Bond, D. R., & Lovley, D. R. (2004). Electron transfer by *Desulfobulbus propionicus* to Fe (III) and graphite electrodes. *Applied and environmental microbiology*, *70*(2), 1234-1237.
- Holmes, D. E., Shrestha, P. M., Walker, D. J., Dang, Y., Nevin, K. P., Woodard, T. L., & Lovley, D. R. (2017). Metatranscriptomic evidence for direct interspecies electron transfer between geobacter and methanotrix species in methanogenic rice paddy soils. *Applied and environmental microbiology*, *83*(9), e00223-00217.
- Imachi, H., Sekiguchi, Y., Kamagata, Y., Hanada, S., Ohashi, A., & Harada, H. (2002). *Pelotomaculum thermopropionicum* gen. nov., sp. nov., an anaerobic, thermophilic, syntrophic propionate-oxidizing bacterium. *International Journal of Systematic and Evolutionary Microbiology*, *52*, 1729-1735.
- Imachi, H., Sekiguchi, Y., Kamagata, Y., Hanada, S., Ohashi, A., & Harada, H. (2002). *Pelotomaculum thermopropionicum* gen. nov., sp. nov., an anaerobic, thermophilic, syntrophic propionate-oxidizing bacterium. *International journal of systematic and evolutionary microbiology*, *52*(5), 1729-1735.

- Jabari, L., Gannoun, H., Cayol, J. L., Hedi, A., Sakamoto, M., Falsen, E., . . . Fardeau, M. L. (2012). *Macellibacteroides fermentans* gen. nov., sp nov., a member of the family Porphyromonadaceae isolated from an upflow anaerobic filter treating abattoir wastewaters. *International Journal of Systematic and Evolutionary Microbiology*, *62*, 2522-2527.
- Kanehisa, M., Sato, Y., & Morishima, K. (2016). BlastKOALA and GhostKOALA: KEGG Tools for Functional Characterization of Genome and Metagenome Sequences. *Journal of Molecular Biology*, *428*(4), 726-731. doi:10.1016/j.jmb.2015.11.006
- Kato, S., Hashimoto, K., & Watanabe, K. (2012a). Methanogenesis facilitated by electric syntrophy via (semi)conductive iron-oxide minerals. *Environmental Microbiology*, *14*(7), 1646-1654.
- Kato, S., Hashimoto, K., & Watanabe, K. (2012b). Microbial interspecies electron transfer via electric currents through conductive minerals. *Proceedings of the National Academy of Sciences of the United States of America*, *109*(25), 10042-10046.
- Kato, S., & Watanabe, K. (2010). Ecological and Evolutionary Interactions in Syntrophic Methanogenic Consortia. *Microbes and Environments*, *25*(3), 145-151.
- Kenealy, W. R., Cao, Y., & Weimer, P. J. (1995). Production of caproic acid by cocultures of ruminal cellulolytic bacteria and *Clostridium kluyveri* grown on cellulose and ethanol. *Appl Microbiol Biotechnol*, *44*(3-4), 507-513.
- Kim, J., Kim, K., Ye, H., Lee, E., Shin, C., McCarty, P. L., & Bae, J. (2011). Anaerobic Fluidized Bed Membrane Bioreactor for Wastewater Treatment. *Environmental Science & Technology*, *45*(2), 576-581. doi:10.1021/es1027103
- Kono, T., Mehrotra, S., Endo, C., Kizu, N., Matusda, M., Kimura, H., . . . Ashida, H. (2017). A RuBisCO-mediated carbon metabolic pathway in methanogenic archaea. *Nature Communications*, *8*. doi:ARTN 1400710.1038/ncomms14007
- Kosaka, T., Uchiyama, T., Ishii, S., Enoki, M., Imachi, H., Kamagata, Y., . . . Watanabe, K. (2006a). Reconstruction and regulation of the central

- catabolic pathway in the thermophilic propionate-oxidizing syntroph *Pelotomaculum thermopropionicum*. *J Bacteriol*, 188(1), 202-210. doi:10.1128/JB.188.1.202-210.2006
- Kosaka, T., Uchiyama, T., Ishii, S., Enoki, M., Imachi, H., Kamagata, Y., . . . Watanabe, K. (2006b). Reconstruction and regulation of the central catabolic pathway in the thermophilic propionate-oxidizing syntroph *Pelotomaculum thermopropionicum*. *Journal of Bacteriology*, 188(1), 202-210.
- Kouzuma, A., Kato, S., & Watanabe, K. (2015). Microbial interspecies interactions: recent findings in syntrophic consortia. *Front Microbiol*, 6, 477. doi:10.3389/fmicb.2015.00477
- Kozich, J. J., Westcott, S. L., Baxter, N. T., Highlander, S. K., & Schloss, P. D. (2013). Development of a dual-index sequencing strategy and curation pipeline for analyzing amplicon sequence data on the MiSeq Illumina sequencing platform. *Appl Environ Microbiol*, 79(17), 5112-5120. doi:10.1128/AEM.01043-13
- Kucek, L. A., Spirito, C. M., & Angenent, L. T. (2016). High n-caprylate productivities and specificities from dilute ethanol and acetate: chain elongation with microbiomes to upgrade products from syngas fermentation. *Energy & Environmental Science*, 9(11), 3482-3494.
- Kuznetsov, Y. I., & Ibatullin, K. A. (2002). On the inhibition of the carbon dioxide corrosion of steel by carboxylic acids. *Protection of Metals*, 38(5), 439-443. doi:Doi 10.1023/A:1020342728236
- LaBarge, N., Ye, Y., Kim, K.-Y., Yilmazel, Y. D., Saikaly, P. E., Hong, P.-Y., & Logan, B. E. (2016). Impact of acclimation methods on microbial communities and performance of anaerobic fluidized bed membrane bioreactors. *Environmental Science: Water Research & Technology*, 2(6), 1041-1048.
- Latif, H., Zeidan, A. A., Nielsen, A. T., & Zengler, K. (2014). Trash to treasure: production of biofuels and commodity chemicals via syngas fermenting microorganisms. *Current Opinion in Biotechnology*, 27, 79-87.

- Leang, C., Qian, X., Mester, T., & Lovley, D. R. (2010). Alignment of the c-type cytochrome OmcS along pili of *Geobacter sulfurreducens*. *Appl Environ Microbiol*, *76*(12), 4080-4084. doi:10.1128/AEM.00023-10
- Lee, M. J., & Zinder, S. H. (1988). Isolation and Characterization of a Thermophilic Bacterium Which Oxidizes Acetate in Syntrophic Association with a Methanogen and Which Grows Acetogenically on H₂-CO₂. *Applied and environmental microbiology*, *54*(1), 124 - 129.
- Leng, L., Yang, P. X., Mao, Y. P., Wu, Z. Y., Zhang, T., & Lee, P. H. (2017). Thermodynamic and physiological study of caproate and 1,3-propanediol co-production through glycerol fermentation and fatty acids chain elongation. *Water Research*, *114*, 200-209.
- Leng, L., Yang, P. X., Singh, S., Zhuang, H. C., Xu, L. J., Chen, W. H., . . . Lee, P. H. (2018). A review on the bioenergetics of anaerobic microbial metabolism close to the thermodynamic limits and its implications for digestion applications. *Bioresource Technology*, *247*, 1095-1106. doi:10.1016/j.biortech.2017.09.103
- Li, W. W., & Yu, H. Q. (2011). From wastewater to bioenergy and biochemicals via two-stage bioconversion processes: A future paradigm. *Biotechnology Advances*, *29*(6), 972-982. doi:10.1016/j.biotechadv.2011.08.012
- Liebergessell, M., Hustede, E., Timm, A., Steinbuchel, A., Fuller, R. C., Lenz, R. W., & Schlegel, H. G. (1991). Formation of Poly(3-Hydroxyalkanoates) by Phototrophic and Chemolithotrophic Bacteria. *Archives of Microbiology*, *155*(5), 415-421. doi:Doi 10.1007/Bf00244955
- Liu, F., Rotaru, A.-E., Shrestha, P. M., Malvankar, N. S., Nevin, K. P., & Lovley, D. R. (2012). Promoting direct interspecies electron transfer with activated carbon. *Energy & Environmental Science*, *5*(10), 8982-8989.
- Liu, F. H., Rotaru, A. E., Shrestha, P. M., Malvankar, N. S., Nevin, K. P., & Lovley, D. R. (2012). Promoting direct interspecies electron transfer with activated carbon. *Energy & Environmental Science*, *5*(10), 8982-8989. doi:10.1039/c2ee22459c
- Liu, W., Cai, W., Guo, Z., Wang, L., Yang, C., Varrone, C., & Wang, A. (2016). Microbial electrolysis contribution to anaerobic digestion of waste

- activated sludge, leading to accelerated methane production. *Renewable Energy*, *91*, 334-339.
- Liu, W., He, Z., Yang, C., Zhou, A., Guo, Z., Liang, B., . . . Wang, A. J. (2016). Microbial network for waste activated sludge cascade utilization in an integrated system of microbial electrolysis and anaerobic fermentation. *Biotechnol Biofuels*, *9*(1), 83. doi:10.1186/s13068-016-0493-2
- Liu, Y., Balkwill, D. L., Aldrich, H. C., Drake, G. R., & Boone, D. R. (1999). Characterization of the anaerobic propionate-degrading syntrophs *Smithella propionica* gen. nov., sp. nov. and *Syntrophobacter wolinii*. *International Journal of Systematic Bacteriology*, *49 Pt 2*, 545-556. doi:10.1099/00207713-49-2-545
- Liu, Y., & Whitman, W. B. (2008). Metabolic, phylogenetic, and ecological diversity of the methanogenic archaea. *Ann N Y Acad Sci*, *1125*(1), 171-189. doi:10.1196/annals.1419.019
- Liu, Y. H., He, P. J., Shao, L. M., Zhang, H., & Lu, F. (2017). Significant enhancement by biochar of caproate production via chain elongation. *Water Research*, *119*, 150-159.
- Lovley, D. R. (2011). Live wires: direct extracellular electron exchange for bioenergy and the bioremediation of energy-related contamination. *Energy & Environmental Science*, *4*(12), 4896-4906.
- Ma, J., Wang, Z., Zou, X., Feng, J., & Wu, Z. (2013). Microbial communities in an anaerobic dynamic membrane bioreactor (AnDMBR) for municipal wastewater treatment: Comparison of bulk sludge and cake layer. *Process Biochemistry*, *48*(3), 510-516.
- Madden, T. L., Tatusov, R. L., & Zhang, J. (1996). Applications of network BLAST server. *Methods Enzymol*, *266*, 131-141.
- Malvankar, N. S., Yalcin, S. E., Tuominen, M. T., & Lovley, D. R. (2014). Visualization of charge propagation along individual pili proteins using ambient electrostatic force microscopy. *Nature nanotechnology*, *9*(12), 1012-1017.

- Marshall, C. W., LaBelle, E. V., & May, H. D. (2013). Production of fuels and chemicals from waste by microbiomes. *Current Opinion in Biotechnology*, 24(3), 391-397.
- Marti-Herrero, J., Alvarez, R., Rojas, M. R., Aliaga, L., Cespedes, R., & Carbonell, J. (2014). Improvement through low cost biofilm carrier in anaerobic tubular digestion in cold climate regions. *Bioresource Technology*, 167, 87-93.
- McCarty, P. L. (2001). The development of anaerobic treatment and its future. *Water Science and Technology*, 44(8), 149-156.
- McCarty, P. L., & Bae, J. (2011). Model to Couple Anaerobic Process Kinetics with Biological Growth Equilibrium Thermodynamics. *Environmental Science & Technology*, 45(16), 6838-6844. doi:10.1021/es2009055
- McCarty, P. L., & Smith, D. P. (1986). Anaerobic wastewater treatment. *Environmental Science & Technology*, 20(12), 1200-1206.
- McInerney, M. J., Sieber, J. R., & Gunsalus, R. P. (2009). Syntrophy in anaerobic global carbon cycles. *Current Opinion in Biotechnology*, 20(6), 623-632. doi:10.1016/j.copbio.2009.10.001
- Morgan-Sagastume, F., Pratt, S., Karlsson, A., Cirne, D., Lant, P., & Werker, A. (2011). Production of volatile fatty acids by fermentation of waste activated sludge pre-treated in full-scale thermal hydrolysis plants. *Bioresource Technol*, 102(3), 3089-3097. doi:10.1016/j.biortech.2010.10.054
- Morita, M., Malvankar, N. S., Franks, A. E., Summers, Z. M., Giloteaux, L., Rotaru, A. E., . . . Lovley, D. R. (2011a). Potential for Direct Interspecies Electron Transfer in Methanogenic Wastewater Digester Aggregates. *Mbio*, 2(4). doi:ARTN e00159-1110.1128/mBio.00159-11
- Morita, M., Malvankar, N. S., Franks, A. E., Summers, Z. M., Giloteaux, L., Rotaru, A. E., . . . Lovley, D. R. (2011b). Potential for direct interspecies electron transfer in methanogenic wastewater digester aggregates. *MBio*, 2(4), e00159-00111. doi:10.1128/mBio.00159-11

- Morris, B. E., Henneberger, R., Huber, H., & Moissl-Eichinger, C. (2013). Microbial syntrophy: interaction for the common good. *FEMS Microbiol Rev*, 37(3), 384-406. doi:10.1111/1574-6976.12019
- Müller, N., Worm, P., Schink, B., Stams, A. J., & Plugge, C. M. (2010). Syntrophic butyrate and propionate oxidation processes: from genomes to reaction mechanisms. *Environmental microbiology reports*, 2(4), 489-499.
- Murrell, P. (2012). *R graphics*. In *R Series* (pp. 1 online resource (536 pages)). Retrieved from <https://www.taylorfrancis.com/books/9781439831779>
- Narihiro, T., Nobu, M. K., Tamaki, H., Kamagata, Y., Sekiguchi, Y., & Liu, W. T. (2016). Comparative Genomics of Syntrophic Branched-Chain Fatty Acid Degrading Bacteria. *Microbes and Environments*, 31(3), 288-292.
- Niu, L., Song, L., & Dong, X. (2008). Proteiniborus ethanolicus gen. nov., sp. nov., an anaerobic protein-utilizing bacterium. *Int J Syst Evol Microbiol*, 58(Pt 1), 12-16. doi:10.1099/ijms.0.65108-0
- Nurk, S., Bankevich, A., Antipov, D., Gurevich, A., Korobeynikov, A., Lapidus, A., . . . Pevzner, P. A. (2013). Assembling Genomes and Mini-metagenomes from Highly Chimeric Reads. In M. Deng, R. Jiang, F. Sun, & X. Zhang (Eds.), *Research in Computational Molecular Biology: 17th Annual International Conference, RECOMB 2013, Beijing, China, April 7-10, 2013. Proceedings* (pp. 158-170). Berlin, Heidelberg: Springer Berlin Heidelberg.
- Pan, X., Angelidaki, I., Alvarado-Morales, M., Liu, H., Liu, Y., Huang, X., & Zhu, G. (2016). Methane production from formate, acetate and H₂/CO₂; focusing on kinetics and microbial characterization. *Bioresour Technol*, 218, 796-806. doi:10.1016/j.biortech.2016.07.032
- Parks, D. H., Imelfort, M., Skennerton, C. T., Hugenholtz, P., & Tyson, G. W. (2015). CheckM: assessing the quality of microbial genomes recovered from isolates, single cells, and metagenomes. *Genome Research*, 25(7), 1043-1055. doi:10.1101/gr.186072.114
- Patel, G. B., & Sprott, G. D. (1990). Methanosaeta-Concillii Gen-Nov, Sp-Nov (Methanothrix-Concillii) and Methanosaeta-Thermoacetophila Nom-Rev,

- Comb-Nov. *International Journal of Systematic Bacteriology*, 40(1), 79-82.
- Plugge, C. M., Balk, M., & Stams, A. J. (2002). *Desulfotomaculum thermobenzoicum* subsp. *thermosyntrophicum* subsp. nov., a thermophilic, syntrophic, propionate-oxidizing, spore-forming bacterium. *Int J Syst Evol Microbiol*, 52(Pt 2), 391-399. doi:10.1099/00207713-52-2-391
- Plugge, C. M., Henstra, A. M., Worm, P., Swarts, D. C., Paulitsch-Fuchs, A. H., Scholten, J. C. M., . . . McInerney, M. J. (2012). Complete genome sequence of *Syntrophobacter fumaroxidans* strain (MPOBT). *Standards in Genomic Sciences*, 7(1), 91-106.
- Reguera, G., McCarthy, K. D., Mehta, T., Nicoll, J. S., Tuominen, M. T., & Lovley, D. R. (2005). Extracellular electron transfer via microbial nanowires. *Nature*, 435(7045), 1098-1101. doi:10.1038/nature03661
- Renz, M. (2005). Ketonization of carboxylic acids by decarboxylation: Mechanism and scope. *European Journal of Organic Chemistry*(6), 979-988. doi:10.1002/ejoc.200400546
- Ritalahti, K. M., Justicia-Leon, S. D., Cusick, K. D., Ramos-Hernandez, N., Rubin, M., Dornbush, J., & Löffler, F. E. (2012). *Sphaerochaeta globosa* gen. nov., sp nov and *Sphaerochaeta pleomorpha* sp nov., free-living, spherical spirochaetes. *International Journal of Systematic and Evolutionary Microbiology*, 62, 210-216.
- Rittmann, B. E., & McCarty, P. L. (2001). *Environmental biotechnology : principles and applications*. Boston: McGraw-Hill.
- Rotaru, A.-E., Shrestha, P. M., Liu, F., Markovaite, B., Chen, S., Nevin, K. P., & Lovley, D. R. (2014). Direct interspecies electron transfer between *Geobacter metallireducens* and *Methanosarcina barkeri*. *Applied and environmental microbiology*, 80(15), 4599-4605. doi:10.1128/AEM.00895-14
- Rotaru, A.-E., Shrestha, P. M., Liu, F., Shrestha, M., Shrestha, D., Embree, M., . . . Lovley, D. R. (2014). A new model for electron flow during anaerobic digestion: direct interspecies electron transfer to *Methanosaeta* for the

- reduction of carbon dioxide to methane. *Energy Environ. Sci.*, 7(1), 408-415. doi:10.1039/c3ee42189a
- Rotaru, A. E., Shrestha, P. M., Liu, F. H., Shrestha, M., Shrestha, D., Embree, M., . . . Lovley, D. R. (2014). A new model for electron flow during anaerobic digestion: direct interspecies electron transfer to *Methanosaeta* for the reduction of carbon dioxide to methane. *Energy & Environmental Science*, 7(1), 408-415.
- Sarkar, N., Ghosh, S. K., Bannerjee, S., & Aikat, K. (2012). Bioethanol production from agricultural wastes: An overview. *Renewable Energy*, 37(1), 19-27.
- Schink, B. (1997). Energetics of syntrophic cooperation in methanogenic degradation. *Microbiol Mol Biol Rev*, 61(2), 262-280.
- Schloss, P. D., Westcott, S. L., Ryabin, T., Hall, J. R., Hartmann, M., Hollister, E. B., . . . Weber, C. F. (2009). Introducing mothur: open-source, platform-independent, community-supported software for describing and comparing microbial communities. *Appl Environ Microbiol*, 75(23), 7537-7541. doi:10.1128/AEM.01541-09
- Schoberth, S., & Gottschalk, G. (1969). Considerations on the energy metabolism of *Clostridium kluuyveri*. *Arch Mikrobiol*, 65(4), 318-328.
- Scholten, J. C., & Conrad, R. (2000). Energetics of syntrophic propionate oxidation in defined batch and chemostat cocultures. *Appl Environ Microbiol*, 66(7), 2934-2942.
- Seedorf, H., Fricke, W. F., Veith, B., Bruggemann, H., Liesegang, H., Strittmatter, A., . . . Gottschalk, G. (2008). The genome of *Clostridium kluuyveri*, a strict anaerobe with unique metabolic features. *Proceedings of the National Academy of Sciences of the United States of America*, 105(6), 2128-2133.
- Seedorf, H., Fricke, W. F., Veith, B., Bruggemann, H., Liesegang, H., Strittmatter, A., . . . Gottschalk, G. (2008). The genome of *Clostridium kluuyveri*, a strict anaerobe with unique metabolic features. *Proc Natl Acad Sci U S A*, 105(6), 2128-2133. doi:10.1073/pnas.0711093105

- Seemann, T. (2014). Prokka: rapid prokaryotic genome annotation. *Bioinformatics*, *30*(14), 2068-2069. doi:10.1093/bioinformatics/btu153
- Segata, N., Bornigen, D., Morgan, X. C., & Huttenhower, C. (2013). PhyloPhlAn is a new method for improved phylogenetic and taxonomic placement of microbes. *Nature Communications*, *4*.
- Shrestha, P. M., Rotaru, A. E., Summers, Z. M., Shrestha, M., Liu, F. H., & Lovley, D. R. (2013). Transcriptomic and Genetic Analysis of Direct Interspecies Electron Transfer. *Applied and Environmental Microbiology*, *79*(7), 2397-2404.
- Smith, D. P., & Mccarty, P. L. (1989). Energetic and Rate Effects on Methanogenesis of Ethanol and Propionate in Perturbed Cstrs. *Biotechnology and Bioengineering*, *34*(1), 39-54.
- Smith, K. S., & Ingram-Smith, C. (2007). Methanosaeta, the forgotten methanogen? *Trends in microbiology*, *15*(4), 150-155.
- Stams, A. J. M., & Plugge, C. M. (2009). Electron transfer in syntrophic communities of anaerobic bacteria and archaea. *Nature Reviews Microbiology*, *7*(8), 568-577. doi:10.1038/nrmicro2166
- Steinbusch, K. J. J., Hamelers, H. V. M., Plugge, C. M., & Buisman, C. J. N. (2011). Biological formation of caproate and caprylate from acetate: fuel and chemical production from low grade biomass. *Energy Environ. Sci.*, *4*(1), 216-224. doi:10.1039/c0ee00282h
- Summers, Z. M., Fogarty, H. E., Leang, C., Franks, A. E., Malvankar, N. S., & Lovley, D. R. (2010). Direct exchange of electrons within aggregates of an evolved syntrophic coculture of anaerobic bacteria. *Science*, *330*(6009), 1413-1415.
- Sung, Y., Fletcher, K. F., Ritalaliti, K. M., Apkarian, R. P., Ramos-Hernandez, N., Sanford, R. A., . . . Löffler, F. E. (2006). *Geobacter lovleyi* sp nov strain SZ, a novel metal-reducing and tetrachloroethene-dechlorinating bacterium. *Applied and Environmental Microbiology*, *72*(4), 2775-2782.
- Takahashi, S., Tomita, J., Nishioka, K., Hisada, T., & Nishijima, M. (2014). Development of a prokaryotic universal primer for simultaneous analysis

- of Bacteria and Archaea using next-generation sequencing. *Plos One*, 9(8), e105592. doi:10.1371/journal.pone.0105592
- Thauer, R. K., Jungermann, K., & Decker, K. (1977). Energy conservation in chemotrophic anaerobic bacteria. *Bacteriol Rev*, 41(1), 100-180.
- Thauer, R. K., Kaster, A. K., Seedorf, H., Buckel, W., & Hedderich, R. (2008). Methanogenic archaea: ecologically relevant differences in energy conservation. *Nature Reviews Microbiology*, 6(8), 579-591.
- Thiele, J. H., & Zeikus, J. G. (1988). Control of Interspecies Electron Flow during Anaerobic Digestion: Significance of Formate Transfer versus Hydrogen Transfer during Syntrophic Methanogenesis in Flocs. *Appl Environ Microbiol*, 54(1), 20-29.
- Tomlinson, N., & Barker, H. A. (1954). Carbon dioxide and acetate utilization by clostridium kluyveri. I. Influence of nutritional conditions on utilization patterns. *J Biol Chem*, 209(2), 585-595.
- Venkiteswaran, K., Bocher, B., Maki, J., & Zitomer, D. (2015). Relating Anaerobic Digestion Microbial Community and Process Function. *Microbiol Insights*, 8(Suppl 2), 37-44. doi:10.4137/MBI.S33593
- Wang, Q., Garrity, G. M., Tiedje, J. M., & Cole, J. R. (2007). Naive Bayesian classifier for rapid assignment of rRNA sequences into the new bacterial taxonomy. *Appl Environ Microbiol*, 73(16), 5261-5267. doi:10.1128/AEM.00062-07
- Weimer, P. J., Nerdahl, M., & Brandl, D. J. (2015). Production of medium-chain volatile fatty acids by mixed ruminal microorganisms is enhanced by ethanol in co-culture with Clostridium kluyveri. *Bioresour Technol*, 175, 97-101. doi:10.1016/j.biortech.2014.10.054
- Wickham, H. (2009). *Ggplot2 : elegant graphics for data analysis*. New York: Springer.
- Willems, A., & Collins, M. D. (1996). Phylogenetic relationships of the genera Acetobacterium and Eubacterium sensu stricto and reclassification of Eubacterium alactolyticum as Pseudoramibacter alactolyticus gen nov, comb nov. *International Journal of Systematic Bacteriology*, 46(4), 1083-1087.

- Wu, B., Li, Y., Lim, W., Lee, S. L., Guo, Q., Fane, A. G., & Liu, Y. (2017). Single-stage versus two-stage anaerobic fluidized bed bioreactors in treating municipal wastewater: Performance, foulant characteristics, and microbial community. *Chemosphere*, *171*, 158-167.
- Wu, Y. W., Tang, Y. H., Tringe, S. G., Simmons, B. A., & Singer, S. W. (2014). MaxBin: an automated binning method to recover individual genomes from metagenomes using an expectation-maximization algorithm. *Microbiome*, *2*. doi:Artn 2610.1186/2049-2618-2-26
- Xiong, B. Y., Richard, T. L., & Kumar, M. (2015). Integrated acidogenic digestion and carboxylic acid separation by nanofiltration membranes for the lignocellulosic carboxylate platform. *Journal of Membrane Science*, *489*, 275-283.
- Xu, J., Guzman, J. J. L., Andersen, S. J., Rabaey, K., & Angenent, L. T. (2015). In-line and selective phase separation of medium-chain carboxylic acids using membrane electrolysis. *Chemical Communications*, *51*(31), 6847-6850.
- Ye, D., Quensen, J. F., 3rd, Tiedje, J. M., & Boyd, S. A. (1999). 2-Bromoethanesulfonate, sulfate, molybdate, and ethanesulfonate inhibit anaerobic dechlorination of polychlorobiphenyls by pasteurized microorganisms. *Appl Environ Microbiol*, *65*(1), 327-329.
- Yu, H. Q., & Mu, Y. (2006). Biological hydrogen production in a UASB reactor with granules. II: Reactor performance in 3-year operation. *Biotechnology and Bioengineering*, *94*(5), 988-995. doi:10.1002/bit.20923
- Zhang, J. X., Mao, L. W., Zhang, L., Loh, K. C., Dai, Y. J., & Tong, Y. W. (2017). Metagenomic insight into the microbial networks and metabolic mechanism in anaerobic digesters for food waste by incorporating activated carbon. *Scientific Reports*, *7*.
- Zhang, S., Chang, J., Lin, C., Pan, Y., Cui, K., Zhang, X., . . . Huang, X. (2017). Enhancement of methanogenesis via direct interspecies electron transfer between Geobacteraceae and Methanosaetaceae conducted by granular activated carbon. *Bioresource Technology*, *245*, 132-137.